LA--13444-T

LA-13444-T
Thesis

Discrete Ordinates Transport Methods for Problems with Highly Forward-Peaked Scattering

Los Alamos
NATIONAL LABORATORY

Los Alamos National Laboratory is operated by the University of California for the United States Department of Energy under contract W-7405-ENG-36.

This thesis was accepted by the Department of Nuclear Engineering, Texas A&M University, College Station, Texas, in partial fulfillment of the requirements for the degree of Doctor of Philosophy. The text and illustrations are the independent work of the author and only the front matter has been edited by the CIC-1 Writing and Editing Staff to conform with Department of Energy and Los Alamos National Laboratory publication policies.

An Affirmative Action/Equal Opportunity Employer

LA-13444-T
Thesis

UC-700
Issued: April 1998

Discrete Ordinates Transport Methods for Problems with Highly Forward-Peaked Scattering

Shawn Daniel Pautz

Los Alamos
NATIONAL LABORATORY
Los Alamos, New Mexico 87545

ACKNOWLEDGMENTS

This research was made possible by the efforts of many, some of whom I wish to acknowledge here. My greatest thanks I reserve for my advisor, Marvin Adams. Thanks are extended to Drs. Paul Nelson, Dmitriy Anistratov, Jim Morel, and Suely Oliveira for serving on my committee and for providing me with additional perspectives. I also thank Dr. James Bramble for serving as a substitute at my final defense.

I would like to thank Dr. Edward Larsen from the University of Michigan for numerous fruitful discussions. My thanks also go to the members of the Radiation Transport Team at Los Alamos National Laboratory for providing me with many tools to support my work, especially Todd Wareing, John McGhee, and Jim Morel.

Part of this research was completed with the support of a National Science Foundation Graduate Research Fellowship. This work also was supported financially by Texas A&M University and Los Alamos National Laboratory. I thank all of the individuals who made such support possible.

I would like to thank the transport research team at Texas A&M University for providing a stimulating and creative environment. The transport research team is: Michael Zika, Chris Castrianni, Chris Gesh, Kelly Thompson, Gilles Ramone, Halim Alsaed, and Daryl Hawkins.

TABLE OF CONTENTS

CHAPTER Page

LIST OF FIGURES

FIGURE Page

LIST OF TABLES

TABLE Page

TABLE Page

DISCRETE ORDINATES TRANSPORT METHODS FOR PROBLEMS WITH HIGHLY FORWARD-PEAKED SCATTERING

by

SHAWN DANIEL PAUTZ

ABSTRACT

We examine the solutions of the discrete ordinates (S_N) method for problems with highly forward-peaked scattering kernels. We derive conditions necessary to obtain reasonable solutions in a certain forward-peaked limit, the Fokker-Planck (FP) limit. We also analyze the acceleration of the iterative solution of such problems and offer improvements to it.

We extend the analytic Fokker-Planck limit analysis to the S_N equations. This analysis shows that in this asymptotic limit the S_N solution satisfies a pseudospectral discretization of the FP equation, provided that the scattering term is handled in a certain way (which we describe) and that the analytic transport solution satisfies an analytic FP equation. Similar analyses of various spatially discretized S_N equations reveal that they too produce solutions that satisfy discrete FP equations, given the same provisions. Numerical results agree with these theoretical predictions.

We define a multidimensional angular multigrid (ANMG) method to accelerate the iterative solution of highly forward-peaked problems. Our analyses show that a straightforward application of this scheme is subject to high-frequency instabilities. However, by applying a diffusive filter to the ANMG corrections we are able to stabilize this

method. Fourier analyses of model problems show that the resulting method is effective at accelerating the convergence rate when the scattering is forward-peaked. Our numerical results demonstrate that these analyses are good predictors of the actual performance of the ANMG method.

CHAPTER I

INTRODUCTION

Over the last several decades a variety of deterministic numerical schemes have been developed to approximately solve the linear Boltzmann transport equation. These methods have been developed primarily to solve neutron transport problems. Most neutron transport problems of interest are characterized by isotropic or mildly anisotropic scattering. For such problems numerical transport schemes have become increasingly accurate and robust; many are applicable to multidimensional problems. Advances have also been made in the development of acceleration methods that are effective at increasing the convergence rate of the iterative solution of such problems.

The transport equation is not limited to the description of mildly anisotropic neutron transport; it also is a valid description in most cases of the transport of neutrons in highly anisotropically scattering media and for other types of particles such as electrons and photons. In many physical problems the scattering is highly "forward-peaked", which means that the average scattering angle is very small. Such problems include the transport of charged particles such as ions and electrons,[1–3] high-energy x-rays and gamma rays,[4] visible light in certain media, and very high-energy neutrons.[5] These types of physical problems are encountered in such situations as inertially and magnetically confined fusion, medical physics,[6–8] electron microscopy,[9,10] shielding of electronic components in spacecraft,[11] ion implantation in electronics,[12] atmospheric and interstellar transport of light,[13–16] gamma-ray well-logging,[17] and accelerator-driven processes.

This dissertation follows the style and format of *Nuclear Science and Engineering*.

The nature of these problems impacts the accuracy and efficiency of the deterministic transport schemes that are used to model them. One generally needs to use higher-order angular quadratures (i.e. finer angular resolution) and to calculate many more scattering moments than are needed to obtain a sufficiently accurate solution in most neutron transport problems. For charged-particle calculations the energy loss per scattering event can be small, requiring a finer energy group structure. These requirements directly impact the amount of memory and CPU time needed, especially in multidimensional calculations. Furthermore, most acceleration methods developed for neutron transport problems lose their effectiveness when the scattering is forward-peaked, which greatly increases the number of iterations required to sufficiently converge the solution.

As a consequence of these computational demands the development, analysis, and application of deterministic transport methods for forward-peaked scattering problems has lagged behind advances in methods for isotropic and weakly anisotropic problems. Most applications have been limited to one-dimensional transport.[18–25] However, the development of much faster computers with more memory and of more efficient transport schemes has made multidimensional calculations more feasible.[26–28] One particular development, the angular multigrid (ANMG) acceleration method of Morel and Manteuffel,[29] greatly reduces the number of iterations required to solve forward-peaked problems, although it has only been developed for one-dimensional geometry. The prospect of a greater range of forward-peaked scattering problems that can be feasibly modeled, especially in multidimensions, creates the need for a better understanding of the accuracy of these methods and for more effective acceleration methods.

The purpose of this work is twofold. First, we will study the accuracy of common deterministic transport methods when they are applied to highly forward-peaked scattering problems, both in one-dimensional and multidimensional geometries. Specifically, we will extend the asymptotic Fokker-Planck analyses of Pomraning[30] to discrete ordinates (commonly called S_N) transport schemes.[31] These analyses will reveal the conditions under which discrete ordinates methods produce reasonable solutions to forward-peaked scattering problems. Second, we will analyze the convergence rate of transport iterations for multidimensional forward-peaked scattering problems and make improvements by extending the ANMG method to the multidimensional setting. Our analysis will show the stability and effectiveness of the ANMG scheme. In situations where it is unstable we will propose, analyze, and test modifications that stabilize this acceleration method without unduly compromising its effectiveness.

This work contributes the following new results to the body of knowledge about computational methods for forward-peaked transport problems:

1. We show that if the scattering source is calculated in a specific manner, then the discrete ordinates solution limits to the solution of a discretized Fokker-Planck equation in the same asymptotic limit in which the exact transport solution limits to an exact Fokker-Planck solution. This is a highly desirable result that provides a measure of confidence in the application of discrete ordinates methods to forward-peaked problems.

2. We show that if the scattering source is calculated in that same specific manner, then several common methods for spatially discretizing the discrete ordinates equations produce solutions that limit to the solutions of spatially and angularly discretized Fokker-Planck

equations. This again is a highly desirable result that increases confidence in the use of discrete ordinates methods for forward-peaked problems.

3. We show that if the scattering source is calculated in the "standard" discrete ordinates manner, then the discrete ordinates solution will in general be poor or will not exist in the Fokker-Planck limit.

4. We analyze in two dimensions the ANgular MultiGrid (ANMG) method previously developed and tested for 1D problems. We find that the scheme is unstable in 2D for the discrete ordinates method with no spatial discretization and with fine-mesh spatial discretization.

5. We devise a diffusive filter for the ANMG corrections and show that this successfully stabilizes the method in 2D. We show that the filtered ANMG method is superior to the diffusion synthetic acceleration (DSA) method that is commonly used in iterations for forward-peaked problems.

The remainder of this work is organized as follows. In Chapter II we will review the asymptotic Fokker-Planck analysis of Pomraning, as applied to analytic transport, and extend it to the discrete ordinates transport method. We will obtain conditions under which the discrete ordinates method produces reasonable solutions in this forward-peaked limit. In Chapter III we will extend these Fokker-Planck analyses to spatially discretized S_N methods in one and two dimensions and also obtain necessary and/or sufficient conditions under which reasonable solutions are obtained. In Chapter IV we will review and analyze the effectiveness of common acceleration methods for highly forward-peaked scattering problems. We will extend the ANMG method to multidimensions and develop modifications necessary to ensure its stability and effectiveness. In Chapter V we will extend the ANMG method to spatially

discrete problems and analyze its stability and effectiveness. In Chapter VI we will present numerical results that support the results of the Fokker-Planck and ANMG analyses. Finally, in Chapter VII we offer some concluding remarks and suggestions for future work.

CHAPTER II

FOKKER-PLANCK ANALYSIS OF THE SPATIALLY ANALYTIC TRANSPORT EQUATION

Previous studies have examined the convergence properties of solutions to discrete ordinates (S_N) discretizations of the transport equation.[32–37] Numerous studies have also examined the convergence and stability properties of spatially discretized S_N equations.[38–56] Generally speaking, given fixed cross sections and geometry the discrete solutions converge to the exact solutions as the spatial and angular discretizations are made increasingly fine, at least for "reasonable" discretization methods. The key feature of these studies is that material properties (i.e. cross sections) are held constant while the discretizations are made vanishingly small. Given sufficient refinement of the discretization, one can achieve an arbitrarily small error in the discrete solution.

A related question is how the accuracy of a particular discrete transport method is related to the cross sections, given fixed problem geometry and a fixed angular and spatial discretization. A scaling parameter, ϵ, is introduced into the cross section definitions such that each cross section varies like ϵ to some power as $\epsilon \rightarrow 0$. For many "scalings" of physical interest the analytic transport solution limits to the solution of some simpler operator.[30,57–66] In this same limit various transport discretization methods may or may not produce solutions that limit to discretized solutions of the simpler analytic operator. For example, numerous spatial discretization schemes have been examined in the thick diffusion limit.[48,50,52,63,67–84] These schemes are considered "good" in this limit if their solutions satisfy

valid discretizations of the diffusion equation; their accuracy is identical (in this limit) to the accuracy of the discrete diffusion solution.

The object of the present study is to determine and assess the behavior of discrete ordinate transport solutions in the limit of forward-peaked scattering, namely the Fokker-Planck limit. A scaling parameter, δ, will be used to define a cross section scaling such that the scattering becomes increasingly forward-peaked as $\delta \rightarrow 0$. Experience in numerical methods analysis[85–88] would suggest that the asymptotic form of the error of the discrete ordinates method could be described by $E = O\left(N^i \delta^j\right)$, where N is the order of the angular quadrature and i and j are constants that are determined by the particular discretization method and by the unscaled cross sections. The studies mentioned in the first paragraph indicate that i will be negative for any reasonable type of quadrature. The question we wish to address is what j is (presuming the form of the error given above is valid), given a particular transport discretization and a cross section scaling parameter δ that describes how forward-peaked the scattering is.

Rather than addressing the above question directly, we wish to break this question into two parts, as is done in the thick diffusion limit studies. For problems involving certain kinds of very highly forward-peaked scattering the solution of the Fokker-Planck (FP) equation has been found to be a good approximation to the analytic transport solution.[30,61,89] The first part of our accuracy question is to find the conditions under which discretizations of the transport equation yield "reasonable" discretizations of the Fokker-Planck equation. In these cases the two-part question of the accuracy of various transport discretizations is reduced to the presumably simpler second part, the question of the accuracy of the corresponding Fokker-Planck discretizations. Our study will not actually address this reduced problem.

This chapter examines the fully analytic transport equation and the spatially analytic discrete ordinates equations in the limit of forward-peaked scattering (the Fokker-Planck limit). We derive conditions under which the equations asymptotically yield solutions that satisfy a (discretized) Fokker-Planck equation.

II.A. Analytic Transport

In this section we briefly review Pomraning's asymptotic analysis[30] of the fully analytic transport equation in the Fokker-Planck limit, which we restrict to the monoenergetic case. The analytic transport equation in general geometry is:

$$\begin{aligned} &\boldsymbol{\Omega}\cdot\boldsymbol{\nabla}\psi\left(\mathbf{r},\boldsymbol{\Omega}\right)+\left(\sigma_a+\sigma_{s0}\right)\psi\left(\mathbf{r},\boldsymbol{\Omega}\right) \\ &=\sum_{n=0}^{\infty}\sum_{m=m_L}^{m_H}\left(\frac{2n+1}{c_{norm}}\right)Y_{nm}\left(\boldsymbol{\Omega}\right)\varphi_{nm}\left(\mathbf{r}\right)\sigma_{sn}\left(\mathbf{r}\right)+q\left(\mathbf{r},\boldsymbol{\Omega}\right), \end{aligned} \tag{1}$$

where

$$\sigma_{sn}=\int_{-1}^{1}d\mu_0 P_n\left(\mu_0\right)\sigma_s\left(\mu_0\right), \qquad \varphi_{nm}\left(\mathbf{r}\right)=\int_{4\pi}d\boldsymbol{\Omega}' Y_{nm}^{*}\left(\boldsymbol{\Omega}'\right)\psi\left(\mathbf{r},\boldsymbol{\Omega}'\right), \tag{2}$$

and where $\sigma_s\left(\mu_0\right)$ is the cross section for scattering through an angle whose cosine is μ_0. The parameter c_{norm} is a normalization factor that depends on n, m, and the normalization chosen for the definition of $Y_{nm}\left(\boldsymbol{\Omega}\right)$, and the parameters m_L and m_H depend on the geometry. For Cartesian geometries m_L and m_H are given by

$$\left(m_L,m_H\right)=\begin{cases}\left(0,0\right), & 1D\\ \left(0,n\right), & 2D\\ \left(-n,n\right), & 3D\end{cases}. \tag{3}$$

Following Pomraning,[30] we make the following definitions and scalings:

$$\delta = 1 - \langle \overline{\mu_0} \rangle = \frac{\langle \sigma_{s0} \rangle - \langle \sigma_{s1} \rangle}{\langle \sigma_{s0} \rangle}, \tag{4a}$$

$$\gamma = \left\langle \overline{(1-\mu_0)^2} \right\rangle = \frac{4\langle \sigma_{s0} \rangle - 6\langle \sigma_{s1} \rangle + 2\langle \sigma_{s2} \rangle}{3\langle \sigma_{s0} \rangle}, \tag{4b}$$

$$A(\mathbf{r}) = \frac{1 - \overline{\mu_0}(\mathbf{r})}{\delta}, \qquad B(\mathbf{r}) = \frac{\overline{(1-\mu_0)^2}(\mathbf{r})}{\gamma}, \tag{4c}$$

$$y = \frac{1-\mu_0}{\delta}, \tag{4d}$$

$$\sigma_{sn}(\mathbf{r}) = \frac{\hat{\sigma}_{sn}(\mathbf{r})}{\delta}, \qquad \sigma_a(\mathbf{r}) = \hat{\sigma}_a(\mathbf{r}), \tag{4e}$$

$$\sigma_{tr}(\mathbf{r}) = \sigma_a(\mathbf{r}) + \sigma_{s0}(\mathbf{r})\left(1 - \overline{\mu_0}(\mathbf{r})\right) = \hat{\sigma}_a(\mathbf{r}) + \hat{\sigma}_{s0}(\mathbf{r}) A(\mathbf{r}), \tag{4f}$$

where $\overline{\mu_0}$ is the average scattering cosine, $\hat{\sigma}_{sn}$ and $\hat{\sigma}_a$ are $O(1)$, δ and γ are small, and $\langle \cdot \rangle$ indicates a typical value. We require that $A(\mathbf{r})$ and $B(\mathbf{r})$ be $O(1)$, i.e. that $1 - \overline{\mu_0}(\mathbf{r})$ and $\overline{(1-\mu_0)^2}(\mathbf{r})$ scale with δ and γ, respectively. The idea is to examine what happens to the solution as δ approaches zero. Physically, this corresponds to a diminishing distance between scatters but also a diminishing average scattering angle. These are balanced such that σ_{tr} is $O(1)$ and independent of δ.

We rewrite the integral for σ_{sn} in terms of y and expand $P_n(\mu_0)$ in a Taylor series about $\mu_0 = 1$:

$$\sigma_{sn}(\mathbf{r}) = \int_0^{2/\delta} dy \left\{ P_n(1) - P_n'(1)\, y\delta + O\left(y^2\delta^2\right) \right\} \hat{\sigma}_s(\mathbf{r}, y). \tag{5}$$

By making use of the following identities for P_n,

$$P_n(1) = 1, \qquad P_n'(1) = \frac{n(n+1)}{2}, \tag{6}$$

we can rewrite Eq. (5) as

$$\sigma_{sn}(\mathbf{r}) = \int_0^{2/\delta} dy \left\{ 1 - \frac{n(n+1)}{2} y\delta + O\left(y^2\delta^2\right) \right\} \hat{\sigma}_s(\mathbf{r}, y). \tag{7}$$

Rewriting Eq. (7) in terms of μ_0 and performing the integration yields the following asymptotic form for σ_{sn}:

$$\sigma_{sn}(\mathbf{r}) = \sigma_{s0}(\mathbf{r}) \left[1 - \frac{n(n+1)}{2} A(\mathbf{r}) \delta + O(\gamma) \right]. \tag{8}$$

Substitution of this expression into the transport equation leads (after some manipulation) to the following intermediate result:

$$\begin{aligned} & \mathbf{\Omega} \cdot \nabla \psi(\mathbf{r}, \mathbf{\Omega}) + \hat{\sigma}_a(\mathbf{r}) \psi(\mathbf{r}, \mathbf{\Omega}) \\ & + \frac{\hat{\sigma}_{s0}(\mathbf{r})}{\delta} \left\{ \psi(\mathbf{r}, \mathbf{\Omega}) - \sum_{n=0}^{\infty} \sum_{m=m_L}^{m_H} \left(\frac{2n+1}{c_{norm}} \right) Y_{nm}(\mathbf{\Omega}) \varphi_{nm}(\mathbf{r}) \right\} \\ = & - \frac{(\sigma_{tr}(\mathbf{r}) - \hat{\sigma}_a(\mathbf{r}))}{2} \sum_{n=0}^{\infty} \sum_{m=m_L}^{m_H} \left(\frac{2n+1}{c_{norm}} \right) n(n+1) Y_{nm}(\mathbf{\Omega}) \varphi_{nm}(\mathbf{r}) \\ & + q(\mathbf{r}, \mathbf{\Omega}) + O\left(\frac{\gamma}{\delta}\right). \end{aligned} \tag{9}$$

Equation (9) is an equivalent form for the transport equation that is obtained when the scattering cross section is asymptotically made forward-peaked. When the preceding analysis was previously reported by Pomraning,[30] he obtained the Fokker-Planck equation by noting

that the term in braces in Eq. (9) is identically zero. In order to illuminate the discrete analyses in subsequent sections, however, we wish to proceed by a slightly more formal route. Our goal is to discern how the transport solution, $\psi(\mathbf{r}, \mathbf{\Omega})$, behaves in the limit as δ tends to zero. Therefore we propose the asymptotic ansatz:

$$\psi = \psi^{(0)} + \delta\psi^{(1)} + \delta^2\psi^{(2)} + \cdots, \tag{10a}$$

$$\varphi_{nm} = \varphi_{nm}^{(0)} + \delta\varphi_{nm}^{(1)} + \delta^2\varphi_{nm}^{(2)} + \cdots, \tag{10b}$$

where we will be primarily interested in the leading-order term. We insert this ansatz into Eq. (2) and consider terms of $O(1)$ to find:

$$\varphi_{nm}^{(0)}(\mathbf{r}) = \int_{4\pi} d\mathbf{\Omega}' Y_{nm}^{*}(\mathbf{\Omega}')\,\psi^{(0)}(\mathbf{r}, \mathbf{\Omega}') \equiv \left(D\psi^{(0)}\right)_{nm}. \tag{11}$$

We insert the ansatz into Eq. (9) and consider terms of $O\left(\delta^{-1}\right)$ to find:

$$\psi^{(0)}(\mathbf{r}, \mathbf{\Omega}) = \sum_{n=0}^{\infty} \sum_{m=m_L}^{m_H} \left(\frac{2n+1}{c_{norm}}\right) Y_{nm}(\mathbf{\Omega})\,\varphi_{nm}^{(0)}(\mathbf{r}) \equiv \left(M\varphi^{(0)}\right)_{\mathbf{\Omega}}. \tag{12}$$

We have not included an $O(\gamma)$ term in Eq. (12), since it is easily shown that $\gamma \rightarrow 0$ as $\delta \rightarrow 0$, i.e. that there are no $O(1)$ components in γ. Equations (11) and (12) define the transformation from $\varphi^{(0)}$ to $\psi^{(0)}$ and its inverse. While Eqs. (11) and (12) are rather obvious in the problem we are now analyzing, we will see later that their discretized counterparts play key roles in the behavior of discrete solutions. In particular, we will find that for some discretizations the D and M operators are not inverses, and hence the discrete versions of the two equations might not both be satisfied (we will note exceptions later). Thus, in such cases we will have a contradiction, implying that the asymptotic ansatz is not valid.

The $O(\delta)$ terms in Eq. (2) yield

$$\varphi_{nm}^{(1)}(\mathbf{r}) = \int_{4\pi} d\mathbf{\Omega}' Y_{nm}^{*}(\mathbf{\Omega}')\,\psi^{(1)}(\mathbf{r},\mathbf{\Omega}') = \left(D\psi^{(1)}\right)_{nm}. \tag{13}$$

The $O(1)$ terms in Eq. (9) yield

$$\begin{aligned}
&\mathbf{\Omega}\cdot\boldsymbol{\nabla}\psi^{(0)}(\mathbf{r},\mathbf{\Omega}) + \hat{\sigma}_a(\mathbf{r})\,\psi^{(0)}(\mathbf{r},\mathbf{\Omega}) \\
&+\hat{\sigma}_{s0}(\mathbf{r})\left\{\psi^{(1)}(\mathbf{r},\mathbf{\Omega}) - \sum_{n=0}^{\infty}\sum_{m=m_L}^{m_H}\left(\frac{2n+1}{c_{norm}}\right)Y_{nm}(\mathbf{\Omega})\,\varphi_{nm}^{(1)}(\mathbf{r})\right\} \\
= &-\frac{(\sigma_{tr}(\mathbf{r}) - \hat{\sigma}_a(\mathbf{r}))}{2}\sum_{n=0}^{\infty}\sum_{m=m_L}^{m_H}\left(\frac{2n+1}{c_{norm}}\right)n(n+1)\,Y_{nm}(\mathbf{\Omega})\,\varphi_{nm}^{(0)}(\mathbf{r}) \\
&+q(\mathbf{r},\mathbf{\Omega}) + O\left(\frac{\gamma}{\delta}\right).
\end{aligned} \tag{14}$$

We have included the $O(\gamma/\delta)$ term in Eq. (14) as if it were $O(1)$; this is not necessarily true and will be discussed momentarily. Note that we have not directly obtained an expression for $\psi^{(1)}$ and $\varphi^{(1)}$ that is analogous to Eq. (12). However, Eq. (13) and the fact that $M = D^{-1}$ require such an expression for consistency. Therefore the term in braces in Eq. (14) disappears.

Now we can use the identity:

$$\left[\frac{\partial}{\partial\mu}\left(1-\mu^2\right)\frac{\partial}{\partial\mu} + \left(\frac{1}{1-\mu^2}\right)\frac{\partial^2}{\partial\phi^2} + n(n+1)\right]Y_{nm}(\mathbf{\Omega}) = 0 \tag{15}$$

to rewrite the summation on the right hand side of Eq. (14), thereby obtaining a Fokker-Planck equation with an extra $O(\gamma/\delta)$ term:

$$\begin{aligned}
&\boldsymbol{\Omega}\cdot\boldsymbol{\nabla}\psi^{(0)}(\mathbf{r},\boldsymbol{\Omega})+\hat{\sigma}_a(\mathbf{r})\,\psi^{(0)}(\mathbf{r},\boldsymbol{\Omega})\\
&=\frac{\sigma_{tr}(\mathbf{r})-\hat{\sigma}_a(\mathbf{r})}{2}\left[\frac{\partial}{\partial\mu}\left(1-\mu^2\right)\frac{\partial}{\partial\mu}+\left(\frac{1}{1-\mu^2}\right)\frac{\partial^2}{\partial\phi^2}\right]\psi^{(0)}(\mathbf{r},\boldsymbol{\Omega})\\
&+q(\mathbf{r},\boldsymbol{\Omega})+O\left(\frac{\gamma}{\delta}\right).
\end{aligned}\tag{16}$$

The $O(\gamma/\delta)$ term in Eq. (16) is significant. It is a function only of the scattering kernel. The FP equation is not an asymptotic limit of the transport equation unless the scattering kernel is such that $\gamma \rightarrow 0$ more rapidly than $\delta \rightarrow 0$, i.e., such that

$$\left\langle\overline{(1-\mu_0)^2}\right\rangle\Big/\langle(1-\bar{\mu}_0)\rangle\rightarrow 0\tag{17}$$

as $\bar{\mu}_0 \rightarrow 1$. The Henyey-Greenstein kernel,[13] for example, does not have this limit. For more discussion see references 30 and 61.

II.B. Discrete Ordinates

We now turn our attention to the discrete-ordinates discretization of the transport equation. The standard discrete-ordinates version of the transport equation (1) is (with the asymptotic form of σ_{sn} inserted):

$$\begin{aligned}
&\boldsymbol{\Omega}_k\cdot\boldsymbol{\nabla}\psi_k(\mathbf{r})+(\sigma_a+\sigma_{s0})\,\psi_k(\mathbf{r})\\
&=\sum_{n=0}^{N-1}\sum_{m=m_L}^{m_H}\left(\frac{2n+1}{c_{norm}}\right)Y_{nm}(\boldsymbol{\Omega}_k)\,\tilde{\varphi}_{nm}(\mathbf{r})\,\frac{\hat{\sigma}_{s0}(\mathbf{r})}{\delta}\left[1-\frac{n(n+1)}{2}A(\mathbf{r})\,\delta+O(\gamma)\right]\\
&+q(\mathbf{r},\boldsymbol{\Omega}_k),
\end{aligned}\tag{18}$$

where

$$\tilde{\varphi}_{nm}(\mathbf{r}) \equiv \sum_{k=1}^{K} w_k Y_{nm}^{*}(\mathbf{\Omega}_k)\,\psi_k(\mathbf{r}). \tag{19}$$

Here the w_k and $\mathbf{\Omega}_k$ are the quadrature weights and angles, respectively, of a quadrature of order N. In standard quadratures $K = N$ in $1D$, $K = N(N+2)/2$ in $2D$, and $K = N(N+2)$ in $3D$. Note that the scattering order in Eq. (18) is truncated at $N-1$. Manipulation of Eq. (18) yields the discretized (in angle) version of Eq. (9):

$$\begin{aligned}
&\mathbf{\Omega}_k \cdot \nabla\psi_k(\mathbf{r}) + \hat{\sigma}_a(\mathbf{r})\,\psi_k(\mathbf{r}) \\
&+\frac{\hat{\sigma}_{s0}(\mathbf{r})}{\delta}\left\{\psi_k(\mathbf{r}) - \sum_{n=0}^{N-1}\sum_{m=m_L}^{m_H}\left(\frac{2n+1}{c_{norm}}\right) Y_{nm}(\mathbf{\Omega}_k)\,\tilde{\varphi}_{nm}(\mathbf{r})\right\} \\
= &-\frac{(\sigma_{tr}(\mathbf{r}) - \hat{\sigma}_a(\mathbf{r}))}{2}\sum_{n=0}^{N-1}\sum_{m=m_L}^{m_H}\left(\frac{2n+1}{c_{norm}}\right) n(n+1)\,Y_{nm}(\mathbf{\Omega}_k)\,\tilde{\varphi}_{nm}(\mathbf{r}) \\
&+q(\mathbf{r},\mathbf{\Omega}_k) + O\left(\frac{\gamma}{\delta}\right).
\end{aligned} \tag{20}$$

We insert the asymptotic ansatz of Eqs. (10) into Eq. (19) and consider terms of $O(1)$ to find:

$$\tilde{\varphi}_{nm}^{(0)}(\mathbf{r}) = \sum_{k=1}^{K} w_k Y_{nm}^{*}(\mathbf{\Omega}_k)\,\psi_k^{(0)}(\mathbf{r}) \equiv \left(D_N\psi^{(0)}\right)_{nm}. \tag{21}$$

We insert the ansatz into Eq. (20) and consider terms of $O\left(\delta^{-1}\right)$ to find:

$$\psi_k^{(0)}(\mathbf{r}) = \sum_{n=0}^{N-1}\sum_{m=m_L}^{m_H}\left(\frac{2n+1}{c_{norm}}\right) Y_{nm}(\mathbf{\Omega}_k)\,\tilde{\varphi}_{nm}^{(0)}(\mathbf{r}) \equiv \left(M_N\tilde{\varphi}^{(0)}\right)_k, \tag{22}$$

where there is no $O(\gamma)$ term for the reasons discussed in the previous section. Equations (21) and (22) are always satisfied if D_N and M_N are inverses of each other. Unlike in analytic

transport, however, this may not be true. In one-dimensional slab and spherical geometry it will be true only if the quadrature set exactly integrates polynomials of degree $2N-1$, as is the case with the Gauss-Legendre (GL) set. In standard multidimensional quadrature sets D_N and M_N are generally not one-to-one and onto operators, in which case they cannot be inverses of each other. If D_N and M_N are not inverses of each other, then Eqs. (21) and (22) may not be consistent (with possible exceptions discussed below); if they are inconsistent then the asymptotic ansatz of Eqs. (10) is not valid. In such a case there is no $O(1)$ solution to Eqs. (18) and (19).

Assuming that $D_N = M_N^{-1}$, and thus that Eqs. (21) and (22) are consistent, then the $O(\delta)$ terms in Eq. (19) yield:

$$\tilde{\varphi}_{nm}^{(1)}(\mathbf{r}) = \sum_{k=1}^{K} w_k Y_{nm}^{*}(\mathbf{\Omega}_k)\,\psi_k^{(1)}(\mathbf{r}) = \left(D_N \psi^{(1)}\right)_{nm}. \tag{23}$$

The $O(1)$ terms in Eq. (20) yield:

$$\begin{aligned}
&\mathbf{\Omega}_k \cdot \nabla \psi_k^{(0)}(\mathbf{r}) + \hat{\sigma}_a(\mathbf{r})\,\psi_k^{(0)}(\mathbf{r}) \\
&+\hat{\sigma}_{s0}(\mathbf{r})\left\{\psi_k^{(1)}(\mathbf{r}) - \sum_{n=0}^{N-1}\sum_{m=m_L}^{m_H}\left(\frac{2n+1}{c_{norm}}\right) Y_{nm}(\mathbf{\Omega}_k)\,\tilde{\varphi}_{nm}^{(1)}(\mathbf{r})\right\} \\
= \; &-\frac{(\sigma_{tr}(\mathbf{r}) - \hat{\sigma}_a(\mathbf{r}))}{2}\sum_{n=0}^{N-1}\sum_{m=m_L}^{m_H}\left(\frac{2n+1}{c_{norm}}\right) n(n+1)\, Y_{nm}(\mathbf{\Omega}_k)\,\tilde{\varphi}_{nm}^{(0)}(\mathbf{r}) \\
&+q(\mathbf{r},\mathbf{\Omega}_k) + O\left(\frac{\gamma}{\delta}\right).
\end{aligned} \tag{24}$$

The scattering term on the left side of Eq. (24) will disappear only if

$$\psi_k^{*(1)}(\mathbf{r}) = \psi_k^{(1)}(\mathbf{r}), \tag{25}$$

where

$$\psi_k^{*(1)}(\mathbf{r}) \equiv \sum_{n=0}^{N-1} \sum_{m=m_L}^{m_H} \left(\frac{2n+1}{c_{norm}}\right) Y_{nm}(\mathbf{\Omega}_k)\, \tilde{\varphi}_{nm}^{(1)}(\mathbf{r}). \tag{26}$$

This is already satisfied by the (assumed) condition $D_N = M_N^{-1}$. Equations (15) and (24) thus yield:

$$\begin{aligned} & \mathbf{\Omega}_k \cdot \nabla \psi_k^{(0)}(\mathbf{r}) + \hat{\sigma}_a(\mathbf{r})\, \psi_k^{(0)}(\mathbf{r}) \\ = \; & \frac{\sigma_{tr}(\mathbf{r}) - \hat{\sigma}_a(\mathbf{r})}{2} \left\{ \left[\frac{\partial}{\partial \mu}(1-\mu^2) \frac{\partial}{\partial \mu} + \left(\frac{1}{1-\mu^2}\right) \frac{\partial^2}{\partial \phi^2} \right] \tilde{\psi}^{(0)}(\mathbf{r}, \mathbf{\Omega}) \right\}_{\mathbf{\Omega}=\mathbf{\Omega}_k} \\ & + q(\mathbf{r}, \mathbf{\Omega}_k) + O\left(\frac{\gamma}{\delta}\right). \end{aligned} \tag{27}$$

where we define $\tilde{\psi}^{(0)}(\mathbf{r}, \mathbf{\Omega})$ to be the $(N-1)$-order polynomial interpolant through the points $\left\{\mathbf{\Omega}_k, \tilde{\psi}^{(0)}(\mathbf{r}, \mathbf{\Omega}_k)\right\}$ in one-dimensional slab and spherical geometry (the definition in multidimensional geometry will be described below). Thus, assuming that $O(\gamma/\delta) \rightarrow 0$ as $\delta \rightarrow 0$, Eq. (27) is a "pseudospectral" discretization[90] of the angular variable in the exact FP equation. (Pseudospectral methods use collocation to determine coefficients in a global function expansion.)

The above discussion indicates that the transformation from discrete values to angular moments and back to discrete values should be the identity. If Eqs. (19) and (26) define the discrete-to-moments and moments-to-discrete transformations, then we will not have the identity unless the quadrature set is Gauss-Legendre in one-dimensional slab or spherical geometry. Given a different quadrature set and/or multidimensional geometry, then, the S_N method may not limit to a discretization of the FP equation unless Eq. (19) and/or (26) is replaced.

Morel[91] reached the same conclusion via a completely different analysis, and offered suggestions for replacing the offending equation(s). The simplest suggestion in one-dimensional slab and spherical geometry is to use for $\tilde{\varphi}_{n0}$ the *exact* moments of the $(N-1)$-order polynomial, $\tilde{\psi}$, that goes through the points $\left\{\mathbf{\Omega}_k, \tilde{\psi}\left(\mathbf{r}, \mathbf{\Omega}_k\right)\right\}$; i.e. to solve Eq. (2) exactly instead of using Eq. (19), thereby redefining D_N. Morel labeled this "Galerkin" quadrature, since he derived it by means of a Galerkin weighting method. The use of the exact moments causes Eq. (25) to be satisfied regardless of quadrature set, and Eq. (27) then follows.

In multidimensional geometries the Galerkin quadrature has a more complex definition. Recall that D_N and M_N are not one-to-one and onto in standard multi-dimensional quadrature sets. For example, level symmetric quadrature sets of order N have $N\left(N+2\right)/2$ and $N\left(N+2\right)$ quadrature points in two and three dimensions, respectively, whereas there are $N\left(N+1\right)/2$ and N^2 spherical harmonics of order $N-1$ or less in the respective dimensions.[92] In order to satisfy Eq. (25) in all circumstances we must first increase the number of spherical harmonics in our flux expansion by using harmonics of higher orders. Morel[91] and Reed[93] proposed suitable spherical harmonic interpolation spaces for multidimensional geometries. For two-dimensional geometries the following interpolation space is suggested:

$$\left\{ Y_{nm} : \begin{array}{ll} 0 \leq m \leq n, & if\ 0 \leq n \leq N-1 \\ 0 < m\ odd \leq N, & if\ n = N \end{array} \right\}. \tag{28}$$

The interpolation space suggested for three dimensions is:

$$\left\{ Y_{nm} : \begin{array}{cc} -n \le m \le n, & if\ 0 \le n \le N-1, \\ \left.\begin{array}{c} -n \le m < 0 \\ and\ 0 < m\ odd \le N \end{array}\right), & if\ n = N \\ -(N+1) \le m\ even < 0, & if\ n = N+1 \end{array} \right\}. \tag{29}$$

The Galerkin quadrature is then defined by adjusting the limits of the summations in Eq. (26) in order to augment M_N and then redefining $D_N \equiv M_N^{-1}$. As in the one-dimensional case Eq. (25) will be satisfied regardless of the discrete angle set when the Galerkin treatment is used, and Eq. (27) then follows, where $\tilde{\psi}^{(0)}(\mathbf{r}, \mathbf{\Omega})$ is now defined as the spherical harmonic interpolant (corresponding to the selected interpolation space) through the points $\left\{ \mathbf{\Omega}_k, \tilde{\psi}^{(0)}(\mathbf{r}, \mathbf{\Omega}_k) \right\}$.

We note that the use of the Galerkin quadrature allows the selection of a greater variety of discrete angle sets in Eq. (18) since the corresponding quadrature weights (if they are defined) are not actually used. For example, in problems involving normally incident beams one can specify better boundary conditions with the Lobatto quadrature set, since this set includes the point $\mu = 1$. In these same problems one can define sets that are highly biased toward particular directions. Furthermore, it may be possible to implement adaptive quadratures more easily.

More can be said about the effects of using a non-Gaussian or non-Galerkin quadrature to evaluate Eq. (19). Let us define the scattering ratio matrix $\mathbf{C}$ by

$$\mathbf{C} = \frac{1}{\sigma_t}\mathbf{D}\mathbf{M}\mathbf{\Sigma}, \quad \sigma_t = \sigma_a + \sigma_{s0}, \tag{30}$$

where $\mathbf{D}$ is the discrete-to-moments matrix, $\mathbf{M}$ is the moments-to-discrete matrix, and $\mathbf{\Sigma}$ is a diagonal matrix whose entries are the scattering coefficients $\{\sigma_{sn}\}$ in the order and frequency corresponding to their respective moments in the other matrices. If exact integrals are used then $\mathbf{D} = \mathbf{M}^{-1}$, and $\mathbf{C}$ will be a diagonal matrix whose entries are the scattering ratios $\{\sigma_{sn}/\sigma_t\}$. In a non-multiplying medium each diagonal term (and hence each eigenvalue of $\mathbf{C}$) will be non-negative and will not exceed unity. If, however, inexact integrations are used, not only will $\mathbf{C}$ differ from $\mathbf{\Sigma}/\sigma_t$, but there is also the possibility of introducing one or more eigenvalues whose absolute values exceed unity. This is physically equivalent to artificially introducing multiplication into the medium. Depending on the amount of leakage present, Eqs. (18) and (19) then may not have a steady-state solution, certainly not in the limit as $\delta \rightarrow 0$. This inconsistency is clearly unacceptable when a steady state solution is known to exist.

We remark that the condition $D = M^{-1}$ is certainly sufficient for obtaining the correct FP limit, but it is not strictly necessary. We need only to satisfy the condition that $(I - MD)\,\tilde{\Psi} = 0$ in order to satisfy Eqs. (21), (22), and (25), i.e. that $\tilde{\Psi}$ be in the null space of $I - MD$. If $MD \neq I$, then certain angular eigenmodes cannot be present in a stable solution. It is entirely possible that the proper selection of boundary conditions and sources could result in a solution that does not contain any of the unstable modes. Alternatively, one could filter out the unstable mode components of the scattering source; this would stabilize the solution, but this will yield a different solution than that obtained when exact integrations are used. Our recommendation is to avoid these complications altogether by simply using the exact inverse of M.

In summary, the discrete ordinates discretization of the transport equation (1) yields a pseudospectral discretization of the Fokker-Planck equation under the scaling defined in the previous section, provided that the Fokker-Planck equation is the asymptotic limit in the analytic case and that the scattering source is calculated carefully (in a nonstandard way, in general). The "nonstandard" scattering source may be obtained by means of the Gauss-Legendre quadrature set, by forming the interpolant of the angular flux and calculating its exact moments, or perhaps by a number of other ways. A different, albeit stable, solution may be obtained by suppressing the unstable eigenmodes of the scattering source (which would limit to a discrete FP solution with a reduced angular function space), but we do not recommend this alternative when inherently stable and less drastic approaches exist.

CHAPTER III

FOKKER-PLANCK ANALYSIS OF THE SPATIALLY DISCRETIZED DISCRETE ORDINATES EQUATIONS

In the previous chapter we analyzed the asymptotic behavior of the spatially analytic transport and discrete ordinates equations in the Fokker-Planck limit. In this chapter we extend our asymptotic analysis to include spatial discretizations. We will study the diamond difference (DD), the linear discontinuous (LD) and the linear moments (LM) methods[39,40] as examples of spatial discretizations of the transport equation in one-dimensional slab geometry. In two-dimensional Cartesian geometry we will examine several related finite element methods on rectangles: the bilinear discontinuous (BLD), the lumped bilinear discontinuous (LBLD) and the simple corner balance (SCB) methods.[71,72,94] For the methods analyzed we find that if a reasonable Fokker-Planck limit is obtained in the spatially analytic case, then a reasonable limit is also obtained in the spatially discrete case.

III.A. Slab Geometry

III.A.1. Diamond Difference

We begin with the DD-S_N discretization of Eq. (1), with the asymptotic cross sections from Eq. (8):

$$\frac{\mu_k}{\Delta x_i}\left(\psi_{k,i+\frac{1}{2}}-\psi_{k,i-\frac{1}{2}}\right)+\left(\hat{\sigma}_{ai}+\frac{\hat{\sigma}_{s0i}}{\delta}\right)\psi_{ki}$$

$$=\sum_{n=0}^{N-1}M_{N,kn}\tilde{\varphi}_{ni}\frac{\hat{\sigma}_{s0i}}{\delta}\left[1-\frac{n\left(n+1\right)}{2}A_i\delta+O\left(\gamma\right)\right]+q_i\left(\mu_k\right), \quad (31a)$$

$$\psi_{ki} = \frac{1}{2}\left(\psi_{k,i+\frac{1}{2}} + \psi_{k,i-\frac{1}{2}}\right), \tag{31b}$$

$$\begin{pmatrix} \psi_{k,\frac{1}{2}} \\ \psi_{k,I+\frac{1}{2}} \end{pmatrix} = \begin{pmatrix} \psi_{k,inc}\left(x_{\frac{1}{2}}\right), & \mu_k > 0 \\ \psi_{k,inc}\left(x_{I+\frac{1}{2}}\right), & \mu_k < 0 \end{pmatrix}, \tag{31c}$$

$$\tilde{\varphi}_{ni} = \sum_{k=1}^{N} D_{N,nk}\psi_{ki}, \tag{31d}$$

where f_i is the cell-average value of f:

$$f_i = \frac{1}{\Delta x_i}\int_{x_{i-\frac{1}{2}}}^{x_{i+\frac{1}{2}}} dx f(x). \tag{32}$$

We remark that the spatial mesh stays fixed in our analysis, which means as $\delta \to 0$, $\sigma_{s0i}\Delta x_i$ increases and $\sigma_{tr,i}\Delta x_i$ does not change.

We insert the asymptotic ansatz of Eqs. (10) into Eqs. (31) and consider the terms of $O(1)$ in Eq. (31d) to find:

$$\tilde{\varphi}_{ni}^{(0)} = \sum_{k=1}^{N} D_{N,nk}\psi_{ki}^{(0)}. \tag{33}$$

We consider terms of $O\left(\delta^{-1}\right)$ in Eq. (31a) to find:

$$\psi_{ki}^{(0)} = \sum_{n=0}^{N-1} M_{N,kn}\tilde{\varphi}_{ni}^{(0)}. \tag{34}$$

As we have already discussed in the previous chapter, if $D_N \neq M_N^{-1}$ then Eqs. (33) and (34) may be inconsistent, in which case there is no $O(1)$ solution to Eqs. (31).

Assuming that $D_N = M_N^{-1}$, then the $O(\delta)$ terms in Eq. (31d) yield:

$$\tilde{\varphi}_{ni}^{(1)} = \sum_{k=1}^{N} D_{N,nk} \psi_{ki}^{(1)}. \tag{35}$$

The $O(1)$ terms in the remaining Eqs. (31) yield:

$$\mu_k \left(\frac{\psi_{k,i+\frac{1}{2}}^{(0)} - \psi_{k,i-\frac{1}{2}}^{(0)}}{\Delta x_i} \right) + \hat{\sigma}_{ai} \psi_{ki}^{(0)} + \hat{\sigma}_{s0i} \left\{ \psi_{ki}^{(1)} - \sum_{n=0}^{N-1} M_{N,kn} \tilde{\varphi}_{ni}^{(1)} \right\}$$

$$= \frac{-\left(\sigma_{tr,i} - \hat{\sigma}_{ai}\right)}{2} \sum_{n=0}^{N-1} M_{N,kn} n(n+1) \tilde{\varphi}_{ni}^{(0)} + q_i(\mu_k) + O\left(\frac{\gamma}{\delta}\right), \tag{36a}$$

$$\psi_{k,i+\frac{1}{2}}^{(0)} = \begin{cases} \psi_{k,inc}\left(x_{\frac{1}{2}}\right), & \mu_k > 0, \quad i = 0 \\ \psi_{k,inc}\left(x_{I+\frac{1}{2}}\right), & \mu_k < 0, \quad i = I \\ 2\psi_{ki}^{(0)} - \psi_{k,i-\frac{1}{2}}^{(0)}, & \mu_k > 0, \quad i > 0 \\ 2\psi_{k,i+1}^{(0)} - \psi_{k,i+\frac{3}{2}}^{(0)}, & \mu_k < 0, \quad i < I \end{cases}. \tag{36b}$$

The term in braces in Eq. (36a) disappears because we have assumed that $D_N = M_N^{-1}$. Equations (15) and (36a) thus yield:

$$\mu_k \left[\frac{\psi_{k,i+\frac{1}{2}}^{(0)} - \psi_{k,i-\frac{1}{2}}^{(0)}}{\Delta x_i} \right] + \hat{\sigma}_{ai} \psi_{ki}^{(0)}$$

$$= \frac{\left(\sigma_{tr,i} - \hat{\sigma}_{ai}\right)}{2} \left[\frac{\partial}{\partial \mu} \left(1 - \mu^2\right) \frac{\partial}{\partial \mu} \tilde{\psi}_i^{(0)} \right]_{\mu = \mu_k} + q_i(\mu_k), \tag{37}$$

assuming that $\gamma/\delta \to 0$ as $\delta \to 0$. The boundary conditions are given by the leading order terms in Eq. (31c):

$$\begin{pmatrix} \psi_{k,\frac{1}{2}}^{(0)} \\ \psi_{k,I+\frac{1}{2}}^{(0)} \end{pmatrix} = \begin{pmatrix} \psi_{k,inc}\left(x_{\frac{1}{2}}\right), & \mu_k > 0 \\ \psi_{k,inc}\left(x_{I+\frac{1}{2}}\right), & \mu_k < 0 \end{pmatrix}. \tag{38}$$

Thus, given that $D_N = M_N^{-1}$ and that γ has no $O(\delta)$ components, the leading-order DD-S_N solution satisfies a DD-pseudospectral discretization of the FP equation. (It is no surprise that these conditions are required, since they were required even without spatial discretization.) The asymptotic boundary conditions are identical to the ones specified for the unscaled problem.

III.A.2. Linear Discontinuous

The scaled LD-S_N discretization of Eq. (1) consists of Eqs. (31a), (31d), and the following:

$$\frac{3\mu_k}{\Delta x_i}\left(\psi_{k,i+\frac{1}{2}} + \psi_{k,i-\frac{1}{2}} - 2\psi_{ki}\right) + \left(\hat{\sigma}_{ai} + \frac{\hat{\sigma}_{s0i}}{\delta}\right)\psi^x_{ki}$$

$$= \sum_{n=0}^{N-1} M_{N,kn}\tilde{\varphi}^x_{ni}\frac{\hat{\sigma}_{s0i}}{\delta}\left[1 - \frac{n(n+1)}{2}A_i\delta + O(\gamma)\right] + q^x_i(\mu_k), \qquad (39a)$$

$$\psi_{k,i+\frac{1}{2}} = \begin{cases} \psi_{k,inc}\left(x_{\frac{1}{2}}\right), & \mu_k > 0, \quad i = 0 \\ \psi_{k,inc}\left(x_{I+\frac{1}{2}}\right), & \mu_k < 0, \quad i = I \\ \psi_{ki} + \psi^x_{ki}, & \mu_k > 0, \quad i \geq 1 \\ \psi_{k,i+1} - \psi^x_{k,i+1}, & \mu_k < 0, \quad i < I \end{cases}, \qquad (39b)$$

$$\tilde{\varphi}^x_{ni} = \sum_{k=1}^{N} D_{N,nk}\psi^x_{ki}, \qquad (39c)$$

where f^x_i is the first spatial moment of f in a cell:

$$f^x_i = \frac{3}{\Delta x_i}\int_{x_{i-\frac{1}{2}}}^{x_{i+\frac{1}{2}}} dx\left[\frac{x - x_i}{\Delta x_i/2}\right] f(x) \qquad (40)$$

By means of the same asymptotic analysis as before we find that $D_N = M_N^{-1}$ is a sufficient condition for there to be an $O(1)$ solution. Given this condition, we obtain Eqs. (35), (36a) and the following:

$$\tilde{\varphi}_{ni}^{x(1)} = \sum_{k=1}^{N} D_{N,nk}\psi_{ki}^{x(1)}, \tag{41a}$$

$$3\mu_k\left[\frac{\psi_{k,i+\frac{1}{2}}^{(0)} + \psi_{k,i-\frac{1}{2}}^{(0)} - 2\psi_{ki}^{(0)}}{\Delta x_i}\right] + \hat{\sigma}_{ai}\psi_{ki}^{x(0)} + \hat{\sigma}_{s0i}\left\{\psi_{ki}^{x(1)} - \sum_{n=0}^{N-1} M_{N,kn}\tilde{\varphi}_{ni}^{x(1)}\right\}$$

$$= \frac{-\left(\sigma_{tr,i} - \hat{\sigma}_{ai}\right)}{2}\sum_{n=0}^{N-1} M_{N,kn}\tilde{\varphi}_{ni}^{x(0)} n(n+1) + q_i^x(\mu_k) + O\left(\frac{\gamma}{\delta}\right), \tag{41b}$$

$$\psi_{k,i+\frac{1}{2}}^{(0)} = \begin{cases} \psi_{k,inc}\left(x_{\frac{1}{2}}\right), & \mu_k > 0, \quad i = 0 \\ \psi_{k,inc}\left(x_{I+\frac{1}{2}}\right), & \mu_k < 0, \quad i = I \\ \psi_{ki}^{(0)} + \psi_{ki}^{x(0)}, & \mu_k > 0, \quad i \geq 1 \\ \psi_{k,i+1}^{(0)} - \psi_{k,i+1}^{x(0)}, & \mu_k < 0, \quad i < I \end{cases}. \tag{41c}$$

We obtain Eq. (37) and the following under the same conditions as in the DD analysis:

$$3\mu_k\left(\frac{\psi_{k,i+\frac{1}{2}}^{(0)} + \psi_{k,i-\frac{1}{2}}^{(0)} - 2\psi_{ki}^{(0)}}{\Delta x_i}\right) + \hat{\sigma}_{ai}\psi_{ki}^{x(0)}$$

$$= \frac{\left(\sigma_{tr,i} - \hat{\sigma}_{ai}\right)}{2}\left[\frac{\partial}{\partial\mu}\left(1-\mu^2\right)\frac{\partial}{\partial\mu}\tilde{\psi}_i^{x(0)}\right]_{\mu=\mu_k} + q_i^x(\mu_k). \tag{42}$$

The leading-order terms in Eq. (39b) yield the leading-order boundary conditions of Eq. (38). Therefore the leading-order LD-S_N solution satisfies an LD-pseudospectral discretization of the FP equation, given the previously stated constraints on the cross section and the quadrature; the asymptotic boundary conditions are equal to the ones in the unscaled problem.

III.A.3. Linear Moments

The scaled LM-S_N discretization of Eq. (1) consists of Eqs. (31a), (31d), (39a), (39c), and the following:

$$\begin{aligned}\psi_{k,exit,i} &= \psi_{k,inc,i}e^{-(\tau_{aki}+\tau_{ski}/\delta)} \\ &\quad +\alpha_{ki}\sum_{n=0}^{N-1} M_{N,kn}\frac{\hat{\sigma}_{s0i}}{\delta}\left[1-\frac{n(n+1)}{2}A_i\delta+O(\gamma)\right]\tilde{\varphi}_{ni} \\ &\quad \pm\beta_{ki}\sum_{n=0}^{N-1} M_{N,kn}\frac{\hat{\sigma}_{s0i}}{\delta}\left[1-\frac{n(n+1)}{2}A_i\delta+O(\gamma)\right]\tilde{\varphi}^x_{ni} \\ &\quad +\alpha_{ki}q_i(\mu_k) \pm \beta_{ki}q^x_i(\mu_k),\ \mu_k \gtrless 0, \end{aligned} \tag{43a}$$

$$\alpha_{ki} = \frac{\left[1-e^{-(\tau_{aki}+\tau_{ski}/\delta)}\right]}{\hat{\sigma}_{ai}+\hat{\sigma}_{s0i}/\delta}, \tag{43b}$$

$$\beta_{ki} = \frac{\left[1+e^{-(\tau_{aki}+\tau_{ski}/\delta)}-\frac{2}{\tau_{aki}+\tau_{ski}/\delta}\left[1-e^{-(\tau_{aki}+\tau_{ski}/\delta)}\right]\right]}{\hat{\sigma}_{ai}+\hat{\sigma}_{s0i}/\delta}, \tag{43c}$$

$$\begin{pmatrix}\psi_{k,inc,i}\\ \psi_{k,exit,i}\end{pmatrix} = \begin{pmatrix}\psi_{k,i\mp\frac{1}{2}}\\ \psi_{k,i\pm\frac{1}{2}}\end{pmatrix},\ \mu_k \gtrless 0, \tag{43d}$$

$$\begin{pmatrix}\psi_{k,\frac{1}{2}}\\ \psi_{k,I+\frac{1}{2}}\end{pmatrix} = \begin{pmatrix}\psi_{k,inc}\left(x_{\frac{1}{2}}\right), & \mu_k>0\\ \psi_{k,inc}\left(x_{I+\frac{1}{2}}\right), & \mu_k<0\end{pmatrix}, \tag{43e}$$

where $\tau_{aki}=\hat{\sigma}_{ai}\Delta x_i/|\mu_k|$ and $\tau_{ski}=\hat{\sigma}_{s0i}\Delta x_i/|\mu_k|$. The asymptotic analysis of Eqs. (31a), (31d), (39a), and (39c) that we performed previously yields Eqs. (35), (36a), (41a), and (41b), provided that $D_N = M_N^{-1}$. The asymptotic analysis of Eq. (43) is more complicated. We recognize that the exponential terms are of higher order than any power of δ; we also note that a denominator term such as $\hat{\sigma}_{ai}+\hat{\sigma}_{s0i}/\delta$ is $O\left(\delta^{-1}\right)$. Therefore the $O(1)$ terms in Eq.

(43a) yield

$$\psi^{(0)}_{k,exit,i} = \sum_{n=0}^{N-1} M_{N,kn} \left(\tilde{\varphi}^{(0)}_{ni} \pm \tilde{\varphi}^{x(0)}_{ni} \right) + O\left(\frac{\gamma}{\delta}\right), \ \mu_k \gtrless 0. \tag{44}$$

We may rewrite Eq. (44) with the help of Eq. (34) and the leading order term of Eq. (39c):

$$\psi^{(0)}_{k,exit,i} = \psi^{(0)}_{ki} \pm \psi^{x(0)}_{ki} + O\left(\frac{\gamma}{\delta}\right), \ \mu_k \gtrless 0. \tag{45}$$

Equation (41c) is obtained by combining Eq. (45) with the leading order terms of Eqs. (43d) and (43e). If γ has no $O(\delta)$ terms we obtain Eqs. (37) and (42). The leading-order boundary conditions are again given by Eq. (38). Therefore the leading-order LM-S_N solution is identical to the leading-order LD-S_N solution: it satisfies an LD-pseudospectral discretization of the FP equation. Once again, the constraints on the cross section and the quadrature apply.

There is a similarity between the results of the FP asymptotic analysis of the LM method and the results of diffusion limit analyses of characteristics methods (CMs),[78] of which the LM method is an example. The diffusion limit analyses show that in this limit the solution to a CM discretization satisfies a discontinuous finite element (DFEM) discretization of the diffusion equation. In particular, the LM solution limits to an LD-diffusion solution. In a similar fashion, our FP analysis shows that the LM solution limits to an LD-FP solution in the FP limit. Although we have not analyzed other CM discretizations in the FP limit it seems reasonable to expect that they too will produce solutions that satisfy some DFEM-FP discretization.

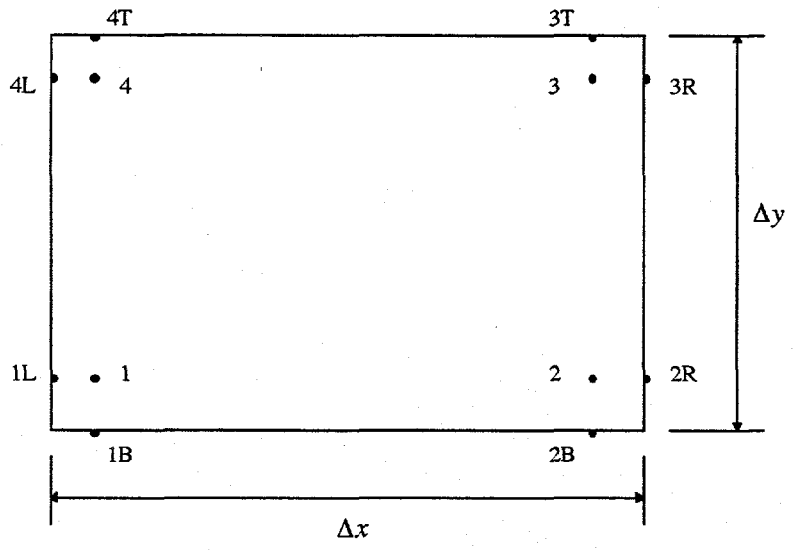

Fig. 1. Typical 2-D FEM element.

III.B. X-Y Geometry

We now will study some related discontinuous finite element (FEM) schemes in two-dimensional Cartesian geometry: the bilinear discontinuous (BLD), the lumped bilinear discontinuous (LBLD) and the simple corner balance (SCB) methods. Our study will be restricted to rectangular grids; a typical element is shown in Figure 1. Various points in the element are labeled. The numbers refer to the corner in which the point is located, and the letters refer to the side (L for left side, B for bottom, etc.). The points are the locations (real or conceptual) where unknown flux quantities are defined. The FEM discretizations are all defined by the following equations:

$$\frac{\mu_k}{\Delta x_i}\mathbf{U}\begin{bmatrix}\psi^L_{k,1,i,j}\\ \psi^R_{k,2,i,j}\\ \psi^R_{k,3,i,j}\\ \psi^L_{k,4,i,j}\end{bmatrix}+\frac{\eta_k}{\Delta y_j}\mathbf{N}\begin{bmatrix}\psi^B_{k,1,i,j}\\ \psi^B_{k,2,i,j}\\ \psi^T_{k,3,i,j}\\ \psi^T_{k,4,i,j}\end{bmatrix}$$

$$+\left(\frac{\mu_k}{\Delta x_i}\mathbf{K}+\frac{\eta_k}{\Delta y_j}\mathbf{L}+\left\{\hat{\sigma}_{a,ij}+\frac{\hat{\sigma}_{s0,ij}}{\delta}\right\}\mathbf{M}\right)\begin{bmatrix}\psi_{k,1,i,j}\\ \psi_{k,2,i,j}\\ \psi_{k,3,i,j}\\ \psi_{k,4,i,j}\end{bmatrix}$$

$$=\sum_{n,m}M_{N,k,nm}\frac{\hat{\sigma}_{s0,ij}}{\delta}\left(1-\frac{n\left(n+1\right)}{2}A_{ij}\delta+O\left(\gamma\right)\right)\mathbf{M}\begin{bmatrix}\tilde{\varphi}_{nm,1,i,j}\\ \tilde{\varphi}_{nm,2,i,j}\\ \tilde{\varphi}_{nm,3,i,j}\\ \tilde{\varphi}_{nm,4,i,j}\end{bmatrix}$$

$$+\mathbf{M}\begin{bmatrix}q_{1,i,j}\\ q_{2,i,j}\\ q_{3,i,j}\\ q_{4,i,j}\end{bmatrix}, \tag{46a}$$

$$\begin{bmatrix}\tilde{\varphi}_{nm,1,i,j}\\ \tilde{\varphi}_{nm,2,i,j}\\ \tilde{\varphi}_{nm,3,i,j}\\ \tilde{\varphi}_{nm,4,i,j}\end{bmatrix}=\sum_k D_{N,nm,k}\begin{bmatrix}\psi_{k,1,i,j}\\ \psi_{k,2,i,j}\\ \psi_{k,3,i,j}\\ \psi_{k,4,i,j}\end{bmatrix}, \tag{46b}$$

$$\psi^L_{k,1,i,j}=\begin{cases}f^L_{k,1,j}, & \mu_k>0,\quad i=1\\ \psi_{k,2,i-1,j}, & \mu_k>0,\quad 2\le i\le I,\quad 1\le j\le J\\ \psi_{k,1,i,j}, & \mu_k<0,\quad 1\le i\le I\end{cases}, \tag{46c}$$

$$\psi^L_{k,4,i,j}=\begin{cases}f^L_{k,4,j}, & \mu_k>0,\quad i=1\\ \psi_{k,3,i-1,j}, & \mu_k>0,\quad 2\le i\le I,\quad 1\le j\le J\\ \psi_{k,4,i,j}, & \mu_k<0,\quad 1\le i\le I\end{cases}, \tag{46d}$$

$$\psi^R_{k,2,i,j}=\begin{cases}\psi_{k,2,i,j}, & \mu_k>0,\quad 1\le i\le I\\ \psi_{k,1,i+1,j}, & \mu_k<0,\quad 1\le i\le I-1,\quad 1\le j\le J\\ f^R_{k,2,j}, & \mu_k<0,\quad i=I\end{cases}, \tag{46e}$$

$$\psi^R_{k,3,i,j} = \begin{cases} \psi_{k,3,i,j}, & \mu_k > 0, \quad 1 \le i \le I \\ \psi_{k,4,i+1,j}, & \mu_k < 0, \quad 1 \le i \le I-1, \quad 1 \le j \le J \\ f^R_{k,3,j}, & \mu_k < 0, \quad i = I \end{cases}, \tag{46f}$$

$$\psi^B_{k,1,i,j} = \begin{cases} f^B_{k,1,i}, & \eta_k > 0, \quad j = 1 \\ \psi_{k,4,i,j-1}, & \eta_k > 0, \quad 2 \le j \le J, \quad 1 \le i \le I \\ \psi_{k,1,i,j}, & \eta_k < 0, \quad 1 \le j \le J \end{cases}, \tag{46g}$$

$$\psi^B_{k,2,i,j} = \begin{cases} f^B_{k,2,i}, & \eta_k > 0, \quad j = 1 \\ \psi_{k,3,i,j-1}, & \eta_k > 0, \quad 2 \le j \le J, \quad 1 \le i \le I \\ \psi_{k,2,i,j}, & \eta_k < 0, \quad 1 \le j \le J \end{cases}, \tag{46h}$$

$$\psi^T_{k,3,i,j} = \begin{cases} \psi_{k,3,i,j}, & \eta_k > 0, \quad 1 \le j \le J \\ \psi_{k,2,i,j+1}, & \eta_k < 0, \quad 1 \le j \le J-1, \quad 1 \le i \le I \\ f^T_{k,3,i}, & \eta_k < 0, \quad j = J \end{cases}, \tag{46i}$$

$$\psi^T_{k,4,i,j} = \begin{cases} \psi_{k,4,i,j}, & \eta_k > 0, \quad 1 \le j \le J \\ \psi_{k,1,i,j+1}, & \eta_k < 0, \quad 1 \le j \le J-1, \quad 1 \le i \le I \\ f^T_{k,4,i}, & \eta_k < 0, \quad j = J \end{cases}, \tag{46j}$$

where f is the boundary incident flux, the limits on (n, m) are determined by the quadrature used, and the matrices **U**, **N**, **K**, **L**, and **M** are given by

$$\mathbf{U} = \begin{cases} \frac{1}{6}\begin{bmatrix} -2 & 0 & 0 & -1 \\ 0 & 2 & 1 & 0 \\ 0 & 1 & 2 & 0 \\ -1 & 0 & 0 & -2 \end{bmatrix}, & BLD, LBLD \\ \frac{1}{2}\begin{bmatrix} -1 & 0 & 0 & 0 \\ 0 & 1 & 0 & 0 \\ 0 & 0 & 1 & 0 \\ 0 & 0 & 0 & -1 \end{bmatrix}, & SCB \end{cases}, \tag{46k}$$

$$\mathbf{N} = \begin{cases} \frac{1}{6}\begin{bmatrix} -2 & -1 & 0 & 0 \\ -1 & -2 & 0 & 0 \\ 0 & 0 & 2 & 1 \\ 0 & 0 & 1 & 2 \end{bmatrix}, & BLD, LBLD \\ \frac{1}{2}\begin{bmatrix} -1 & 0 & 0 & 0 \\ 0 & -1 & 0 & 0 \\ 0 & 0 & 1 & 0 \\ 0 & 0 & 0 & 1 \end{bmatrix}, & SCB \end{cases}, \tag{46l}$$

$$\mathbf{K} = \begin{cases} \frac{1}{12}\begin{bmatrix} 2 & 2 & 1 & 1 \\ -2 & -2 & -1 & -1 \\ -1 & -1 & -2 & -2 \\ 1 & 1 & 2 & 2 \end{bmatrix}, & BLD, LBLD \\ \frac{1}{4}\begin{bmatrix} 1 & 1 & 0 & 0 \\ -1 & -1 & 0 & 0 \\ 0 & 0 & -1 & -1 \\ 0 & 0 & 1 & 1 \end{bmatrix}, & SCB \end{cases}, \tag{46m}$$

$$\mathbf{L} = \begin{cases} \frac{1}{12}\begin{bmatrix} 2 & 1 & 1 & 2 \\ 1 & 2 & 2 & 1 \\ -1 & -2 & -2 & -1 \\ -2 & -1 & -1 & -2 \end{bmatrix}, & BLD, LBLD \\ \frac{1}{4}\begin{bmatrix} 1 & 0 & 0 & 1 \\ 0 & 1 & 1 & 0 \\ 0 & -1 & -1 & 0 \\ -1 & 0 & 0 & -1 \end{bmatrix}, & SCB \end{cases}, \tag{46n}$$

$$\mathbf{M} = \begin{cases} \frac{1}{36}\begin{bmatrix} 4 & 2 & 1 & 2 \\ 2 & 4 & 2 & 1 \\ 1 & 2 & 4 & 2 \\ 2 & 1 & 2 & 4 \end{bmatrix}, & BLD \\ \frac{1}{4}\begin{bmatrix} 1 & 0 & 0 & 0 \\ 0 & 1 & 0 & 0 \\ 0 & 0 & 1 & 0 \\ 0 & 0 & 0 & 1 \end{bmatrix}, & LBLD, SCB \end{cases}. \tag{46o}$$

We insert the asymptotic ansatz of Eq. (10) into Eq. (46) and consider terms of $O(1)$ in Eq. (46b) to find:

$$\begin{bmatrix} \tilde{\varphi}^{(0)}_{nm,1,i,j} \\ \tilde{\varphi}^{(0)}_{nm,2,i,j} \\ \tilde{\varphi}^{(0)}_{nm,3,i,j} \\ \tilde{\varphi}^{(0)}_{nm,4,i,j} \end{bmatrix} = \sum_k D_{N,nm,k} \begin{bmatrix} \psi^{(0)}_{k,1,i,j} \\ \psi^{(0)}_{k,2,i,j} \\ \psi^{(0)}_{k,3,i,j} \\ \psi^{(0)}_{k,4,i,j} \end{bmatrix}. \tag{47}$$

We consider terms of $O\left(\delta^{-1}\right)$ in Eq. (46a) to find:

$$\begin{bmatrix} \psi^{(0)}_{k,1,i,j} \\ \psi^{(0)}_{k,2,i,j} \\ \psi^{(0)}_{k,3,i,j} \\ \psi^{(0)}_{k,4,i,j} \end{bmatrix} = \sum_{n,m} M_{N,k,nm} \begin{bmatrix} \tilde{\varphi}^{(0)}_{nm,1,i,j} \\ \tilde{\varphi}^{(0)}_{nm,2,i,j} \\ \tilde{\varphi}^{(0)}_{nm,3,i,j} \\ \tilde{\varphi}^{(0)}_{nm,4,i,j} \end{bmatrix}, \tag{48}$$

where we have noted that $\mathbf{M}$ can be eliminated since it is invertible. As before, if $D_N = M_N^{-1}$, then Eqs. (47) and (48) will be consistent. We shall assume that this is the case; then the $O\left(\delta\right)$ terms in Eq. (46b) yield:

$$\begin{bmatrix} \tilde{\varphi}^{(1)}_{nm,1,i,j} \\ \tilde{\varphi}^{(1)}_{nm,2,i,j} \\ \tilde{\varphi}^{(1)}_{nm,3,i,j} \\ \tilde{\varphi}^{(1)}_{nm,4,i,j} \end{bmatrix} = \sum_{k} D_{N,nm,k} \begin{bmatrix} \psi^{(1)}_{k,1,i,j} \\ \psi^{(1)}_{k,2,i,j} \\ \psi^{(1)}_{k,3,i,j} \\ \psi^{(1)}_{k,4,i,j} \end{bmatrix}. \tag{49}$$

The $O\left(1\right)$ terms in the remaining Eqs. (46) yield:

$$\frac{\mu_k}{\Delta x_i}\mathbf{U} \begin{bmatrix} \psi^{L(0)}_{k,1,i,j} \\ \psi^{R(0)}_{k,2,i,j} \\ \psi^{R(0)}_{k,3,i,j} \\ \psi^{L(0)}_{k,4,i,j} \end{bmatrix} + \frac{\eta_k}{\Delta y_j}\mathbf{N} \begin{bmatrix} \psi^{B(0)}_{k,1,i,j} \\ \psi^{B(0)}_{k,2,i,j} \\ \psi^{T(0)}_{k,3,i,j} \\ \psi^{T(0)}_{k,4,i,j} \end{bmatrix}$$

$$+ \left(\frac{\mu_k}{\Delta x_i}\mathbf{K} + \frac{\eta_k}{\Delta y_j}\mathbf{L} + \hat{\sigma}_{a,ij}\mathbf{M} \right) \begin{bmatrix} \psi^{(0)}_{k,1,i,j} \\ \psi^{(0)}_{k,2,i,j} \\ \psi^{(0)}_{k,3,i,j} \\ \psi^{(0)}_{k,4,i,j} \end{bmatrix}$$

$$+ \hat{\sigma}_{s0,ij}\mathbf{M} \left\{ \begin{bmatrix} \psi^{(1)}_{k,1,i,j} \\ \psi^{(1)}_{k,2,i,j} \\ \psi^{(1)}_{k,3,i,j} \\ \psi^{(1)}_{k,4,i,j} \end{bmatrix} - \sum_{n,m} M_{N,k,nm} \begin{bmatrix} \tilde{\varphi}^{(1)}_{nm,1,i,j} \\ \tilde{\varphi}^{(1)}_{nm,2,i,j} \\ \tilde{\varphi}^{(1)}_{nm,3,i,j} \\ \tilde{\varphi}^{(1)}_{nm,4,i,j} \end{bmatrix} \right\}$$

$$= \frac{-\left(\sigma_{tr,ij} - \hat{\sigma}_{a,ij}\right)}{2} \sum_{n,m} M_{N,k,nm} n\left(n+1\right) \mathbf{M} \begin{bmatrix} \tilde{\varphi}^{(0)}_{nm,1,i,j} \\ \tilde{\varphi}^{(0)}_{nm,2,i,j} \\ \tilde{\varphi}^{(0)}_{nm,3,i,j} \\ \tilde{\varphi}^{(0)}_{nm,4,i,j} \end{bmatrix}$$

$$+\mathbf{M} \begin{bmatrix} q_{1,i,j} \\ q_{2,i,j} \\ q_{3,i,j} \\ q_{4,i,j} \end{bmatrix} + O\left(\frac{\gamma}{\delta}\right), \tag{50a}$$

$$\psi^{L(0)}_{k,1,i,j} = \begin{cases} f^{L}_{k,1,j}, & \mu_k > 0, \quad i = 1 \\ \psi^{(0)}_{k,2,i-1,j}, & \mu_k > 0, \quad 2 \le i \le I, \quad 1 \le j \le J \\ \psi^{(0)}_{k,1,i,j}, & \mu_k < 0, \quad 1 \le i \le I \end{cases}, \tag{50b}$$

$$\psi^{L(0)}_{k,4,i,j} = \begin{cases} f^{L}_{k,4,j}, & \mu_k > 0, \quad i = 1 \\ \psi^{(0)}_{k,3,i-1,j}, & \mu_k > 0, \quad 2 \le i \le I, \quad 1 \le j \le J \\ \psi^{(0)}_{k,4,i,j}, & \mu_k < 0, \quad 1 \le i \le I \end{cases}, \tag{50c}$$

$$\psi^{R(0)}_{k,2,i,j} = \begin{cases} \psi^{(0)}_{k,2,i,j}, & \mu_k > 0, \quad 1 \le i \le I \\ \psi^{(0)}_{k,1,i+1,j}, & \mu_k < 0, \quad 1 \le i \le I-1, \quad 1 \le j \le J \\ f^{R}_{k,2,j}, & \mu_k < 0, \quad i = I \end{cases}, \tag{50d}$$

$$\psi^{R(0)}_{k,3,i,j} = \begin{cases} \psi^{(0)}_{k,3,i,j}, & \mu_k > 0, \quad 1 \le i \le I \\ \psi^{(0)}_{k,4,i+1,j}, & \mu_k < 0, \quad 1 \le i \le I-1, \quad 1 \le j \le J \\ f^{R}_{k,3,j}, & \mu_k < 0, \quad i = I \end{cases}, \tag{50e}$$

$$\psi^{B(0)}_{k,1,i,j} = \begin{cases} f^{B}_{k,1,i}, & \eta_k > 0, \quad j = 1 \\ \psi^{(0)}_{k,4,i,j-1}, & \eta_k > 0, \quad 2 \le j \le J, \quad 1 \le i \le I \\ \psi^{(0)}_{k,1,i,j}, & \eta_k < 0, \quad 1 \le j \le J \end{cases}, \tag{50f}$$

$$\psi^{B(0)}_{k,2,i,j} = \begin{cases} f^{B}_{k,2,i}, & \eta_k > 0, \quad j = 1 \\ \psi^{(0)}_{k,3,i,j-1}, & \eta_k > 0, \quad 2 \le j \le J, \quad 1 \le i \le I \\ \psi^{(0)}_{k,2,i,j}, & \eta_k < 0, \quad 1 \le j \le J \end{cases}, \tag{50g}$$

$$\psi^{T(0)}_{k,3,i,j} = \begin{cases} \psi^{(0)}_{k,3,i,j}, & \eta_k > 0, \quad 1 \le j \le J \\ \psi^{(0)}_{k,2,i,j+1}, & \eta_k < 0, \quad 1 \le j \le J-1, \quad 1 \le i \le I \\ f^{T}_{k,3,i}, & \eta_k < 0, \quad j = J \end{cases}, \tag{50h}$$

$$\psi^{T(0)}_{k,4,i,j} = \begin{cases} \psi^{(0)}_{k,4,i,j}, & \eta_k > 0, \quad 1 \le j \le J \\ \psi^{(0)}_{k,1,i,j+1}, & \eta_k < 0, \quad 1 \le j \le J-1, \quad 1 \le i \le I \\ f^{T}_{k,4,i}, & \eta_k < 0, \quad j = J \end{cases}. \tag{50i}$$

Eqs. (50b)-(50i) express the leading-order boundary conditions, which are simply the conditions applied to the unscaled problem. By our assumption of $D_N = M_N^{-1}$, the term in braces in Eq. (50a) disappears. Equations (15) and (50a) thus yield:

$$\begin{aligned} &\frac{\mu_k}{\Delta x_i}\mathbf{U}\begin{bmatrix} \psi^{L(0)}_{k,1,i,j} \\ \psi^{R(0)}_{k,2,i,j} \\ \psi^{R(0)}_{k,3,i,j} \\ \psi^{L(0)}_{k,4,i,j} \end{bmatrix} + \frac{\eta_k}{\Delta y_j}\mathbf{N}\begin{bmatrix} \psi^{B(0)}_{k,1,i,j} \\ \psi^{B(0)}_{k,2,i,j} \\ \psi^{T(0)}_{k,3,i,j} \\ \psi^{T(0)}_{k,4,i,j} \end{bmatrix} \\ &+\left(\frac{\mu_k}{\Delta x_i}\mathbf{K} + \frac{\eta_k}{\Delta y_j}\mathbf{L} + \hat{\sigma}_{a,ij}\mathbf{M}\right)\begin{bmatrix} \psi^{(0)}_{k,1,i,j} \\ \psi^{(0)}_{k,2,i,j} \\ \psi^{(0)}_{k,3,i,j} \\ \psi^{(0)}_{k,4,i,j} \end{bmatrix} \\ &= \frac{(\sigma_{tr,ij} - \hat{\sigma}_{a,ij})}{2}\mathbf{M}\left\{\left[\frac{\partial}{\partial\mu}\left(1-\mu^2\right)\frac{\partial}{\partial\mu} + \left(\frac{1}{1-\mu^2}\right)\frac{\partial^2}{\partial\phi^2}\right]\begin{bmatrix} \tilde{\psi}^{(0)}_{1,i,j}(\mathbf{\Omega}) \\ \tilde{\psi}^{(0)}_{2,i,j}(\mathbf{\Omega}) \\ \tilde{\psi}^{(0)}_{3,i,j}(\mathbf{\Omega}) \\ \tilde{\psi}^{(0)}_{4,i,j}(\mathbf{\Omega}) \end{bmatrix}\right\}_{\mathbf{\Omega}=\mathbf{\Omega}_k} \\ &+\mathbf{M}\begin{bmatrix} q_{1,i,j} \\ q_{2,i,j} \\ q_{3,i,j} \\ q_{4,i,j} \end{bmatrix}, \end{aligned} \tag{51}$$

assuming that $\gamma/\delta \rightarrow 0$ as $\delta \rightarrow 0$. Thus, given that $D_N = M_N^{-1}$ and that γ has no $O(\delta)$ components, the leading-order FEM-S_N solution satisfies a FEM-pseudospectral discretization of the FP equation.

In summary, the last two chapters have shown that some transport problems with forward-peaked scaling are described by the Fokker-Planck equation, while others are not; this is a function strictly of the scattering kernel. If the analytic problem does limit to the FP equation, then the discrete ordinates equations limit to a pseudospectral discretization of the FP equation, provided that the scattering source is treated carefully. If the discrete ordinates equations limit to a pseudospectral discretization of the FP equation, then (at least for the cases studied) reasonable spatial discretizations of the discrete ordinates equations limit to related spatial discretizations of the pseudospectral-FP equation. We have noted some similarities between the FP and diffusion limit analyses of characteristics methods. Finally, the leading order boundary conditions in the FP limit are identical to the boundary conditions for the unscaled problem.

CHAPTER IV

ANGULAR MULTIGRID ACCELERATION OF THE SPATIALLY ANALYTIC DISCRETE ORDINATES EQUATIONS

In the previous two chapters we analyzed discrete ordinates transport methods in the limit of highly forward-peaked scattering (the Fokker-Planck limit). We noted that in that limit the exact transport solution satisfies, to leading order, the Fokker-Planck equation, provided that the scattering kernel satisfies a certain condition. We then identified conditions under which certain discretized transport solutions satisfy, to leading order, reasonable discretizations of the Fokker-Planck equation. Assuming that these FP discretizations have the desired accuracy for problems of interest, we therefore have identified conditions under which certain transport methods produce reliable results for certain forward-peaked problems.

We now turn our attention to defining efficient methods for obtaining solutions to these transport discretizations. In most realistic problems it is necessary to use iterative solution methods. However, the convergence rates of iterative methods can be arbitrarily slow. It is therefore necessary to create computational acceleration schemes that improve the iterative convergence rate. The effectiveness of a given acceleration scheme may depend on the underlying physical problem and the discretization scheme.

In this chapter we consider the acceleration of the spatially analytic, multidimensional discrete ordinates method in the FP limit. We extend the angular multigrid method,[29,95] previously defined for slab geometry, to the multidimensional setting. Our analysis shows that the basic angular multigrid scheme is unstable in multidimensional calculations, but we introduce modifications that make it stable and effective.

IV.A. Development of the Angular Multigrid Acceleration Method for Discrete Ordinates Calculations

IV.A.1. Acceleration of General Iterative Methods

We begin by examining a general linear iterative method in order to construct the framework and terminology that will organize our development of iterative methods for transport calculations. This general presentation is a modification of one given by Morel.[96] Let the following be a linear system that we wish to solve:

$$Hf = q, \tag{52}$$

where H is a "high-order" operator and q is a "source". In many linear systems of interest it is very difficult to directly invert H. It often is possible, however, to "split" H into two operators, at least one of which is "easily" inverted:

$$H = A - B. \tag{53}$$

We then can define the following iterative method:

$$Af^{(l+1)} = Bf^{(l)} + q, \tag{54}$$

where l is the iteration number and $f^{(0)}$ is an arbitrary initial iterate. Multiplication by A^{-1} yields

$$f^{(l+1)} = Zf^{(l)} + A^{-1}q, \tag{55}$$

where $Z = A^{-1}B$ is the "iteration operator." Examination of the eigenvalues of Z reveals the effectiveness of the iterative method. If the spectral radius ρ of Z (defined as the maximum of the absolute values of the eigenvalues) is greater than unity, the iteration can diverge, and the iterative method is not practically useful. If $\rho \ll 1$, the iterative method will converge rapidly. If $\rho \lesssim 1$, the iterative method will converge, albeit slowly. This last case is common among iterative methods. Modifications of these methods are required to decrease the spectral radii and thus to increase the convergence rates.

In order to develop an approach to increase the iterative convergence rate, let us examine the error at each iteration. The error in an iterative approximation to the solution is given by

$$e^{(l)} = f - f^{(l)}. \tag{56}$$

Manipulation of Eqs. (52)-(56) yields an exact expression for the error:

$$He^{(l+1)} = Br^{(l+1)}, \tag{57}$$

where $r^{(l+1)} \equiv f^{(l+1)} - f^{(l)}$ is the "residual". Given the exact error $e^{(l+1)}$, we could use Eq. (56) to obtain the exact discrete solution after a single iteration. Unfortunately, Eq. (57) is just as difficult to solve as the original problem, Eq. (52), since we must invert H in both cases. However, if we could solve Eq. (57) approximately in an efficient manner, we could add the resulting error estimate to the current iterate and therefore obtain a better iterative approximation. We do so by replacing Eq. (57) with the following approximation:

$$L\tilde{e}^{(l+1)} = Br^{(l+1)}, \tag{58}$$

where L is a "low-order" approximation to H and is "easily" inverted. This suggests the following iterative scheme:

$$f^{(l+\frac{1}{2})} = Zf^{(l)} + A^{-1}q, \tag{59a}$$

$$\tilde{e}^{(l+\frac{1}{2})} = L^{-1}Br^{(l+\frac{1}{2})}, \tag{59b}$$

$$f^{(l+1)} = f^{(l+\frac{1}{2})} + \tilde{e}^{(l+\frac{1}{2})}. \tag{59c}$$

This can be written in the equivalent form:

$$f^{(l+1)} = \left(I - L^{-1}H\right) Zf^{(l)} + \left(I + L^{-1}B\right) A^{-1}q, \tag{60}$$

with the new iteration operator $Z' = (I - L^{-1}H)\, Z$. Clearly, if $L \approx H$ then the spectral radius of Z' will be small and the iterative method will converge rapidly. The modification to the basic iteration in Eq. (55) is called an "acceleration method", and L is often called a "preconditioner", since its application changes the eigenvalues and thus the condition number of the iteration operator.

There are several criteria that L needs to meet for it to define a good acceleration method. First, L must produce a good estimate of those error modes that have the slowest convergence rate in the original iterative method. In other words, if we decompose the error into the eigenvectors of Z, we must produce a good estimate for those error eigenmodes corresponding to the eigenvalues of greatest absolute magnitude. In such a case L will be "effective". Second, L must be "stable": it must not greatly overestimate any error modes, or those modes will diverge in the new iterative method. Finally, L must be "easily" inverted. We

must be able to invert L directly or iteratively at a reasonable computational cost, otherwise there will be no advantage in using the new iterative method.

How does one find an acceleration method that meets the above criteria? Potential candidates are those operators that are asymptotic limits of the high-order operator, assuming that the high-order operator is reasonably close to the corresponding limit. These asymptotic operators are generally simpler, and thus easier to invert, than the high-order operator, yet they may behave similarly. This is the approach of diffusion synthetic acceleration (DSA), which we shall encounter later in this chapter. Alternatively, one may use an operator that results from a cruder discretization of the original problem, since it will presumably share many of the important properties of the high-order operator but will be easier to invert. This is the approach taken by the various multigrid schemes. Whatever the candidate acceleration method is, it must be carefully analyzed to determine its stability and effectiveness for the class of problems of interest.

IV.A.2. Source Iteration

The integro-differential transport operator is very difficult to directly invert for all but the simplest problems. In most cases an appropriate discretization of the monoenergetic equation can be solved by means of source iteration. The source iteration method for the discrete ordinates (S_N) discretization is given in operator notation by

$$[\Omega \cdot \nabla + \sigma_t]_N \Psi^{(l+1)} = M_N \Sigma_N D_N \Psi^{(l)} + \mathbf{q}, \tag{61}$$

where the N subscript indicates the quadrature order for which the operators are defined. The term "source" iteration is derived from the fact that we iterate on the right side of Eq. (61), which is the scattering source.

In order to determine rigorously the effectiveness of source iteration we would need to examine all of the eigenvalues of the source iteration operator. This is usually done by means of a Fourier analysis, which we shall describe and use in the next section. However, we can place a lower bound on the spectral radius of the source iteration operator in a homogeneous infinite medium by restricting our attention to "flat" modes, i.e. those error modes that vary slowly spatially. For such modes the gradient operator $\mathbf{\Omega} \cdot \mathbf{\nabla}$ becomes negligible compared to the removal operator σ_t, yielding the following simpler iteration:

$$\sigma_{t,N} \mathbf{\Psi}^{(l+1)} = M_N \Sigma_N D_N \mathbf{\Psi}^{(l)} + \mathbf{q}, \tag{62}$$

which, assuming that $D_N = M_N^{-1}$, can be rewritten as

$$\mathbf{\Phi}^{(l+1)} = C_N \mathbf{\Phi}^{(l)} + \frac{1}{\sigma_{t,N}} D_N \mathbf{q}, \tag{63}$$

where $C_N = \Sigma_N / \sigma_{t,N}$. We will assume throughout the following chapters that $D_N = M_N^{-1}$, for reasons described in the previous chapters. Therefore the eigenvalues corresponding to these flat modes are $\{\sigma_{sn} / \sigma_t\}$. We define $c \equiv \sigma_{s0} / \sigma_t$ as the scattering ratio; as $c \rightarrow 1$ the source iteration method converges arbitrarily slowly. A full Fourier analysis of an infinite-medium problem would reveal that the flat mode corresponding to c is indeed the slowest converging mode. Therefore, although the source iteration method is stable for non-

multiplying media, it can have arbitrarily slow convergence. Methods must be found to accelerate these slowly converging flat modes.

IV.A.3. Diffusion Synthetic Acceleration

Some transport problems are diffusive, meaning that the transport operator is "close" to the asymptotic diffusion limit.[57] Such problems are characterized by large, nearly isotropic scattering cross sections, small absorption cross sections and optically thick media. Consequently the scattering ratio is close to unity and the source iteration method has a slow convergence rate.

Since the diffusion equation is a good approximation to these problems (and for a wider class of problems it is a good approximation for flat, slowly converging modes), it is a good candidate as an acceleration method for source iteration. Over the last 30 years the diffusion synthetic acceleration (DSA) method has been developed extensively.[48,50,52,73,74,76,81,94,96–115] The basic DSA scheme uses a diffusion equation to estimate and correct the errors in the zeroth flux moment:

$$[\Omega \cdot \nabla + \sigma_t]_N \Psi^{(l+\frac{1}{2})} = M_N \Sigma_N \Phi^{(l)}, \tag{64a}$$

$$\Phi^{(l+\frac{1}{2})} = D_N \Psi^{(l+\frac{1}{2})}, \tag{64b}$$

$$\left[-\nabla \cdot \frac{1}{3\sigma_t} \nabla + \sigma_a\right] f^{(l)} = \sigma_{s0} \left(\varphi_0^{(l+\frac{1}{2})} - \varphi_0^{(l)}\right), \tag{64c}$$

$$\varphi_{nm}^{(l+1)} = \begin{cases} \varphi_0^{(l+\frac{1}{2})} + f^{(l)}, & n = 0 \\ \varphi_{nm}^{(l+\frac{1}{2})}, & n > 0 \end{cases}, \tag{64d}$$

where we have omitted a fixed source term since it does not affect the iteration operator and we are only interested in the iterative convergence properties. We shall continue to omit the fixed source in future analyses, in which case $\Psi^{(l)}$ and $\Phi^{(l)}$ may be interpreted as the iterative errors rather than the actual solution estimates.

Let us examine the effect of DSA on the iterative convergence rate of flat error modes, as we did for source iteration. For flat modes Eq. (64) may be rewritten as

$$\sigma_{t,N}\Phi^{\left(l+\frac{1}{2}\right)} = \Sigma_N \Phi^{(l)}, \tag{65a}$$

$$\sigma_a f^{(l)} = \sigma_{s0}\left(\varphi_0^{\left(l+\frac{1}{2}\right)} - \varphi_0^{(l)}\right), \tag{65b}$$

$$\varphi_{nm}^{(l+1)} = \begin{cases} \varphi_0^{\left(l+\frac{1}{2}\right)} + f^{(l)}, & n = 0 \\ \varphi_{nm}^{\left(l+\frac{1}{2}\right)}, & n > 0 \end{cases}. \tag{65c}$$

Rearrangement of Eq. (65) leads to the following relation for the iteration errors:

$$\varphi_{nm}^{(l+1)} = \begin{cases} 0, & n = 0 \\ c_{n,N}\varphi_{nm}^{(l)}, & n > 0 \end{cases}, \tag{66}$$

where we have defined a general scattering ratio $c_{n,N} \equiv \sigma_{sn,N}/\sigma_{t,N}$. Our emphasis upon the order of the quadrature set by including N in the cross section subscripts will be important in our later multigrid development. If the scattering is isotropic, then Eq. (66) predicts that DSA will converge the flat component of the solution in a single iteration. An analysis of all the iteration modes (not just the flat ones) in a homogeneous infinite-medium model problem reveals that the overall spectral radius of DSA for analytic transport is less than 0.23 in slab geometry[103] and 0.5 in multidimensions[112] when scattering is isotropic, so for problems with isotropic scattering DSA is both stable and effective.

In spatially discretized problems the situation is more complex. Alcouffe[100] and Larsen[103] found that to guarantee the stability of DSA in spatially discretized problems the discretization of the diffusion operator must be consistent with or nearly consistent with the discretization of the transport operator. Furthermore, for DSA to be useful the diffusion operator must be easily inverted. Some of the discrete diffusion operators developed for DSA methods are symmetric and hence relatively easy to invert by the conjugate gradient method[116] or by other means, whereas other proposed diffusion operators are more difficult to invert. In many cases attempts to alter the diffusion operator in order to invert it more easily cause DSA to lose its effectiveness. The development of effective and efficient DSA schemes remains an active field of research.

IV.A.4. Current-Accelerating DSA

The standard DSA method is stable and effective for diffusive problems with isotropic scattering. However, DSA loses its effectiveness as the scattering becomes increasingly anisotropic. Equation (66) shows that $\max\{c_{n,N}\}$ for $n > 0$ is a lower bound on the spectral radius of source iteration with DSA. When the scattering becomes sufficiently anisotropic we must also accelerate higher moments than the zeroth flux moment in order to have an effective scheme.

Morel[96] proposed a variant of DSA in which the "currents" (i.e. the first flux moments) as well as the scalar flux are accelerated. Like DSA, it may be derived as an approximation to transport theory (the P_1 approximation). The modified scheme is given by

$$[\Omega \cdot \nabla + \sigma_t]_N \Psi^{(l+\frac{1}{2})} = M_N \Sigma_N \Phi^{(l)}, \tag{67a}$$

$$\mathbf{\Phi}^{\left(l+\frac{1}{2}\right)} = D_N \mathbf{\Psi}^{\left(l+\frac{1}{2}\right)}, \tag{67b}$$

$$\left[-\boldsymbol{\nabla}\cdot\frac{1}{3\sigma_{tr}}\boldsymbol{\nabla}+\sigma_a\right] f^{(l)} = \sigma_{s0}\left(\varphi_0^{\left(l+\frac{1}{2}\right)}-\varphi_0^{(l)}\right)-\frac{\sigma_{s1}}{\sigma_{tr}}M_J\left(\mathbf{\Phi}^{\left(l+\frac{1}{2}\right)}-\mathbf{\Phi}^{(l)}\right)_{n=1}, \tag{67c}$$

$$\mathbf{h}^{(l)} = -\frac{1}{3\sigma_{tr}}\boldsymbol{\nabla} f^{(l)}+\frac{\sigma_{s1}}{\sigma_{tr}}M_J\left(\mathbf{\Phi}^{\left(l+\frac{1}{2}\right)}-\mathbf{\Phi}^{(l)}\right)_{n=1}, \tag{67d}$$

$$\varphi_{nm}^{(l+1)} = \begin{cases} \varphi_0^{\left(l+\frac{1}{2}\right)}+f^{(l)}, & n=0 \\ \varphi_{1,m}^{\left(l+\frac{1}{2}\right)}+\left(J_M\mathbf{h}^{(l)}\right)_m, & n=1 \\ \varphi_{nm}^{\left(l+\frac{1}{2}\right)}, & n>1 \end{cases}, \tag{67e}$$

where M_J and J_M are matrices that convert the first flux moments to currents and back, respectively. For flat modes this method reduces to

$$\sigma_{t,N}\mathbf{\Phi}^{\left(l+\frac{1}{2}\right)} = \Sigma_N\mathbf{\Phi}^{(l)}, \tag{68a}$$

$$\sigma_a f^{(l)} = \sigma_{s0}\left(\varphi_0^{\left(l+\frac{1}{2}\right)}-\varphi_0^{(l)}\right), \tag{68b}$$

$$\mathbf{h}^{(l)} = \frac{\sigma_{s1}}{\sigma_{tr}}M_J\left(\mathbf{\Phi}^{\left(l+\frac{1}{2}\right)}-\mathbf{\Phi}^{(l)}\right)_{n=1}, \tag{68c}$$

$$\varphi_{nm}^{(l+1)} = \begin{cases} \varphi_0^{\left(l+\frac{1}{2}\right)}+f^{(l)}, & n=0 \\ \varphi_{1,m}^{\left(l+\frac{1}{2}\right)}+\left(J_M\mathbf{h}^{(l)}\right)_m, & n=1 \\ \varphi_{nm}^{\left(l+\frac{1}{2}\right)}, & n>1 \end{cases}. \tag{68d}$$

Combining Eqs. (68) yields the following convergence properties for flat error modes:

$$\varphi_{nm}^{(l+1)} = \begin{cases} 0, & n=0,1 \\ c_{n,N}\varphi_{nm}^{(l)}, & n>1 \end{cases}. \tag{69}$$

Therefore the convergence rate for flat modes is governed by $\max\{c_{n,N}\}$ for $n \geq 2$ rather than $n \geq 1$. Since most physical forward-peaked scattering kernels produce $c_{0,N} \geq c_{1,N} \geq$

$\cdots \geq c_{L,N}$, where L is the order of the scattering, this extended DSA scheme has improved convergence rates over the standard DSA for flat modes without a greatly increased cost. One significant drawback to this modified DSA method that a full analysis reveals is that for multidimensional calculations one of its eigenvalues has a magnitude of $\overline{\mu_0}c/(1-\overline{\mu_0}c)$, so for anisotropic scattering with $\overline{\mu_0}c > 0.5$ (when standard DSA loses its effectiveness) the modified DSA is unstable and thus cannot be used.[112] Additional modifications or other anisotropic acceleration methods must then be implemented.

IV.A.5. Many-Moment Acceleration Methods and Angular Multigrid

In the preceding analyses we have seen that a lower bound on the spectral radius of source iteration is given by $\max\{c_{n,N}\}$ for all n corresponding to "unaccelerated" moments. As the scattering becomes highly forward-peaked ($c_{n,N} \rightarrow 1$) it becomes necessary to accelerate more flux moments than just the zeroth and first ones. Thus we need to define acceleration methods of higher order than diffusion.

Earlier we stated that the asymptotic limits of the transport operator may be good candidates for acceleration methods. In the current study we are interested in problems that are near the FP limit, so the FP equation would seem to be an ideal acceleration operator. Certainly we could expect an analysis to reveal that such an acceleration method would be effective. However, a good acceleration operator must be easily invertible, and experience has also shown that the discretization of the acceleration operator generally must be consistent with the discretization of the transport operator. Pseudospectral discretizations of the FP equation are similar structurally to the S_N transport operator, so inversion methods like source iteration would have the same convergence difficulties. Instead of attempting to find

an inexpensive method of inverting the FP operator, we shall look at other candidates for acceleration methods.

The P_N equations (another anisotropic asymptotic limit[58]) have been investigated as potential acceleration methods in slab geometry.[101,106,117–119] For both isotropic and anisotropic problems the P_N acceleration method has been found to be more effective than DSA for odd values of N. However, because of the increasingly high cost of solving the coupled P_N equations for increasing values of N the most cost-effective acceleration method was determined to be the P_1 scheme (equivalent to Morel's DSA method[96]). Khattab and Larsen[119] defined an easily invertible P_N-like method in which they solve the P_N equations approximately by decoupling them, but this method's effectiveness slowly degrades as the degree of anisotropy increases. The P_N equations are even more difficult to solve in multidimensions, so this approach is not very promising.

A second approach that may be taken in the search for good acceleration methods is to use a more coarsely discretized version of the high-order operator. This approach has been used in situations in which the geometry or the spatial discretization scheme makes it very difficult to construct a consistent and easily invertible DSA operator. Early attempts used S_2 equations to accelerate the zeroth and sometimes the first flux moments.[120–124] More recently the transport synthetic acceleration (TSA) method has been developed; it uses a lower-order transport operator (not necessarily S_2) and modified cross sections to accelerate the zeroth flux moment.[82,125–127] The cross section in the TSA operator has been restricted to isotropic scattering in order to produce a symmetric operator, which is easier to invert than the asymmetric operators that result from anisotropic scattering.

In order to deal effectively with highly anisotropic scattering we propose to modify the above approach by using lower-order discrete ordinates operators with anisotropic scattering to define an acceleration method. Specifically, we will extend the angular multigrid method of Morel and Manteuffel[29] to multidimensional transport. Before we describe their method and our extensions in detail, let us first examine the effectiveness of using a single low-order discrete ordinates operator with anisotropic cross sections to accelerate a high-order S_N calculation. The basic method is the following two-grid scheme:

$$[\Omega \cdot \nabla + \sigma_t]_N \Psi^{(l+\frac{1}{2})} = M_N \Sigma_N \Phi^{(l)}, \tag{70a}$$

$$\Phi^{(l+\frac{1}{2})} = D_N \Psi^{(l+\frac{1}{2})}, \tag{70b}$$

$$[\Omega \cdot \nabla + \sigma_t]_{N'} \Psi'^{(l)} = M_{N'} \Sigma_{N'} \Phi'^{(l)} + M_{N'} P_{N \to N'} \Sigma_N \left(\Phi^{(l+\frac{1}{2})} - \Phi^{(l)} \right), \tag{70c}$$

$$\Phi'^{(l)} = D_{N'} \Psi'^{(l)}, \tag{70d}$$

$$\Phi^{(l+1)} = \Phi^{(l+\frac{1}{2})} + P_{N' \to N} \Phi'^{(l)}, \tag{70e}$$

where $N' < N$. For compactness of notation we have defined the restriction operator $P_{N \to N'}$ and prolongation operator $P_{N' \to N}$:

$$(P_{N \to N'} \Phi)_{(n,m)} = \varphi_{nm}, \quad (n,m) \in Q_{N'}, \tag{71a}$$

$$(P_{N' \to N} \Phi)_{(n,m)} = \begin{cases} \varphi_{nm}, & (n,m) \in Q_{N'} \\ 0, & (n,m) \notin Q_{N'} \end{cases}, \tag{71b}$$

where $Q_{N'}$ is the set of spherical harmonics orders (n,m) that form the interpolatory basis for the quadrature of order N'. Note that Eqs. (70) imply that we actually invert the $S_{N'}$

equations; we shall return to this operation later. As in previous analyses we restrict our attention to flat error modes, which reduces our acceleration scheme to the following:

$$\sigma_{t,N}\Phi^{\left(l+\frac{1}{2}\right)} = \Sigma_N\Phi^{(l)}, \tag{72a}$$

$$\sigma_{t,N'}\Phi'^{(l)} = \Sigma_{N'}\Phi'^{(l)} + P_{N\rightarrow N'}\Sigma_N\left(\Phi^{\left(l+\frac{1}{2}\right)} - \Phi^{(l)}\right), \tag{72b}$$

$$\Phi^{(l+1)} = \Phi^{\left(l+\frac{1}{2}\right)} + P_{N'\rightarrow N}\Phi'^{(l)}. \tag{72c}$$

Combining Eqs. (72) yields the following iteration equation for flat error modes:

$$\varphi_{nm}^{(l+1)} = \begin{cases} 0, & (n,m) \in Q_{N'} \\ c_{n,N}\varphi_{nm}^{(l)}, & (n,m) \notin Q_{N'} \end{cases}. \tag{73}$$

Thus the spectral radius for flat modes is $\max\{c_{n,N}\}$ over only the n corresponding to unaccelerated moments. Since the only constraint that we have placed on N' is that it be less than N, many more moments than the zeroth and first moments may be accelerated, causing the spectral radius to be governed by higher-order scattering ratios than in DSA.

The effectiveness of the above two-grid scheme apparently relies on completely inverting the lower-order discrete ordinates operator. This inversion is, of course, difficult to perform. Source iteration on the $S_{N'}$ operator will converge as slowly as it does for the S_N operator (assuming for now that $c_{n,N'} = c_{n,N}$). Therefore we need to apply an acceleration method to more rapidly invert the $S_{N'}$ operator. We also recognize that we may not need to completely invert the $S_{N'}$ operator; a partial inversion may be sufficient to provide good acceleration at less cost than a full inversion. We reintroduce the DSA acceleration method and assume that a single $S_{N'}$ sweep accelerated by DSA will be effective at accelerating the S_N iteration.

Since the scattering is forward-peaked in many problems of interest and we are interested in multidimensional calculations, we shall use the standard DSA operator rather than the unstable current-accelerating DSA. The modified two-grid scheme is:

$$[\mathbf{\Omega}\cdot\boldsymbol{\nabla}+\sigma_t]_N\,\boldsymbol{\Psi}^{\left(l+\frac{1}{2}\right)} = M_N\Sigma_N\boldsymbol{\Phi}^{(l)}, \tag{74a}$$

$$\boldsymbol{\Phi}^{\left(l+\frac{1}{2}\right)} = D_N\boldsymbol{\Psi}^{\left(l+\frac{1}{2}\right)}, \tag{74b}$$

$$[\mathbf{\Omega}\cdot\boldsymbol{\nabla}+\sigma_t]_{N'}\,\boldsymbol{\Psi}'^{(l)} = M_{N'}P_{N\to N'}\Sigma_N\left(\boldsymbol{\Phi}^{\left(l+\frac{1}{2}\right)}-\boldsymbol{\Phi}^{(l)}\right), \tag{74c}$$

$$\boldsymbol{\Phi}'^{(l)} = D_{N'}\boldsymbol{\Psi}'^{(l)}, \tag{74d}$$

$$\left[-\boldsymbol{\nabla}\cdot\frac{1}{3\sigma_{t,N'}}\boldsymbol{\nabla}+\sigma_a\right]f^{(l)} = P_{N'\to 0}\Sigma_{N'}\boldsymbol{\Phi}'^{(l)}, \tag{74e}$$

$$\boldsymbol{\Phi}^{(l+1)} = \boldsymbol{\Phi}^{\left(l+\frac{1}{2}\right)}+P_{N'\to N}\left(\boldsymbol{\Phi}'^{(l)}+P_{0\to N'}f^{(l)}\right), \tag{74f}$$

where $P_{N'\to 0}$ is the restriction to and $P_{0\to N'}$ the prolongation from the zeroth flux moment. After restricting our attention to flat error modes and manipulating the resulting equations we obtain the following equation for the iteration errors:

$$\varphi_{nm}^{(l+1)} = \begin{cases} 0, & n=0 \\ c_{n,N}c_{n,N'}\varphi_{nm}^{(l)}, & (n,m)\in Q_{N'},\ n\neq 0 \\ c_{n,N}\varphi_{nm}^{(l)}, & (n,m)\notin Q_{N'} \end{cases}. \tag{75}$$

A comparison of Eqs. (73) and (75) shows that failure to completely invert the $S_{N'}$ operator may degrade the effectiveness of the two-grid scheme, depending on the values of $c_{n,N}$ and $c_{n,N'}$. However, this scheme is more effective than accelerating the S_N calculation with DSA alone, since $|c_{n,N}c_{n,N'}|<|c_{n,N}|$. Nevertheless, the convergence may still be arbitrarily slow

if $c_{n,N'} = c_{n,N} \approx 1$ for some value of n. What is needed is a method by which we may reduce the magnitudes of $\{c_{n,N'}\}$.

For this we turn to the extended transport correction. The extended transport correction was originally defined to improve the numerical accuracy of calculations with anisotropic scattering by including the effects of scattering moments of higher order than the cross section expansion used.[128–130] This "correction" consists of subtracting a constant from all of the cross section moments, thereby defining "corrected" cross sections σ_n^*:

$$\sigma_n^* = \sigma_n - \sigma_{corr}, \; n \leq L. \tag{76}$$

The effect of the transport correction is to make the scattering less highly forward-peaked by approximately subtracting a delta function in the forward direction in the differential scattering cross section (which has no effect on the corresponding analytic angular flux solution). If a Galerkin quadrature is not used or if the scattering order is not equal to the maximum order of the spherical harmonics associated with the Galerkin quadrature (i.e. if a full scattering matrix is not used) the discrete ordinates solution is not invariant with respect to the value of σ_{corr}. Standard values for the correction are $\sigma_{corr} = \sigma_L$ or $\sigma_{corr} = \sigma_{L+1}$; it has been found through numerical experience that the solution is improved when the extended transport correction is used.[128,130] The solution is invariant, however, if the discrete-to-moments and moments-to-discrete operators are inverses of each other and a full scattering matrix is used. To see that this is true, examine the following transport corrected discrete ordinates equation:

$$\left[\boldsymbol{\Omega} \cdot \boldsymbol{\nabla} + (\sigma_t - \sigma_{corr})\right]_N \boldsymbol{\Psi} = M_N \left[\Sigma_N - \sigma_{corr} I\right] D_N \boldsymbol{\Psi}. \tag{77}$$

Rearrangement of Eq. (77) gives

$$[\mathbf{\Omega}\cdot\mathbf{\nabla}+\sigma_t]_N\,\mathbf{\Psi}-\sigma_{corr}\mathbf{\Psi}=M_N\Sigma_N D_N\mathbf{\Psi}-\sigma_{corr}M_N D_N\mathbf{\Psi}. \tag{78}$$

If $D_N = M_N^{-1}$ then the terms containing σ_{corr} cancel and we are left with the uncorrected S_N calculation. Although the solution may be invariant, the iterative convergence properties have been altered, since the corrected scattering ratios are given by

$$c^*_{n,N}=\frac{\sigma_{t,N}-\sigma_{corr}}{\sigma_{n,N}-\sigma_{corr}}, \tag{79}$$

and σ_{corr} may be chosen to minimize these ratios, i.e. to make the scattering less anisotropic. In particular, for the DSA-accelerated two-grid scheme we may choose σ_{corr} such that $\left|c^*_{n,N'}\right| < |c_{n,N}|$. This is a crucial step in making this scheme as efficient as possible.

The above concepts were all incorporated by Morel and Manteuffel into their angular multigrid (ANMG) acceleration method, which they developed, analyzed, and tested for slab geometry.[29] Their scheme has the additional feature, inherent in multigrid schemes,[131,132] of a hierarchy of several low-order discrete ordinates operators, with each low-order operator accelerated by an operator of even lower order. (Multigrid schemes had been defined in the past for transport problems,[133,134] but their low-order operators used coarsened spatial discretizations rather than coarsened angular discretizations.) Morel and Manteuffel explicitly described the particular application to an S_{16} calculation, which in their scheme is accelerated by an S_8 sweep, which in turn is accelerated by an S_4 sweep, which in turn is accelerated by a current-accelerating DSA calculation. A transport correction is applied to each S_N operator (or "level"), including the topmost one, in order to optimize the "smoothing"

or convergence rate of those moments not accelerated by lower levels. Their analysis reveals that by using a series of successively lower order S_N operators, each half the order of the previous operator in the series, an upper bound on the spectral radius of 0.6 is obtained with the ANMG scheme. (The angular multigrid method was originally referred to by the acronym AMG, but in order to avoid confusion with the more widely known algebraic multigrid method[135] we will use the acronym ANMG to refer to the angular multigrid method from now on.)

The objective of the remainder of our work is to extend the angular multigrid scheme to multidimensional calculations. Initially we will examine the basic scheme, as expressed by Eqs. (74), with the inclusion of an arbitrary number of additional discrete ordinates levels. Instead of using the unstable current-accelerating DSA we shall substitute an S_2 sweep accelerated by standard DSA as the lowest level. Modifications to the basic scheme will be defined to improve the stability and effectiveness as indicated by full analyses of the multigrid scheme.

IV.B. Fourier Analysis of the Angular Multigrid Acceleration Method

In the previous section we examined the effects of various acceleration schemes on "flat" or slowly spatially varying error modes as a quick and simple indicator of their effectiveness. These analyses show that a lower bound on the iterative spectral radii of common acceleration schemes becomes arbitrarily close to unity as the scattering becomes highly forward-peaked. These same analyses show that a many-moment acceleration method such as the ANMG method can be quite effective at attenuating these flat error modes. This is a necessary property for the ANMG scheme to be a good acceleration method.

In order to completely determine the effectiveness and stability of any acceleration operator, however, we must examine all of its eigenvalues. A key step in this process is to identify small eigenspaces of the solution space that have finite dimension (and therefore a finite number of eigenvalues). Identification of these subspaces generally permits the use of numerical analysis techniques to determine the eigenvalues associated with each subspace. Assuming that all subspaces of the solution space are identified and analyzed, the behavior of the iterative method is completely determined.

In the particular case of linear transport methods, a Fourier analysis is usually applied in order to determine the iterative eigenvalues.[103] The errors are decomposed into Fourier modes (defined below), which are eigenfunctions of the transport operator and most acceleration operators. Subsequent analysis of each Fourier mode determines the effectiveness and stability of the iterative operator with respect to that mode. Not only does this determine the overall stability and effectiveness of the iterative method, but it also reveals details of the iterative behavior, which can suggest further improvements.

We will employ Fourier analyses to determine the stability and effectiveness of the ANMG scheme. First we will demonstrate a Fourier analysis (and the need for additional acceleration in forward-peaked problems) by applying it to the DSA-accelerated S_N method (S_N-DSA) as expressed in Eqs. (64). We introduce the following Fourier ansatz:

$$\psi_k^{(l+\frac{1}{2})} = \omega^l a_k e^{i\boldsymbol{\lambda}\cdot\mathbf{r}}, \tag{80a}$$

$$\varphi_{nm}^{(l+\frac{1}{2})} = \omega^l A_{nm} e^{i\boldsymbol{\lambda}\cdot\mathbf{r}}, \tag{80b}$$

$$\varphi_{nm}^{(l+1)} = \omega^{l+1} B_{nm} e^{i\boldsymbol{\lambda}\cdot\mathbf{r}}, \tag{80c}$$

$$f^{(l)} = \omega^l C_{DSA} e^{i\boldsymbol{\lambda}\cdot\mathbf{r}}. \tag{80d}$$

Equation (80) states that we can express the errors in terms of complex exponential functions with associated spatial frequencies $\boldsymbol{\lambda}$, where in two-dimensional problems $\boldsymbol{\lambda} = (\lambda_x, \lambda_y)$. The total error is a linear combination of the error modes characterized by different $\boldsymbol{\lambda}$'s. Close examination of Eqs. (64) shows that complex exponentials are indeed eigenfunctions of the S_N-DSA operator, so we may analyze each of them independently.

We introduce Eqs. (80) into Eqs. (64) and constrain the equations to an infinite homogeneous medium. Past experience with Fourier analyses has shown that infinite homogeneous medium results are generally in excellent agreement with computational results for the most difficult finite and/or heterogeneous problems, which are analytically intractable. Equations (64a) and (64b) then yield

$$\mathbf{A} = D_N L_N^{-1} M_N \Sigma_N \mathbf{B} \equiv S_N \mathbf{B}, \tag{81}$$

where $L_N = diag\left\{\sigma_{t,N} + i\boldsymbol{\Omega}_k \cdot \boldsymbol{\lambda}\right\}$. Equation (64c) yields

$$C_{DSA} = L_{DSA}^{-1} P_{N\to 0} \Sigma_N \left(\mathbf{A} - \mathbf{B}\right) \equiv S_{DSA}\left(\mathbf{A} - \mathbf{B}\right), \tag{82}$$

where $L_{DSA} = \left[\sigma_{a,N} + \left|\boldsymbol{\lambda}\right|^2 / 3\sigma_{t,N}\right]$. Equation (64d) yields

$$\omega\mathbf{B} - \mathbf{A} = P_{0\to N} C_{DSA}. \tag{83}$$

Finally, we combine Eqs. (81)-(83) to obtain

$$\omega\mathbf{B} = \left[P_{0\to N} S_{DSA}\left(S_N - I_N\right) + S_N\right]\mathbf{B}. \tag{84}$$

Equation (84) is a matrix eigenvalue problem; the dimension of the matrix is equal to the number of quadrature directions. The largest of these eigenvalues in absolute value for a given λ we will call the "modal spectral radius" associated with error modes of this frequency; the spectral radius is the largest modal spectral radius for all λ.

We first analyze Eq. (84) for the S_4 equations in *x-y* geometry with isotropic scattering, no absorption and the standard level-symmetric quadrature set. The results of this analysis are shown in Figure 2. The modal spectral radius is plotted as a function of the modal frequency, where we have converted the frequencies from Cartesian to polar coordinates. (In this and all succeeding analyses $|\lambda|$ is measured in units of transport mean free paths.) As discussed in the previous section this iteration is stable and effective. As $|\lambda| \rightarrow 0$ (i.e. as the modes become flat) the modal spectral radii approach zero, a direct result of the DSA development. At higher frequencies the modal spectral radius is greater than zero yet much less than unity, which shows that DSA produces an imperfect but nevertheless reasonable error estimate at non-zero frequencies. Note also that at certain angles there are somewhat larger modal spectral radii at high frequencies; these angles correspond with quadrature directions. Although the modal spectral radii along these rays are higher than at other angles, the iteration is still quite effective.

Before we examine the effects of a forward-peaked kernel on the modal spectral radii, let us look more closely at the Fokker-Planck kernel and its effect on flat modes. In Chapter II we derived the asymptotic FP scattering kernel, Eq. (8). If we apply the standard transport correction to this kernel, we obtain the standard form of the FP kernel:

$$\sigma_{sn} = \frac{\sigma_{tr} - \hat{\sigma}_a}{2} \left[L(L+1) - n(n+1) \right]. \tag{85}$$

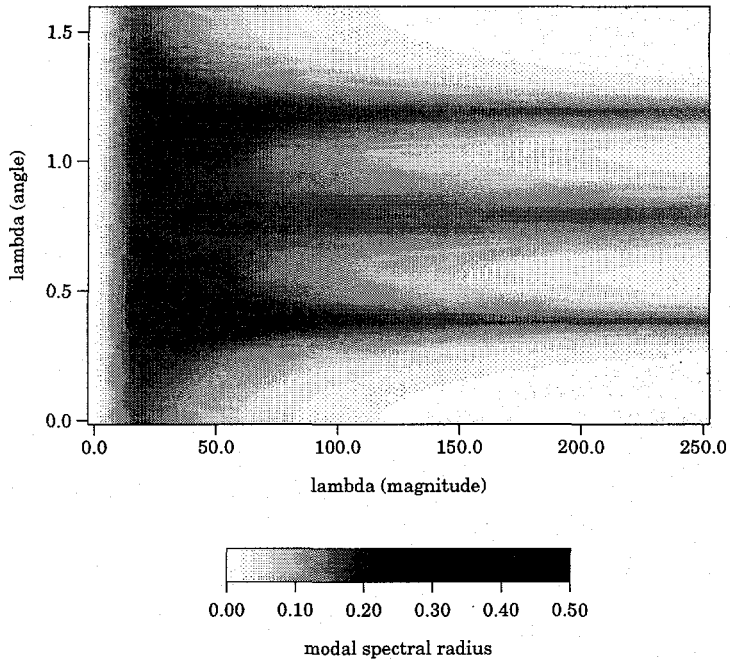

Fig. 2. Fourier analysis of S_4-DSA iteration, isotropic scattering.

In Table I we list values for σ_{sn} and the associated scattering ratios $|c_n|$ for a P_4 expansion ($L = 4$) with $\sigma_{tr} = 1$ and $\hat{\sigma}_a = 0$. The scattering ratios associated with unaccelerated moments form lower bounds on the overall iterative spectral radius. For an S_4-DSA calculation that uses the standard FP kernel, Table I shows that the spectral radius will be at least 0.9. However, we can make some improvements by applying an optimized transport correction. In the S_4-DSA case we subtract the value $(\sigma_4 + \sigma_1)/2$ from all of the scattering moments, resulting in the optimized values of σ_{sn} and $|c_n|$ listed in Table I. With this transport correction the modal spectral radius is reduced to 0.82.

We now apply a Fourier analysis to the S_4-DSA iteration with the optimized FP kernel derived above and no absorption. Solution of Eq. (84) for the modal spectral radii yields the results displayed in Figure 3. The high frequency results are very similar to the isotropic case:

TABLE I

Standard and Optimized P_4 FP Cross Sections and Scattering Ratios

n	σ_{sn} (standard)	$\lvert c_n \rvert$ (standard)	σ_{sn} (optimized)	$\lvert c_n \rvert$ (optimized)
0	10	1.0	5.5	1.0
1	9	0.9	4.5	0.82
2	7	0.7	2.5	0.46
3	4	0.4	-0.5	0.09
4	0	0.0	-4.5	0.82

despite some narrow regions of increased modal spectral radii the iteration scheme is fairly effective. However, at low frequencies the spectral radius is close to unity. The modal spectral radius for $|\lambda| = 0$ is indeed 0.82, as derived above, although for intermediate frequencies it is as high as 0.90, the overall iterative spectral radius. This demonstrates the ineffectiveness of DSA for highly anisotropic scattering and the need to accelerate additional moments.

In Figures 4 and 5 we plot the modal spectral radius for S_6-DSA and S_8-DSA iterations, respectively, with optimized FP kernels. Because of the increased quadrature orders we need to use FP expansions of higher order, so the scattering anisotropy is more extreme. In the S_6 case the flat modal spectral radius with an optimized FP kernel is 0.91 (reduced from 0.95 with the standard FP expansion). The overall S_6-DSA spectral radius is 0.95. In the S_8 case the flat modal spectral radius is 0.95 (reduced from 0.97 with the standard FP expansion). The overall S_8-DSA spectral radius is 0.97. Not only does DSA become even more ineffective as higher order FP expansions are used, but the optimized transport correction also loses effectiveness. The high frequency behavior is similar to that seen in the S_4-DSA results. Note that as we increase the FP expansion order in these analyses we keep $\sigma_{tr} = 1$, which means that σ_t increases. This may explain why the qualitative trends in Figures 3-5 seem to scale to progressively higher frequencies as we increase the quadrature and scattering

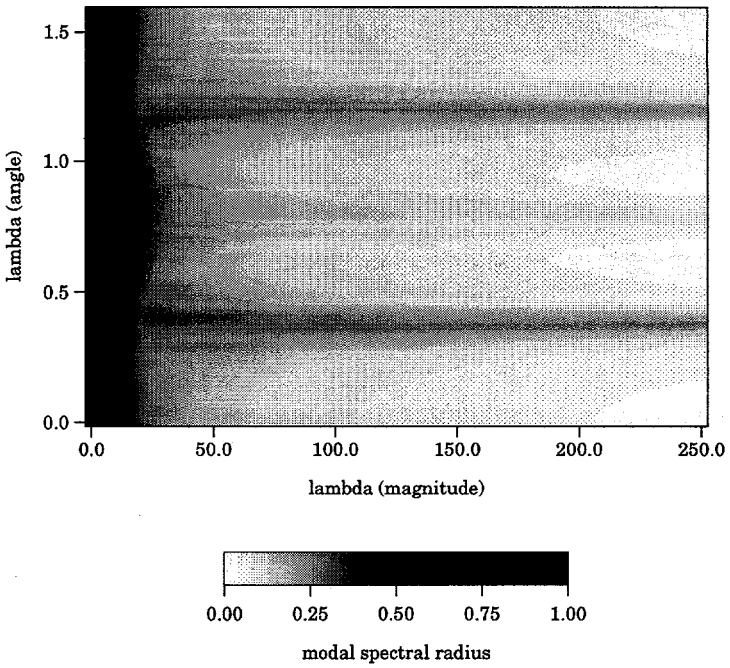

Fig. 3. Fourier analysis of S_4-DSA iteration, optimized FP scattering.

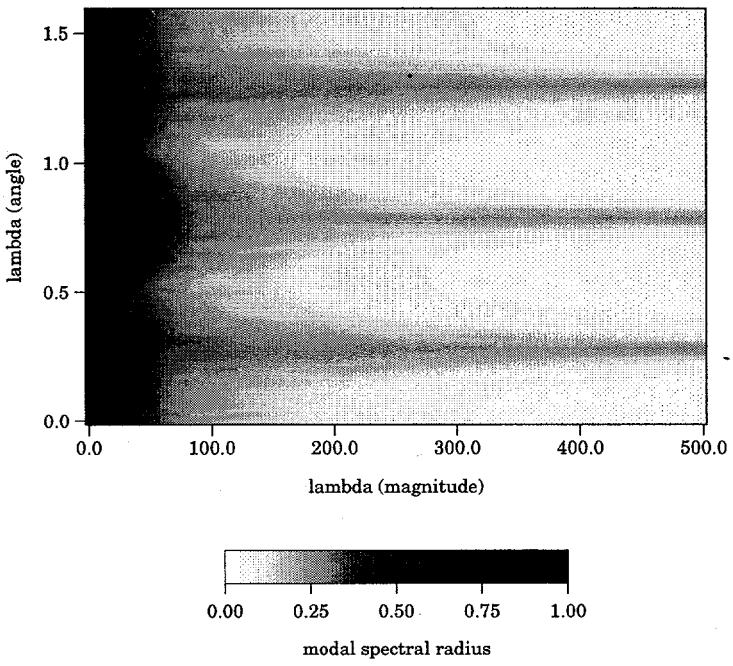

Fig. 4. Fourier analysis of S_6-DSA iteration, optimized FP scattering.

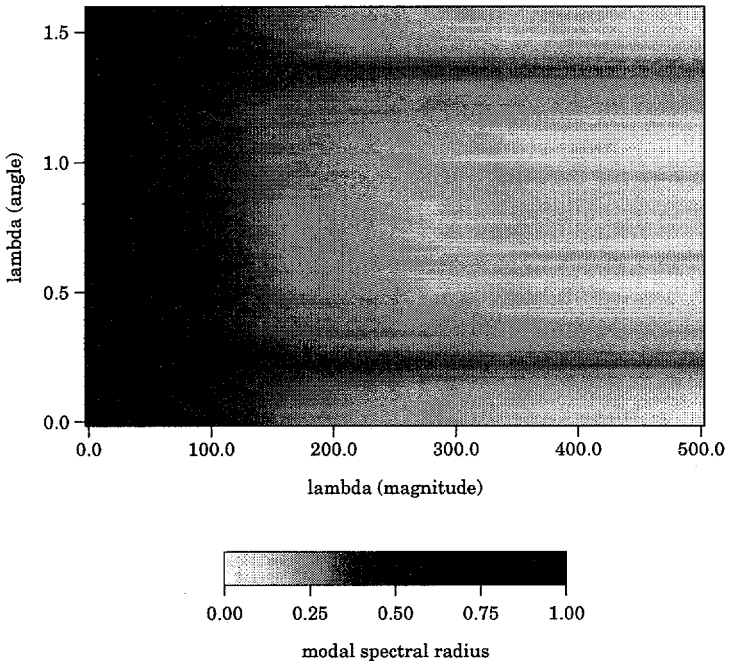

Fig. 5. Fourier analysis of S_8-DSA iteration, optimized FP scattering.

order. One final aspect that these analyses reveal about DSA-accelerated S_N schemes with forward-peaked scattering is that the eigenvalues of greatest absolute value occur in complex conjugate pairs; in contrast, in relatively isotropic problems the dominant eigenvalues are almost always real.[136] This difference will become important when we attempt to confirm our Fourier analyses numerically.

Now that we have demonstrated the Fourier analysis method and have shown in greater detail the ineffectiveness of DSA when applied to forward-peaked problems, we will Fourier analyze several specific examples of the ANMG acceleration method. Our first example is the DSA-accelerated two-grid scheme presented in Eqs. (74). We augment the Fourier ansatz

of Eqs. (80) with the following:

$$\psi_k'^{(l)} = \omega^l c_k' e^{i\boldsymbol{\lambda}\cdot\mathbf{r}}, \tag{86a}$$

$$\varphi_{nm}'^{(l)} = \omega^l C_{nm}' e^{i\boldsymbol{\lambda}\cdot\mathbf{r}}. \tag{86b}$$

We substitute the Fourier ansatz into Eqs. (74). Equations (74a) and (74b) yield Eq. (81). Equations (74c) and (74d) yield

$$\mathbf{C}' = D_{N'} L_{N'}^{-1} M_{N'} P_{N\to N'} \Sigma_N (\mathbf{A} - \mathbf{B}) \equiv S_{N\to N'} (\mathbf{A} - \mathbf{B}). \tag{87}$$

Equation (74e) yields

$$C_{DSA} = L_{DSA}^{-1} P_{N'\to 0} \Sigma_{N'} \mathbf{C}' \equiv S_{DSA} \mathbf{C}'. \tag{88}$$

Equation (74f) yields

$$\omega\mathbf{B} - \mathbf{A} = P_{N'\to N} [\mathbf{C}' + P_{0\to N'} C_{DSA}]. \tag{89}$$

Finally, combining Eqs. (81) and (87)-(89) yields

$$\omega\mathbf{B} = [P_{N'\to N} (P_{0\to N'} S_{DSA} + I_{N'}) S_{N\to N'} (S_N - I_N) + S_N] \mathbf{B}. \tag{90}$$

We solve the above eigenvalue problem for the S_4-S_2-DSA scheme ($N = 4, N' = 2$) with FP scattering and an optimized transport correction on each level ("optimized" will always mean that at each level the absolute values of the scattering ratios corresponding to moments that are unaccelerated at lower levels are minimized). The flat modes of this

scheme will have a modal spectral radius of 0.54. The Fourier analysis results are shown in Figure 6. The multigrid scheme does indeed accelerate low-frequency modes well, as predicted. However, this scheme also excites high-frequency errors that correspond to one of the quadrature directions; the resulting spectral radius is 2.37 (in the figure all modal spectral radii greater than 2.0 are plotted as 2.0). Therefore this specific application of the ANMG method is unstable and cannot be used without modification.

Before we address the question of whether we can stabilize the S_4-S_2-DSA iteration let us first analyze some other ANMG schemes to determine whether high-frequency instabilities are common for plane waves along quadrature directions for this class of acceleration methods. We extend Eqs. (74) to allow for an additional discrete ordinates level. This three-

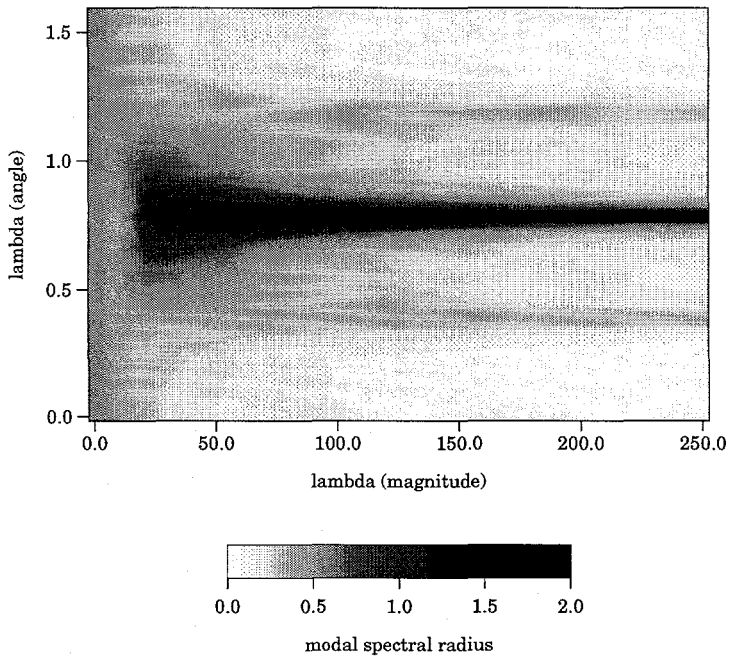

Fig. 6. Fourier analysis of S_4-S_2-DSA iteration, optimized FP scattering.

grid scheme consists of Eqs. (74a)-(74d) and the following:

$$\left[\Omega\cdot\nabla+\sigma_t\right]_{N''}\Psi^{''(l)} = M_{N''}P_{N'\rightarrow N''}\Sigma_{N'}\Phi^{'(l)}, \tag{91a}$$

$$\Phi^{''(l)} = D_{N''}\Psi^{''(l)}, \tag{91b}$$

$$\left[-\nabla\cdot\frac{1}{3\sigma_{t,N''}}\nabla+\sigma_a\right]f^{(l)} = P_{N''\rightarrow 0}\Sigma_{N''}\Phi^{''(l)}, \tag{91c}$$

$$\Phi^{(l+1)} = \Phi^{\left(l+\frac{1}{2}\right)}+P_{N'\rightarrow N}\Phi^{'(l)}+P_{N''\rightarrow N}\Phi^{''(l)}+P_{0\rightarrow N}f^{(l)}. \tag{91d}$$

The extension of these equations to even more grids is obvious. We again augment the Fourier ansatz to include the additional level:

$$\psi_k^{''(l)} = \omega^l c_k'' e^{i\lambda\cdot\mathbf{r}}, \tag{92a}$$

$$\varphi_{nm}^{''(l)} = \omega^l C_{nm}'' e^{i\lambda\cdot\mathbf{r}}. \tag{92b}$$

We substitute the Fourier ansatz into Eqs. (74a)-(74d) and (91). We obtain Eqs. (81) and (87) as before. Equations (91a)-(91b) yield

$$\mathbf{C}'' = D_{N''}L_{N''}^{-1}M_{N''}P_{N'\rightarrow N''}\Sigma_{N'}\mathbf{C}' \equiv S_{N'\rightarrow N''}\mathbf{C}'. \tag{93}$$

Equation (91c) yields

$$C_{DSA} = L_{DSA}^{-1}P_{N''\rightarrow 0}\Sigma_{N''}\mathbf{C}'' \equiv S_{DSA}\mathbf{C}''. \tag{94}$$

Equation (91d) yields

$$\omega\mathbf{B} - \mathbf{A} = P_{N'\rightarrow N}\left[\mathbf{C}' + P_{N''\rightarrow N'}\left(\mathbf{C}'' + P_{0\rightarrow N''}C_{DSA}\right)\right]. \tag{95}$$

Finally, combining Eqs. (81), (87), and (93)-(95) yields

$$\omega\mathbf{B} = \left[P_{N'\rightarrow N}\left\{P_{N''\rightarrow N'}\left(P_{0\rightarrow N''}S_{DSA} + I_{N''}\right)S_{N'\rightarrow N''} + I_{N'}\right\}S_{N\rightarrow N'}\left(S_N - I_N\right) + S_N\right]\mathbf{B}. \tag{96}$$

Equation (96) describes the eigenvalues of a general three-grid iteration.

We now examine the particular schemes S_6-S_4-S_2-DSA and S_8-S_4-S_2-DSA with optimized FP scattering. Our selection of the number of grids and their quadrature orders is identical to that of Morel and Manteuffel (with the addition of the S_2 operator), in which $N' = Half\,(N)$, where

$$Half\,(N) = \begin{cases} \frac{N}{2}, & \frac{N}{2}\ even \\ \frac{N}{2}+1, & \frac{N}{2}\ odd \end{cases}. \tag{97}$$

Our analysis of flat modes with optimized transport corrections gives a modal spectral radius of 0.40 for the S_6-S_4-S_2-DSA iteration and 0.57 for the S_8-S_4-S_2-DSA iteration. The Fourier analyses of these schemes are shown in Figures 7 and 8. We observe the same qualitative behavior seen in the S_4-S_2-DSA iteration. Low-frequency modes are well accelerated by the ANMG method. However, high-frequency instabilities plague this acceleration scheme. The spectral radius for the S_6-S_4-S_2-DSA iteration is 1.62; that of the S_8-S_4-S_2-DSA iteration is 2.44. Additional analyses confirm that these instabilities are not the result solely of the S_2 or DSA operators; accelerating the high-order operator by inverting any of the lower-order discrete ordinates operators creates high-frequency instabilities. It seems reasonable to expect

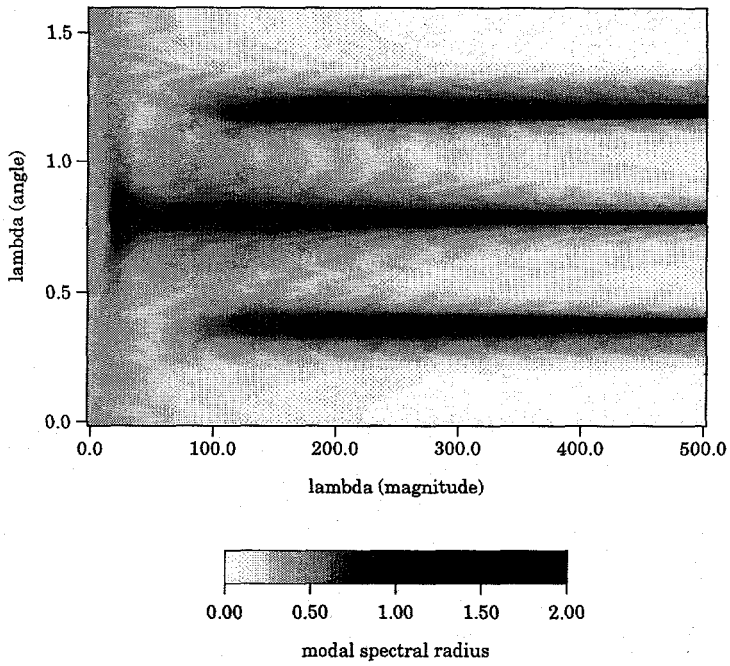

Fig. 7. Fourier analysis of S_6-S_4-S_2-DSA iteration, optimized FP scattering.

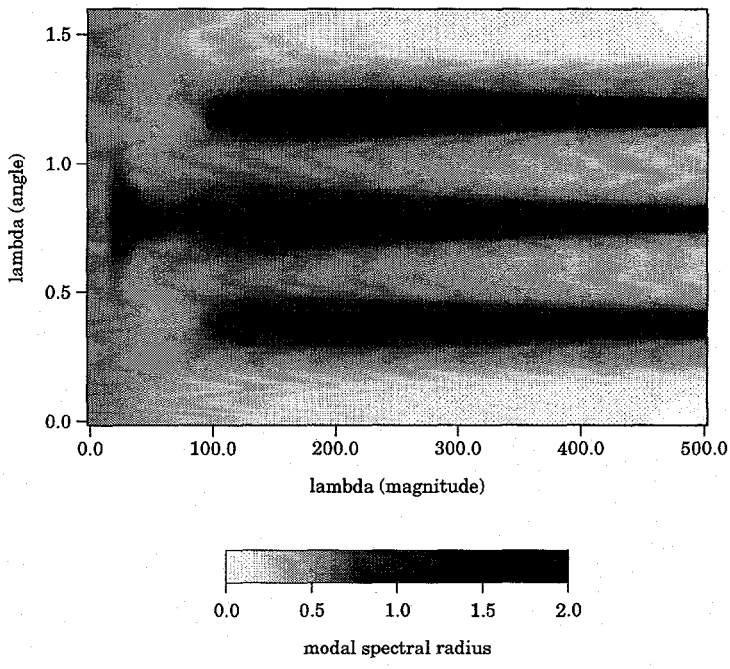

Fig. 8. Fourier analysis of S_8-S_4-S_2-DSA iteration, optimized FP scattering.

that higher-order ANMG methods will also exhibit this general behavior: low-frequency modes will be well accelerated, but the overall iteration will be destabilized by certain high-frequency modes. If we wish to use this type of acceleration method we need to find a way to stabilize the high-frequency corrections without significantly degrading the acceleration of low-frequency modes.

Two observations will guide our development of a stable ANMG acceleration method. First, low-frequency modes are stable and well accelerated by the basic ANMG scheme. If possible, we do not want to define any modifications that alter the low-frequency corrections. Second, the Fourier analyses of ordinary source iteration (with or without DSA acceleration) show that the high-frequency modes are stable and well attenuated by that iteration; it is the ANMG corrections that destabilize these modes. Therefore we desire a modification to the ANMG scheme that produces little or no correction at high frequencies. In summary, we seek an operator that we can apply to the ANMG corrections that is the identity for low-frequency modes and is the zero operator for high-frequency modes. This is a classic description of a low-pass filter; it also may be used as a working definition of an elliptic operator. Desirable properties for such an operator in our situation are that it is easily invertible and easily implemented.

Such an elliptic operator is already in use in the acceleration schemes we have examined so far: it is the diffusion operator for DSA. At high frequencies the ∇^2 term becomes very large, so its inversion results in a vanishingly small correction. On the other hand, at low frequencies the ∇^2 term becomes negligible compared to a non-zero absorption term; if $\sigma_a = \sigma_{s0}$ then we have the identity. We therefore propose to modify the ANMG acceleration

method by replacing the equation for the corrections with the following:

$$\mathbf{f}_{corr}^{(l)} = \mathbf{\Phi}'^{(l)} + P_{N''\rightarrow N'}\mathbf{\Phi}''^{(l)} + P_{N'''\rightarrow N'}\mathbf{\Phi}'''^{(l)}\cdots, \quad (98a)$$

$$\left[-\boldsymbol{\nabla}\cdot\frac{\alpha_f}{3\sigma_f}\boldsymbol{\nabla}+\sigma_f\right] f'^{(l)}_{corr,nm} = \sigma_f f^{(l)}_{corr,nm},\ (n,m)\in Q_{N'}, \quad (98b)$$

$$\mathbf{\Phi}^{(l+1)} = \mathbf{\Phi}^{\left(l+\frac{1}{2}\right)} + P_{N'\rightarrow N}\left[\mathbf{f}'^{(l)}_{corr} + P_{0\rightarrow N'}f^{(l)}_{DSA}\right], \quad (98c)$$

where for now we shall let $\sigma_f = \sigma_{t,N}$.

Note several things about the above modifications. First, we do not propose to filter the DSA corrections; these corrections are small at high frequencies and have already been observed to be stable. Second, the filter contains a tuning parameter α_f; we may adjust this parameter to define the boundary between "low" frequencies and "high" frequencies. Third, at low and high frequencies the filter will in fact limit to the identity and the zero operator, respectively, as desired. Last, the filter is applied to each angular moment independently. One of the ramifications of this is that the filter is easily parallelizable and hence may result in little additional computational cost. It also means that for a given spatial error mode the filter is simply a multiplicative constant for all of the angular moments of that mode. Therefore it does not matter whether we calculate the ANMG corrections and then filter them or if we apply the filter to the residual that drives the ANMG method; the final ANMG corrections are the same. (This reordering of operators would result in the filtering of the DSA corrections, however.)

A Fourier analysis of the filtered ANMG method yields the following eigenvalue problem (written here for the three-grid scheme):

$$\omega \mathbf{B} = \left[P_{N' \to N} \left\{ P_{0 \to N'} S_{DSA} S_{N' \to N''} + F_{aug}^{-1} S_{corr} \right\} S_{N \to N'} \left(S_N - I_N \right) + S_N \right] \mathbf{B}, \qquad (99)$$

where

$$F_{aug} = diag \left\{ 1 + \alpha_f \left| \boldsymbol{\lambda} \right|^2 / 3\sigma_f^2 \right\}, \qquad (100a)$$

$$S_{corr} = P_{N'' \to N'} S_{N' \to N''} + I_{N'}. \qquad (100b)$$

We solve Eq. (99), or its generalization to ANMG methods of an arbitrary number of levels, for the S_4-S_2-DSA-filter, S_6-S_4-S_2-DSA-filter, and S_8-S_4-S_2-DSA-filter iterations with optimized FP scattering and $\alpha_f = 1$. The results are shown in Figures 9-11. These figures show that the spatially analytic ANMG acceleration method is stable and effective for S_N discretizations of order 4, 6, and 8 when the ANMG corrections are diffusively filtered. The spectral radii for the filtered schemes are 0.65, 0.63, and 0.85 for the S_4, S_6, and S_8 schemes, respectively. It is not surprising that the spectral radii are larger than the modal spectral radii for flat modes; this is seen in DSA-accelerated schemes. The spectral radius for the S_8-ANMG iteration is noticeably higher than for the other iterations; a comparison of Figures 8 and 11 shows that in this particular case the filter may be tuned to too high a frequency "cutoff", which we shall define as the frequency of the modes that are reduced in magnitude by a factor of 2 by the filter.

Let us look at the effect of adjusting the filter tuning parameter, α_f. Figure 12 shows the effect of reducing α_f to 0.1 on the S_8 ANMG iteration, which should allow higher frequency

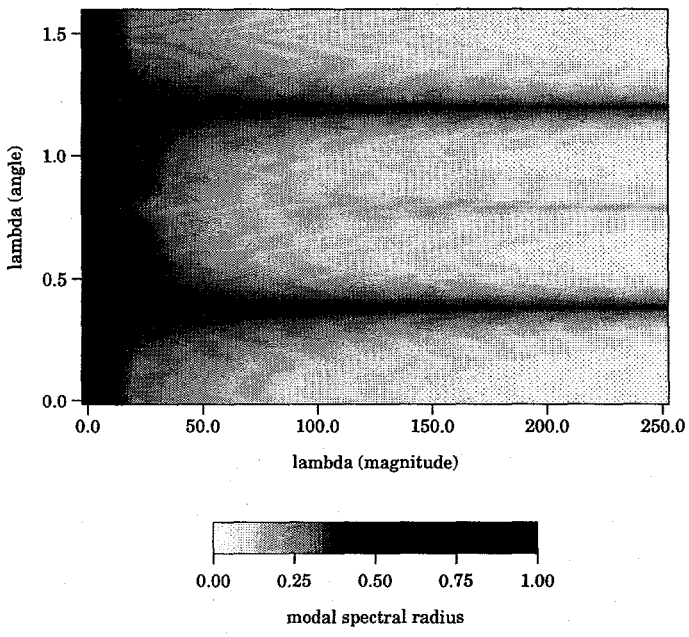

Fig. 9. Fourier analysis of S_4-S_2-DSA-filter iteration, optimized FP scattering $(\alpha_f = 1, \sigma_f = \sigma_{t,4})$.

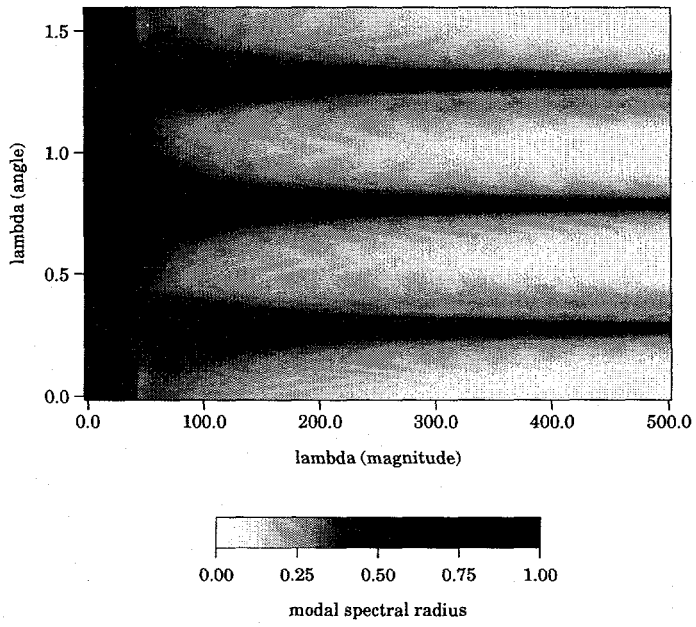

Fig. 10. Fourier analysis of S_6-S_4-S_2-DSA-filter iteration, optimized FP scattering $(\alpha_f = 1, \sigma_f = \sigma_{t,6})$.

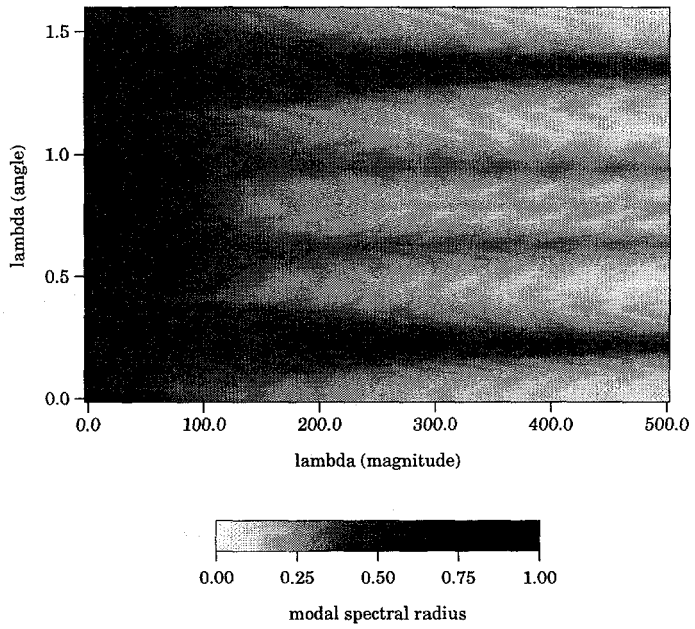

Fig. 11. Fourier analysis of S_8-S_4-S_2-DSA-filter iteration, optimized FP scattering ($\alpha_f = 1, \sigma_f = \sigma_{t,8}$).

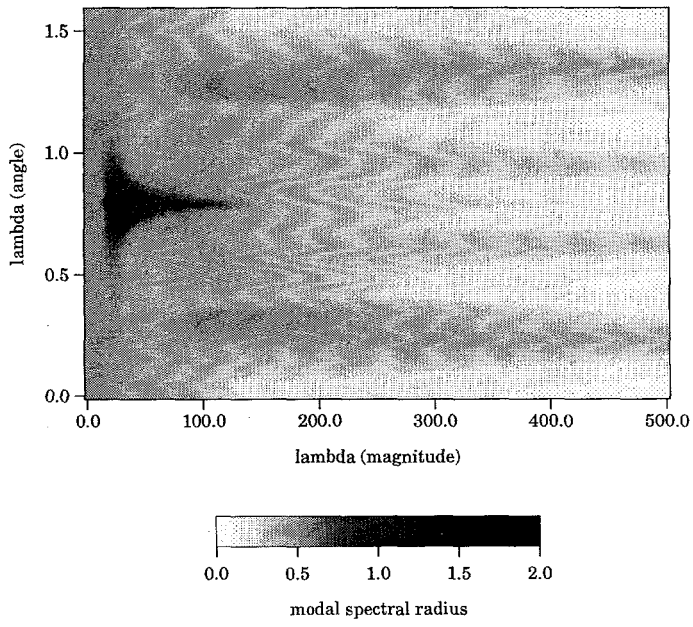

Fig. 12. Fourier analysis of S_8-S_4-S_2-DSA-filter iteration, optimized FP scattering ($\alpha_f = 0.1, \sigma_f = \sigma_{t,8}$).

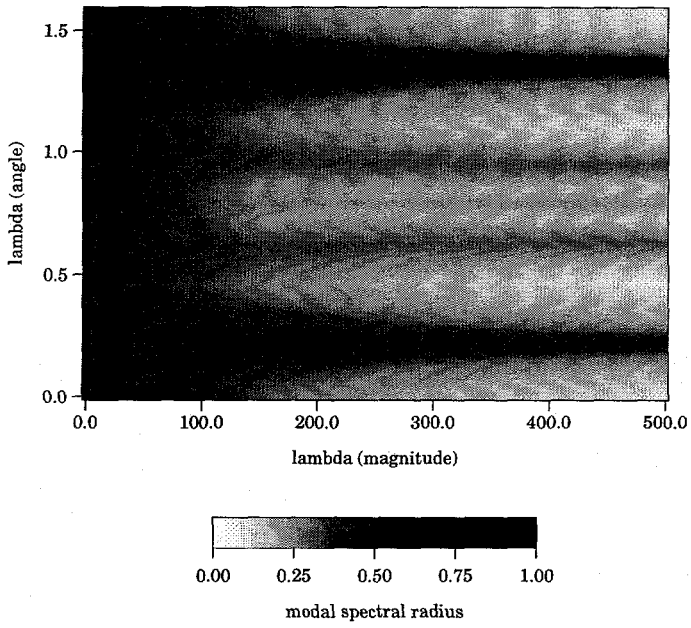

Fig. 13. Fourier analysis of S_8-S_4-S_2-DSA-filter iteration, optimized FP scattering ($\alpha_f = 10, \sigma_f = \sigma_{t,8}$).

corrections to pass through unchanged. The tuning parameter is too low in this case; the high-frequency instabilities are clearly present. Figure 13 shows the effect of increasing α_f to 10 on the S_8 ANMG iteration. Although the marginally stable region in Figure 11 has now been effectively filtered, the modal spectral radii of some other modes of the same frequency magnitude have increased, resulting in an overall spectral radius of 0.72. These results show that the selection of an optimal value for α_f is not trivial. If α_f is too low then the ANMG method is destabilized by high-frequency corrections; if α_f is too high then the ANMG method loses some of its effectiveness.

In practice, it is desirable to use a constant value of α_f that yields an unconditionally stable and effective ANMG acceleration scheme for any S_N order. The appearance of a frequency region of increased modal spectral radii in the filtered S_8-ANMG iteration that was

TABLE II

Spectral Radii of Filtered S_N-ANMG Iterations ($\alpha_f = 1$, $\sigma_f = \sigma_{t,N}$)

N	σ	$\lvert\lambda_{slow}\rvert$
4	0.65	≈ 0
6	0.63	≈ 0
8	0.85	21.4
10	0.95	19.3
12	1.04	20.7
14	1.32	25.4

not present in the S_4 or S_6 schemes suggests that we should examine the ANMG acceleration of some higher-order problems to determine if this is an indicator of an undesirable trend. In Table II we record the spectral radii and the frequencies of the slowest-converging modes of a sequence of filtered S_N-ANMG iterations with $\alpha_f = 1$ and $\sigma_f = \sigma_{t,N}$. As N increases the spectral radius increases rapidly; in fact, the S_{12} and S_{14} iterations are unstable. The parametric study of the previous paragraph leads us to believe that a sufficiently large value of α_f would stabilize these iterations, but this does not guarantee that a constant value of α_f would stabilize S_N-ANMG iterations of an arbitrary order.

In order to determine whether we can define a filter which yields an unconditionally stable ANMG scheme, we first note that the instabilities recorded in Table II occur at approximately the same frequency. Thus we desire a filter that has the same frequency cutoff regardless of S_N order. The filter we have defined in Eq. (98b) does *not* have a constant cutoff frequency when $\sigma_f = \sigma_{t,N}$. The cutoff frequency in this case is

$$\lambda = \sigma_{t,N}\sqrt{\frac{3}{\alpha_f}}. \tag{101}$$

TABLE III

Spectral Radii of Filtered S_N-ANMG Iterations ($\alpha_f = 1$, $\sigma_f = \sigma_{tr}$)

N	σ	$\lvert\lambda_{slow}\rvert$
4	0.70	3.2
6	0.81	4.1
8	0.86	6.7
10	0.90	7.7
12	0.92	8.2
14	0.94	9.3

As the quadrature and scattering orders increase the FP cross section expansion yields an increasing value of $\sigma_{t,N}$, which increases the cutoff frequency. However, σ_{tr} is constant with respect to the cross section expansion order. Therefore, if we let $\sigma_f = \sigma_{tr}$ we can expect the filter to scale to higher quadrature orders without any changes to its frequency properties; its cutoff frequency is

$$\lambda = \sigma_{tr}\sqrt{\frac{3}{\alpha_f}}. \tag{102}$$

In Table III we record the spectral radii and corresponding slowest-converging frequencies for a sequence of filtered S_N-ANMG iterations with $\alpha_f = 1$ and $\sigma_f = \sigma_{tr}$. All of the iterations examined are stable, although the spectral radii are gradually increasing. Note that the frequencies of the slowest-converging modes are greater than the cutoff frequency, which is about 1.7. Therefore their modal spectral radii are close in value to the corresponding modal spectral radii of simple source iteration, which is stable. We thus expect the ANMG scheme to remain stable for increasingly higher S_N orders when $\alpha_f = 1$ and $\sigma_f = \sigma_{tr}$; the trend in Table III suggests, however, that the scheme may become increasingly ineffective. Nevertheless, since low-frequency modes are better accelerated by the ANMG scheme

than by DSA alone the ANMG scheme should remain more effective than simple DSA-acceleration.

In summary, the analyses of this chapter have shown that common acceleration schemes for discrete ordinates problems with source iteration are ineffective when scattering is highly forward-peaked; numerous flux moments need to be accelerated. The basic (unfiltered) spatially analytic ANMG method is an effective acceleration method for low-frequency modes in these problems, but it generally is subject to high-frequency instabilities. These instabilities can be eliminated by filtering the corrections with an elliptic operator; the diffusion equation is preferred for practical reasons since it is already used for DSA. The filter may be tuned to define the boundary between low and high frequencies; the selection of the tuning parameter affects the stability and effectiveness of the ANMG method. Since all of these results are obtained from analyses of the spatially analytic equations, we need to perform additional analyses to determine whether these properties remain when we apply spatial discretizations to these methods.

CHAPTER V

ANMG ACCELERATION OF THE SPATIALLY DISCRETIZED DISCRETE ORDINATES EQUATIONS

In the previous chapter we extended the angular multigrid scheme to the spatially analytic discrete ordinates equations in x-y geometry. Our analysis showed that the basic ANMG scheme is subject to high-frequency instabilities, but that the method is stable and effective when the ANMG corrections are diffusively filtered. Although we did not examine the method in three dimensions, experience has shown that the qualitative behavior of transport methods in x-y-z geometry is close to that seen in x-y geometry. Therefore we will assume that the spatially analytic ANMG method is stable and effective in x-y-z geometry, unless subsequent numerical tests show otherwise.

We now focus on the application of the ANMG method to the spatially discretized S_N equations in x-y geometry. Conceptually this is simple, since we will be using the same type of operators that we used in the spatially analytic case. The discrete ordinates equations that we choose to examine are the class of finite element methods presented in Eq. (46). As DSA and filter operators we will consider the methods presented in Appendix A. These are the modified 4-step operator[109] and the DSA operator of Wareing, Larsen, and Adams[73] (WLA), as modified by Wareing.[137]

As in the last chapter we will employ Fourier analyses to determine the stability and effectiveness of the various iterative methods. Specifically, we want to determine whether the spatially discretized ANMG method is effective at accelerating flat modes and whether it is subject to high-frequency instabilities. If instabilities are present, we need to determine

whether the candidate filter operators are "discrete elliptic", that is, whether they eliminate high-frequency modes while having little or no effect on flat modes. Assuming that the filters are effective and stable, we want to determine the spectral radii for a variety of ANMG-accelerated discrete ordinates calculations.

V.A. Development of Fourier Analysis Equations

We begin by introducing a Fourier ansatz that is applicable to the FEM framework. We include all of the variables that will be used in the final ANMG method; not all will be used in the methods that precede it in our analyses. Our discrete Fourier ansatz is

$$\psi_{k,c,ij}^{\left(l+\frac{1}{2}\right)} = \omega^l a_{k,c} e^{i(\lambda_x x_i + \lambda_y y_j)}, \tag{103a}$$

$$\varphi_{nm,c,ij}^{\left(l+\frac{1}{2}\right)} = \omega^l A_{nm,c} e^{i(\lambda_x x_i + \lambda_y y_j)}, \tag{103b}$$

$$\varphi_{nm,c,ij}^{(l+1)} = \omega^{l+1} B_{nm,c} e^{i(\lambda_x x_i + \lambda_y y_j)}, \tag{103c}$$

$$\psi_{k,c,ij}^{\prime(l)} = \omega^l c'_{k,c} e^{i(\lambda_x x_i + \lambda_y y_j)}, \tag{103d}$$

$$\varphi_{nm,c,ij}^{\prime(l)} = \omega^l C'_{nm,c} e^{i(\lambda_x x_i + \lambda_y y_j)}, \tag{103e}$$

$$\psi_{k,c,ij}^{\prime\prime(l)} = \omega^l c''_{k,c} e^{i(\lambda_x x_i + \lambda_y y_j)}, \tag{103f}$$

$$\varphi_{nm,c,ij}^{\prime\prime(l)} = \omega^l C''_{nm,c} e^{i(\lambda_x x_i + \lambda_y y_j)}, \tag{103g}$$

$$f_{corr,nm,c,ij}^{(l)} = \omega^l C_{corr,nm,c} e^{i(\lambda_x x_i + \lambda_y y_j)}, \tag{103h}$$

$$f_{corr,nm,c,ij}^{\prime(l)} = \omega^l C'_{corr,nm,c} e^{i(\lambda_x x_i + \lambda_y y_j)}, \tag{103i}$$

$$f^{(l)}_{DSA,c,ij} = \omega^l C_{DSA,c} e^{i(\lambda_x x_i + \lambda_y y_j)}, \tag{103j}$$

where the subscript $c \in \{1,2,3,4\}$ indicates the cell corner in which each variable is defined. Note that we have assigned the same phase $(\lambda_x x_i + \lambda_y y_j)$ to all the variables in a given cell, regardless of their actual location. This is an arbitrary choice, since the selection of a different phase only introduces a multiplicative complex constant into the above ansatz. This constant (and all other multiplicative constants in the Fourier ansatz) will be algebraically eliminated as long as we are consistent in our analysis. The above phase selection has been chosen for its convenience in the following analyses.

In Chapter IV we introduced the Fourier ansatz into the iterative equations to find the transformations between the iterative variables for a given Fourier mode; the combination of these equations yielded an eigenvalue problem. We will do the same thing in the discrete setting, except that we will concentrate more heavily on the transformations defined by each individual operator. The combination of these operators will yield the various iterative equations and corresponding eigenvalue problems.

The first operators we will examine are those defined in the FEM equations in Eq. (46), where we define the left side of Eq. (46a) as the sweep operator, L_N. We substitute the Fourier ansatz of Eq. (103) into L_N and the definitions of Eqs. (46c)-(46j), yielding

$$
\begin{aligned}
L_N \;=\; & \frac{\mu_k}{\Delta x}\mathbf{U}\left[\begin{array}{cccc}
(0,1) & \left(e^{-i\lambda_x\Delta x},0\right) & 0 & 0 \\
\left(0,e^{i\lambda_x\Delta x}\right) & (1,0) & 0 & 0 \\
0 & 0 & (1,0) & \left(0,e^{i\lambda_x\Delta x}\right) \\
0 & 0 & \left(e^{-i\lambda_x\Delta x},0\right) & (0,1)
\end{array}\right]_{(\mu_k>0,\mu_k<0)} \\
& +\frac{\eta_k}{\Delta y}\mathbf{N}\left[\begin{array}{cccc}
(0,1) & 0 & 0 & \left(e^{-i\lambda_y\Delta y},0\right) \\
0 & (0,1) & \left(e^{-i\lambda_y\Delta y},0\right) & 0 \\
0 & \left(0,e^{i\lambda_y\Delta y}\right) & (1,0) & 0 \\
\left(0,e^{i\lambda_y\Delta y}\right) & 0 & 0 & (1,0)
\end{array}\right]_{(\eta_k>0,\eta_k<0)} \\
& +\frac{\mu_k}{\Delta x}\mathbf{K}+\frac{\eta_k}{\Delta y}\mathbf{L}+\sigma_{t,N}\mathbf{M}. \qquad (104)
\end{aligned}
$$

Here we have introduced the notation $(\cdot,\cdot)$; if the left side of the matrix subscripts (i.e. $\mu_k > 0$ or $\eta_k > 0$) is true then (L,R) is evaluated as L, and if the right side is true then (L,R) is evaluated as R.

Next we define the right side of Eq. (46a) as the scattering source operator, Q_N (we ignore the fixed source as usual). Substitution of the Fourier ansatz yields

$$Q_N = M_{N,B}\Sigma_{N,B}\mathbf{M}_B, \qquad (105)$$

where the B subscript indicates that we have defined block matrices. If the original matrix is 4×4 (e.g. $\mathbf{M}$), then the corresponding block matrix is a diagonal block matrix with each block equal to the original matrix. If the original matrix has a dimension equal to the number of quadrature directions (e.g. M_N), then block i,j of the corresponding block matrix is a 4×4 diagonal block with each diagonal element equal to element i,j of the original matrix. The dimension of any of these block matrices is four times the number of quadrature directions.

We can combine the above operators into the following discrete ordinates operators:

$$S_N \equiv D_{N,B} L_{N,B}^{-1} Q_N, \tag{106a}$$

$$S_{N\to N'} \equiv D_{N',B} L_{N',B}^{-1} Q_{N\to N'}, \tag{106b}$$

where

$$Q_{N\to N'} = M_{N',B} P_{N\to N',B} \Sigma_{N,B} \mathrm{M}_B \tag{107}$$

This completes our description of the operators in Eq. (46).

Now we will analyze the diffusion operators that we will use for DSA and for filtering the ANMG corrections. The first operator we will examine is the modified 4-step (M4S) operator of Eq. (A.1a). The left side of this equation is the M4S DSA loss operator, L_{M4S}. Substitution of the Fourier ansatz into L_{M4S} and the definitions of Eqs. (A.1b)-(A.1i) yields the following form for L_{M4S}:

$$\begin{aligned} L_{M4S} &= \frac{\Delta y}{2}\mathbf{G}\left[\begin{array}{cccc} \mathbf{J}_{x1} & \mathbf{J}_{x2} & \mathbf{J}_{x3} & \mathbf{J}_{x4} \end{array}\right] \\ &\quad + \frac{\Delta x}{2}\mathbf{H}\left[\begin{array}{cccc} \mathbf{J}_{y1} & \mathbf{J}_{y2} & \mathbf{J}_{y3} & \mathbf{J}_{y4} \end{array}\right] + \sigma_a \Delta x \Delta y \mathrm{M}, \end{aligned} \tag{108a}$$

$$\mathbf{J}_{x1} = \left[\begin{array}{c} \alpha + \frac{D}{2\Delta x} - \frac{D}{2\Delta x} e^{-i\lambda_x \Delta x} \\ -\frac{D}{2\Delta x} - \left(\alpha - \frac{D}{2\Delta x}\right) e^{i\lambda_x \Delta x} \\ 0 \\ 0 \end{array}\right], \tag{108b}$$

$$\mathbf{J}_{x2} = \left[\begin{array}{c} -\frac{D}{2\Delta x} - \left(\alpha - \frac{D}{2\Delta x}\right) e^{-i\lambda_x \Delta x} \\ \alpha + \frac{D}{2\Delta x} - \frac{D}{2\Delta x} e^{i\lambda_x \Delta x} \\ 0 \\ 0 \end{array}\right], \tag{108c}$$

$$\mathbf{J}_{x3} = \begin{bmatrix} 0 \\ 0 \\ \alpha + \frac{D}{2\Delta x} - \frac{D}{2\Delta x} e^{i\lambda_x \Delta x} \\ -\frac{D}{2\Delta x} - \left(\alpha - \frac{D}{2\Delta x}\right) e^{-i\lambda_x \Delta x} \end{bmatrix}, \tag{108d}$$

$$\mathbf{J}_{x4} = \begin{bmatrix} 0 \\ 0 \\ -\frac{D}{2\Delta x} - \left(\alpha - \frac{D}{2\Delta x}\right) e^{i\lambda_x \Delta x} \\ \alpha + \frac{D}{2\Delta x} - \frac{D}{2\Delta x} e^{-i\lambda_x \Delta x} \end{bmatrix}, \tag{108e}$$

$$\mathbf{J}_{y1} = \begin{bmatrix} \alpha + \frac{D}{2\Delta y} - \frac{D}{2\Delta y} e^{-i\lambda_y \Delta y} \\ 0 \\ 0 \\ -\frac{D}{2\Delta y} - \left(\alpha - \frac{D}{2\Delta y}\right) e^{i\lambda_y \Delta y} \end{bmatrix}, \tag{108f}$$

$$\mathbf{J}_{y2} = \begin{bmatrix} 0 \\ \alpha + \frac{D}{2\Delta y} - \frac{D}{2\Delta y} e^{-i\lambda_y \Delta y} \\ -\frac{D}{2\Delta y} - \left(\alpha - \frac{D}{2\Delta y}\right) e^{i\lambda_y \Delta y} \\ 0 \end{bmatrix}, \tag{108g}$$

$$\mathbf{J}_{y3} = \begin{bmatrix} 0 \\ -\frac{D}{2\Delta y} - \left(\alpha - \frac{D}{2\Delta y}\right) e^{-i\lambda_y \Delta y} \\ \alpha + \frac{D}{2\Delta y} - \frac{D}{2\Delta y} e^{i\lambda_y \Delta y} \\ 0 \end{bmatrix}, \tag{108h}$$

$$\mathbf{J}_{y4} = \begin{bmatrix} -\frac{D}{2\Delta y} - \left(\alpha - \frac{D}{2\Delta y}\right) e^{-i\lambda_y \Delta y} \\ 0 \\ 0 \\ \alpha + \frac{D}{2\Delta y} - \frac{D}{2\Delta y} e^{i\lambda_y \Delta y} \end{bmatrix}. \tag{108i}$$

Similarly, the right side of Eq. (A.1a) is the DSA source operator, Q_{M4S}. The Fourier form of this operator is simply

$$Q_{M4S} = \Delta x \Delta y \mathbf{M} \tag{109}$$

Finally, recognizing that $\mathbf{q}$ in Eq. (A.1a) is the product of σ_{s0} and the zeroth moment of the residual, we may define the overall DSA operator, S_{M4S}:

$$S_{M4S} = L_{M4S}^{-1} Q_{M4S} P_{N\to 0,B} \Sigma_{N,B}, \tag{110}$$

where we assume that we are applying DSA to a discrete ordinates calculation of order N.

If we are using the modified 4-step method as a filter, a Fourier analysis yields a filter operator, F_{M4S}, that is similar to L_{M4S}. The only differences are that all cross sections are replaced by σ_f (including the ones defining the diffusion coefficients) and the diffusion coefficients are multiplied by α_f.

We now examine the modified WLA method, as expressed in Eqs. (A.4) and (A.9). We define the left side of Eq. (A.4) as the continuous DSA loss operator, L_{CD}. The Fourier form of this operator is

$$L_{CD} = \left[\left(\begin{array}{c} \beta_{ij} + \beta_{i-1,j}e^{-i\lambda_x\Delta x} + \beta_{i+1,j}e^{i\lambda_x\Delta x} + \beta_{i,j-1}e^{-i\lambda_y\Delta y} \\ +\beta_{i,j+1}e^{i\lambda_y\Delta y} + \beta_{i-1,j-1}e^{-i(\lambda_x\Delta x+\lambda_y\Delta y)} + \beta_{i-1,j+1}e^{i(-\lambda_x\Delta x+\lambda_y\Delta y)} \\ +\beta_{i+1,j-1}e^{i(\lambda_x\Delta x-\lambda_y\Delta y)} + \beta_{i+1,j+1}e^{i(\lambda_x\Delta x+\lambda_y\Delta y)} \end{array}\right)\right]. \tag{111}$$

The right side of Eq. (A.4) is the continuous DSA source operator, Q_{CD}. Its Fourier form is

$$Q_{CD} = \Delta x\Delta y \left[\begin{array}{c} M_{1,1} + M_{1,2}\left(e^{-i\lambda_x\Delta x} + e^{-i\lambda_y\Delta y}\right) + M_{1,3}e^{-i(\lambda_x\Delta x+\lambda_y\Delta y)} \\ M_{1,1}e^{-i\lambda_x\Delta x} + M_{1,2}\left(1 + e^{-i(\lambda_x\Delta x+\lambda_y\Delta y)}\right) + M_{1,3}e^{-i\lambda_y\Delta y} \\ M_{1,1}e^{-i(\lambda_x\Delta x+\lambda_y\Delta y)} + M_{1,2}\left(e^{-i\lambda_x\Delta x} + e^{-i\lambda_y\Delta y}\right) + M_{1,3} \\ M_{1,1}e^{-i\lambda_y\Delta y} + M_{1,2}\left(1 + e^{-i(\lambda_x\Delta x+\lambda_y\Delta y)}\right) + M_{1,3}e^{-i\lambda_x\Delta x} \end{array}\right]^T. \tag{112}$$

The left side of Eq. (A.9) we define as the discontinuous DSA loss operator, L_{DD}; its Fourier form is

$$L_{DD} = \alpha\Delta y\mathbf{G} + \alpha\Delta x\mathbf{H} + \sigma_a\Delta x\Delta y\mathbf{M}. \tag{113}$$

The right side of Eq. (A.9) is the discontinuous DSA source operator, Q_{DD}. Its Fourier form is

$$Q_{DD} = \alpha \left[\begin{array}{cc} \frac{\Delta x \Delta y}{\alpha} \mathbf{M} & Q_{DD,5} \end{array} \right], \tag{114}$$

where

$$Q_{DD,5} = \left[\begin{array}{c} \Delta y G_{1,1} + \Delta y G_{1,4} e^{i\lambda_y \Delta y} + \Delta x H_{1,1} + \Delta x H_{1,2} e^{i\lambda_x \Delta x} \\ \Delta y G_{2,2} e^{i\lambda_x \Delta x} + \Delta y G_{2,3} e^{i(\lambda_x \Delta x + \lambda_y \Delta y)} + \Delta x H_{2,1} + \Delta x H_{2,2} e^{i\lambda_x \Delta x} \\ \left(\begin{array}{c} \Delta y G_{3,2} e^{i\lambda_x \Delta x} + \Delta y G_{3,3} e^{i(\lambda_x \Delta x + \lambda_y \Delta y)} \\ + \Delta x H_{3,3} e^{i(\lambda_x \Delta x + \lambda_y \Delta y)} + \Delta x H_{3,4} e^{i\lambda_y \Delta y} \end{array} \right) \\ \Delta y G_{4,1} + \Delta y G_{4,4} e^{i\lambda_y \Delta y} + \Delta x H_{4,3} e^{i(\lambda_x \Delta x + \lambda_y \Delta y)} + \Delta x H_{4,4} e^{i\lambda_y \Delta y} \end{array} \right]. \tag{115}$$

Finally, we may combine these operators into the WLA DSA loss operator, L_{WLA}:

$$L_{WLA}^{-1} = L_{DD}^{-1} Q_{DD} \left[\begin{array}{c} I_4 \\ L_{CD}^{-1} Q_{CD} \end{array} \right]. \tag{116}$$

The definitions of Q_{WLA}, S_{WLA}, and F_{WLA} are analogous to those for the modified 4-step method. Q_{WLA} is equal to Q_{M4S}. S_{WLA} is defined as

$$S_{WLA} = L_{WLA}^{-1} Q_{WLA} P_{N \to 0,B} \Sigma_{N,B}. \tag{117}$$

F_{WLA} is equal to L_{WLA} when all cross sections are replaced by σ_f and the diffusion coefficients are multiplied by α_f.

We now combine the operators we have just defined and analyzed into iterative equations and eigenvalue problems. The DSA-accelerated DFEM-S_N equations are analogous to Eq. (64), except that we substitute the spatially discrete operators for the corresponding analytic ones. By the same combination of the Fourier-analyzed operators and equations we obtain an

eigenvalue problem analogous to Eq. (84):

$$\omega \mathbf{B} = \left[P_{0 \to N,B} S_{M4S} \left(S_N - I_{N,B} \right) + S_N \right] \mathbf{B}. \tag{118}$$

If the modified WLA DSA method is used rather than the modified 4-step method, we replace S_{M4S} with S_{WLA} in Eq. (118). The spatially discrete eigenvalue problem for the unfiltered two-grid scheme is analogous to Eq. (90):

$$\omega \mathbf{B} = \left[P_{N' \to N,B} \left(P_{0 \to N'',B} S_{M4S} + I_{N',B} \right) S_{N \to N'} \left(S_N - I_{N,B} \right) + S_N \right] \mathbf{B}. \tag{119}$$

The spatially discrete eigenvalue problem for the unfiltered three-grid scheme is analogous to Eq. (96):

$$\omega \mathbf{B} = \left[\begin{array}{c} P_{N' \to N,B} \left\{ P_{N'' \to N',B} \left(P_{0 \to N'',B} S_{M4S} + I_{N'',B} \right) S_{N' \to N''} + I_{N',B} \right\} \times \\ S_{N \to N'} \left(S_N - I_{N,B} \right) + S_N \end{array} \right] \mathbf{B}. \tag{120}$$

Finally, the spatially discrete eigenvalue problem for the filtered ANMG scheme is analogous to Eq. (99):

$$\omega \mathbf{B} = \left[P_{N' \to N,B} \left\{ P_{0 \to N',B} S_{M4S} S_{N' \to N''} + F_B^{-1} S_{corr} \right\} S_{N \to N'} \left(S_N - I_{N,B} \right) + S_N \right] \mathbf{B}, \tag{121}$$

where F_B is either $F_{M4S,B}$ or $F_{WLA,B}$ and S_{corr} is analogous to Eq. (100b):

$$S_{corr} = P_{N'' \to N',B} S_{N' \to N''} + I_{N',B}. \tag{122}$$

V.B. Fourier Results

In the previous section we derived the Fourier eigenvalue problems for a variety of DFEM discrete ordinates iterations. In this section we solve these eigenvalue problems in order to determine the stability and effectiveness of these iterative schemes. As a baseline case we will use the BLD S_4 equations. We will vary the DFEM method, the quadrature order, and other parameters in order to understand the stability and effectiveness of these iterative methods.

Before we report the results of these studies, we note some differences between spatially discrete and spatially analytic Fourier analyses. In the spatially analytic case we vary only $\boldsymbol{\lambda}$ for a given iterative scheme; in the discrete case we also can vary Δx and Δy. Therefore for every Fourier analysis we might perform in the spatially analytic case there corresponds any number of Fourier analyses in the discrete case. We will select a representative sample of cell dimensions that will reveal the characteristics of the iterative methods for different types of meshes. In addition, a given spatial mesh only supports a limited range of frequencies $\boldsymbol{\lambda}$. Any $\lambda_x \Delta x \times \lambda_y \Delta y$ that lies outside of the range $(0, \pi) \times (0, \pi)$ is, as far as the discrete problem is concerned, identical to some lower frequency that is within this range. Therefore we may limit our search for the iterative spectral radii to the above range of frequencies, whereas in the analytic case we must theoretically examine $\boldsymbol{\lambda}$ of any magnitude.

The search process is conducted by defining a grid of points within the frequency range described above. This grid is defined for the magnitudes and angles of the frequencies rather than their Cartesian components λ_x and λ_y; a 25x50 grid is nominally used. The modal spectral radius for each frequency is calculated and the maximum modal spectral radius (and corresponding frequency) is recorded. A new grid centered on this frequency with a finer grid

spacing and smaller range is defined and the process is repeated. This search on successively finer grids is terminated when two conditions are met: the maximum modal spectral radius found on the most recent grid is within 10^{-4} of the one found on the previous coarser grid and the largest five modal spectral radii found on the most recent grid are within $5\text{x}10^{-4}$ of each other. This process should identify the frequency regions which contain local maxima and then narrow in on the global maximum in most cases.

We begin our Fourier analyses by examining the DSA-accelerated S_4 iteration with BLD spatial discretization, the modified 4-step method, optimized Fokker-Planck scattering, and no absorption. The spectral radii are reported in Table IV. Here we measure the cell thicknesses in units of transport mean free paths, $\sigma_{tr}\Delta x$ and $\sigma_{tr}\Delta y$. We apply an optimized transport correction to the scattering kernel in order to demonstrate the best spectral radii that can be obtained with DSA-acceleration alone. Table IV shows that a spectral radius of 0.90 is obtained regardless of cell dimensions, which is the same value we obtain in the spatially analytic case. This is not surprising, since our spatially analytic results showed that our spectral radius was determined by the flat modes. Not only are the flat modes supported by all mesh sizes, but the vanishingly slow spatial variation of these modes tends to negate the effects of spatial discretization. We also note that the modified 4-step method does not lose its effectiveness as the cell sizes or aspect ratios are varied.

We note in Appendix A that the modified 4-step DSA equations are generally difficult to solve. However, the modified WLA method is relatively easy to solve, albeit at the expense of effectiveness in some situations. In Table V we report the spectral radii for an S_4-DSA calculation that uses the modified WLA method for the DSA operator. Here we can see that this DSA method is ineffective when the mesh cells have a large aspect ratio (where we define

TABLE IV

Fourier Analysis Results, BLD S_4-DSA (M4S) Iteration, Optimized FP Scattering

	$\sigma_{tr}\Delta y$						
$\sigma_{tr}\Delta x$	.001	.01	.1	1	10	100	1000
.001	0.90						
.01	0.90	0.90					
.1	0.90	0.90	0.90				
1	0.90	0.90	0.90	0.90			
10	0.90	0.90	0.90	0.90	0.90		
100	0.90	0.90	0.90	0.90	0.90	0.90	
1000	0.90	0.90	0.90	0.90	0.90	0.90	0.90

TABLE V

Fourier Analysis Results, BLD S_4-DSA (WLA) Iteration, Optimized FP Scattering

	$\sigma_{tr}\Delta y$						
$\sigma_{tr}\Delta x$	.001	.01	.1	1	10	100	1000
.001	0.90						
.01	0.90	0.90					
.1	0.90	0.90	0.90				
1	0.90	0.90	0.90	0.90			
10	0.97	0.97	0.96	0.90	0.90		
100	0.998	0.998	0.997	0.99	0.90	0.91	
1000	0.9998	0.9998	0.9997	0.999	0.99	0.95	0.91

TABLE VI

Fourier Analysis Results, BLD S_6-DSA (WLA) Iteration, Optimized FP Scattering

	$\sigma_{tr}\Delta y$		
$\sigma_{tr}\Delta x$	.01	1	100
.01	0.95		
1	0.95	0.95	
100	0.999	0.99	0.95

the aspect ratio as the ratio of the longer cell side and the shorter cell side). It also appears that some effectiveness is lost as the cells become optically thick. Nevertheless, for most of the cell dimensions studied the modified WLA DSA operator is as effective as the modified 4-step operator. Of course the ANMG method has been developed with the intent of improving on these spectral radii, which are still quite high (and which increase as N increases).

Before we study the stability and effectiveness of the spatially discrete ANMG scheme, let us examine the effectiveness of DSA for higher-order quadratures. In most of the studies to follow we will use the modified WLA method since in actual computations we will implement the scheme that we can easily solve. In Tables VI and VII we report the spectral radii of the S_6-DSA (WLA) and S_8-DSA (WLA) iterations, respectively, with optimized Fokker-Planck scattering (we have reduced the number of studies because of increasing computational cost).

TABLE VII

Fourier Analysis Results, BLD S_8-DSA (WLA) Iteration, Optimized FP Scattering

	$\sigma_{tr}\Delta y$		
$\sigma_{tr}\Delta x$	.01	1	100
.01	0.98		
1	0.98	0.98	
100	0.9995	0.997	0.98

TABLE VIII

Fourier Analysis Results, BLD S_4-S_2-DSA (M4S) Iteration, Optimized FP Scattering

	$\sigma_{tr}\Delta y$						
$\sigma_{tr}\Delta x$	.001	.01	.1	1	10	100	1000
.001	2.34						
.01	2.16	2.11					
.1	1.03	1.03	0.80				
1	0.65	0.65	0.65	0.65			
10	0.65	0.65	0.65	0.65	0.65		
100	0.65	0.65	0.65	0.65	0.65	0.65	
1000	0.65	0.65	0.65	0.65	0.65	0.65	0.65

For cells with high aspect ratios we again have lost DSA effectiveness, but we otherwise obtain nearly the same spectral radii as in the spatially analytic cases.

Now we examine the stability and effectiveness of the unfiltered ANMG scheme. In Table VIII we report the spectral radii of the S_4-S_2-DSA iteration with the modified 4-step DSA and BLD spatial differencing. For very thin cells the iteration is unstable, with spectral radii approaching that of the spatially analytic case (2.37). However, for cells with at least one side longer than about one transport mean free path the iteration is stable and effective. These observations are a direct result of the fact that the ANMG instabilities we have encountered previously occur in high-frequency modes. As we discussed earlier a spatial mesh places an upper limit on the magnitude of the frequencies that can be supported. When the cells become sufficiently thick only stable, low-frequency modes will be observed. Depending on the physical problem and the mesh used, one may not even need to filter or otherwise alter the ANMG corrections for the iteration to be stable and effective, which would save implementation and computational costs.

Now let us look at other ANMG schemes that use the modified WLA method. In Tables IX-XI we report the spectral radii for the S_4-S_2-DSA, the S_6-S_4-S_2-DSA, and the S_8-S_4-S_2-

TABLE IX

Fourier Analysis Results, BLD S_4-S_2-DSA (WLA) Iteration, Optimized FP Scattering

	$\sigma_{tr}\Delta y$						
$\sigma_{tr}\Delta x$	.001	.01	.1	1	10	100	1000
.001	2.34						
.01	2.16	2.11					
.1	1.03	1.03	0.80				
1	0.65	0.65	0.65	0.65			
10	0.91	0.91	0.90	0.78	0.65		
100	0.99	0.99	0.99	0.98	0.89	0.71	
1000	0.999	0.999	0.999	0.998	0.99	0.95	0.74

DSA iterations, respectively, with BLD spatial differencing. A comparison of Tables IX and VIII shows that for thin cells the unfiltered ANMG scheme that uses the modified WLA DSA has the same spectral radii as the scheme that uses the modified 4-step DSA. As before, though, the method is ineffective (although stable) for high aspect ratio cells. We also see some degraded effectiveness for very thick cells. In the S_6 and S_8 cases we observe the same general properties: high-frequency instabilities that appear in meshes consisting of optically thin cells, stability but ineffectiveness when the cells have high aspect ratios, and reasonable effectiveness for other cell dimensions.

In many problems of practical interest the physical medium is optically thick, and the cells that are created by applying a spatial mesh to the problem may be at least several transport mean free paths thick. In these problems the standard ANMG method will be stable

TABLE X

Fourier Analysis Results, BLD S_6-S_4-S_2-DSA (WLA) Iteration, Optimized FP Scattering

	$\sigma_{tr}\Delta y$		
$\sigma_{tr}\Delta x$	.01	1	100
.01	1.21		
1	0.63	0.63	
100	0.99	0.98	0.71

TABLE XI

Fourier Analysis Results, BLD S_8-S_4-S_2-DSA (WLA) Iteration, Optimized FP Scattering

	$\sigma_{tr}\Delta y$		
$\sigma_{tr}\Delta x$	.01	1	100
.01	1.53		
1	0.64	0.64	
100	0.99	0.98	0.71

and effective, as Tables IX-XI indicate. However, there may be situations in which many or all of the cells are optically thin, in which case we must guard against high-frequency instabilities. We have already proposed using a diffusion operator such as the modified 4-step method or the modified WLA method as a low-pass filter to stabilize the ANMG scheme. Earlier in this chapter we stated that their performance depends on whether they are "discrete elliptic", which we defined as eliminating high-frequency modes while leaving low-frequency modes unchanged. Before we apply these filters to the ANMG method to determine their effectiveness in that specific application, let us first examine these operators directly in order to gain insight into their properties.

The first spatially discrete diffusion operator we will examine is the modified 4-step method. It is defined by Eq. (A.1); the Fourier analysis of its operators is given by Eqs. (108)-(110). Recall that if this method is used as a filter we replace all cross sections with σ_f, including the ones embedded in $\mathbf{q}$, and multiply the diffusion coefficients by α_f. If the cells are optically thick ($\sigma_f \Delta x \Delta y$ is large) then the last term in Eq. (108a) and the source term of Eq. (109) dominate; since these terms are equal we obtain the identity in the limit of thick cells, regardless of frequency. Therefore this filter will not alter any ANMG corrections for optically thick cells, which is desirable since there are no instabilities in this situation.

If the cells are optically thin, the behavior of the modified 4-step filter is more complex. Although the individual components of the currents ($\mathbf{J}_{x1}$, etc.) are much larger than the other terms, these terms will cancel each other in the limit of $\boldsymbol{\lambda} \rightarrow 0$. For flat modes we once again obtain the identity, which we desire. On the other hand, the currents will not identically cancel for high-frequency modes, and since these terms become arbitrarily larger than the source term as the frequency is increased and the optical thickness is decreased, we obtain the zero operator in the limit of $\boldsymbol{\lambda} \rightarrow \infty$. This also is a desirable property, since these modes produce the ANMG instabilities. Therefore the modified 4-step operator has the basic properties (in certain limits) that we desire for an ANMG filter.

The filtering properties of the modified WLA method are similar to those of the modified 4-step method, with some slight differences. The modified WLA method is specified by Eqs. (A.4) and (A.9); the Fourier forms of its operators are given in Eqs. (111)-(116). (When the modified WLA method is used as a filter we incorporate σ_f and α_f as described in the previous section.) For spatially thick cells we see that the last term in Eq. (113) and the left portion of the matrix in Eq. (114) dominate, regardless of frequency. These terms are equal, so we obtain the identity in the thick cell limit, as we did with the modified 4-step method. For thin cells we observe that the updated fluxes are set equal to the continuous solution; this is more easily seen in Eq. (A.9). As $\boldsymbol{\lambda} \rightarrow 0$ the diffusion terms in the β coefficients of the continuous equation cancel, and the continuous solution is equal to the average of the associated corner sources. Thus as $\sigma_f \Delta x$, $\sigma_f \Delta y$, and $\boldsymbol{\lambda} \rightarrow 0$ we obtain the "continuous" identity, with all discontinuities eliminated. Since in this limit we expect discontinuities to be vanishingly small anyway, the filter effectively does nothing to modify these modes. On the other hand, as $\boldsymbol{\lambda} \rightarrow \infty$ the diffusion terms dominate, and since they are much larger than the

TABLE XII

Fourier Analysis Results, BLD S_4-S_2-DSA-filter (M4S) Iteration, Optimized FP Scattering ($\alpha_f = 1, \sigma_f = \sigma_{t,4}$)

	$\sigma_{tr}\Delta y$						
$\sigma_{tr}\Delta x$	.001	.01	.1	1	10	100	1000
.001	0.65						
.01	0.65	0.65					
.1	0.65	0.65	0.65				
1	0.65	0.65	0.65	0.65			
10	0.65	0.65	0.65	0.65	0.65		
100	0.65	0.65	0.65	0.65	0.65	0.65	
1000	0.65	0.65	0.65	0.65	0.65	0.65	0.65

source term we obtain the zero operator. Therefore the modified WLA method should be an effective filter for ANMG corrections.

Now that we have theoretical reasons to believe that the modified 4-step and modified WLA methods will be good filters for the ANMG corrections, we will examine their actual performance. In Table XII we report the spectral radii of the S_4-S_2-DSA-filter iteration, where the spatial discretization is BLD, the diffusion operator for both DSA and the filter is the modified 4-step method, the scattering is optimized Fokker-Planck without absorption, $\alpha_f = 1$, and $\sigma_f = \sigma_{t,N}$. We see that the ANMG method works very well when a good DSA and filter operator is used; the spectral radius is 0.65 regardless of cell size. This supports our predictions of the filtering properties of the modified 4-step method.

The performance of the modified WLA method as an ANMG filter is shown in Tables XIII-XV for the S_4-S_2-DSA-filter, S_6-S_4-S_2-DSA-filter, and S_8-S_4-S_2-DSA-filter iterations, respectively, with the same parameters as in the previous case. We see that the instabilities recorded in Tables IX-XI have disappeared in the filtered scheme; the new spectral radii are equal to the ones obtained for the inherently stable, thicker cells. There is some degradation in performance for the inherently stable cells with high aspect ratios when the filter is applied.

TABLE XIII

Fourier Analysis Results, BLD S_4-S_2-DSA-filter (WLA) Iteration, Optimized FP Scattering ($\alpha_f = 1, \sigma_f = \sigma_{t,4}$)

	$\sigma_{tr}\Delta y$						
$\sigma_{tr}\Delta x$	.001	.01	.1	1	10	100	1000
.001	0.65						
.01	0.65	0.65					
.1	0.65	0.65	0.65				
1	0.75	0.72	0.65	0.65			
10	0.98	0.97	0.94	0.80	0.65		
100	0.998	0.998	0.995	0.98	0.89	0.71	
1000	0.9998	0.9998	0.9995	0.998	0.99	0.95	0.74

TABLE XIV

Fourier Analysis Results, BLD S_6-S_4-S_2-DSA-filter (WLA) Iteration, Optimized FP Scattering ($\alpha_f = 1, \sigma_f = \sigma_{t,6}$)

	$\sigma_{tr}\Delta y$		
$\sigma_{tr}\Delta x$	.01	1	100
.01	0.63		
1	0.83	0.63	
100	0.998	0.98	0.71

TABLE XV

Fourier Analysis Results, BLD S_8-S_4-S_2-DSA-filter (WLA) Iteration, Optimized FP Scattering ($\alpha_f = 1, \sigma_f = \sigma_{t,8}$)

	$\sigma_{tr}\Delta y$		
$\sigma_{tr}\Delta x$	.01	1	100
.01	0.90		
1	0.83	0.64	
100	0.998	0.98	0.71

TABLE XVI

Fourier Analysis Results, LBLD S_4-S_2-DSA-filter (WLA) Iteration, Optimized FP Scattering ($\alpha_f = 1, \sigma_f = \sigma_{t,4}$)

	$\sigma_{tr}\Delta y$						
$\sigma_{tr}\Delta x$	.001	.01	.1	1	10	100	1000
.001	0.65						
.01	0.65	0.65					
.1	0.65	0.65	0.65				
1	0.86	0.81	0.65	0.65			
10	0.98	0.98	0.95	0.84	0.65		
100	0.998	0.998	0.995	0.98	0.90	0.72	
1000	0.9998	0.9998	0.9995	0.998	0.99	0.95	0.74

This is not too surprising, since the modified WLA method breaks down in these situations. It does indicate, however, that we want to avoid filtering unless we either must do so to stabilize the iteration or if we have no knowledge of the cell sizes to be used in a given calculation.

As a final analysis of the filtered ANMG scheme we examine other DFEM methods. In Tables XVI and XVII we report the spectral radii for the S_4-S_2-DSA-filter scheme with the modified WLA method and with LBLD and SCB spatial differencing, respectively. The characteristics of these schemes are similar to those seen with BLD differencing. There are no instabilities, but the properties of the modified WLA operator cause the iteration to be ineffective for high aspect ratio cells. Performance is somewhat better for the SCB scheme than for the other DFEM methods for thick cells; the SCB method is already known to behave more physically in this limit.

We remark that in the filtered schemes examined in this section we use $\sigma_f = \sigma_{t,N}$. In the previous chapter our spatially analytic studies revealed that $\sigma_f = \sigma_{tr}$ yields a filter that has better properties as higher quadrature orders are used. Since we have observed that the Fourier analyses of the spatially discretized schemes share important properties with the spatially analytic schemes when $\sigma_f = \sigma_{t,N}$, we are confident that we will observe the same

TABLE XVII

Fourier Analysis Results, SCB S_4-S_2-DSA-filter (WLA) Iteration, Optimized FP Scattering ($\alpha_f = 1, \sigma_f = \sigma_{t,4}$)

	$\sigma_{tr}\Delta y$						
$\sigma_{tr}\Delta x$	.001	.01	.1	1	10	100	1000
.001	0.65						
.01	0.65	0.65					
.1	0.65	0.65	0.65				
1	0.87	0.85	0.72	0.65			
10	0.98	0.98	0.96	0.86	0.65		
100	0.998	0.998	0.995	0.98	0.90	0.65	
1000	0.9998	0.9998	0.9995	0.998	0.99	0.90	0.65

behavior for filters that use $\sigma_f = \sigma_{tr}$ in spatially discretized schemes as seen with spatially analytic schemes.

In summary, the analyses of this chapter have shown that the ANMG scheme applied to x-y DFEM S_N calculations shares many of the characteristics of the spatially analytic method. The standard spatially discrete ANMG method is subject to high-frequency instabilities for thin cells. These instabilities disappear when the cells are of intermediate or large thickness; this desirable property obviously cannot be seen in the spatially analytic case. The spatially discrete scheme can be made unconditionally stable by applying a diffusive filter to the corrections. The effectiveness of the entire scheme is limited by the quality of the discrete diffusion operator, since it is necessary to accelerate the zeroth flux moment in order for the ANMG corrections to be effective.

CHAPTER VI

NUMERICAL RESULTS

In Chapters II and III we showed that under certain conditions the spatially analytic and spatially discretized S_N equations limit to discrete versions of the Fokker-Planck equation when the scattering is highly forward-peaked. In Chapters IV and V we developed an angular multigrid (ANMG) iteration method that is stable and effective for multidimensional S_N calculations with highly forward-peaked scattering. In this chapter we present numerical results that confirm the predictions of these analyses.

VI.A. Fokker-Planck Asymptotic Limit

In this section we will present numerical results that support our Fokker-Planck asymptotic analyses. We will restrict our attention to one-dimensional slab geometry. These results will demonstrate the asymptotic form of the cross section, the asymptotic limit of spatially analytic S_N equations, and the asymptotic limit of several spatial discretizations of the S_N equations.

The specific analytic problem we will examine is defined by Eqs. (1), (2), and

$$\psi(0,\mu) = \delta(1-\mu),\ 0<\mu\leq 1, \tag{123a}$$

$$\psi(L,\mu) = 0,\ -1\leq\mu<0, \tag{123b}$$

$$\sigma_s(\mu_0) = C(\delta)\exp\left(-\frac{1-\mu_0}{\delta}\right), \qquad \sigma_a = 0, \tag{123c}$$

where the value of $C(\delta)$ is such that $\sigma_{tr} = 0.1$. This problem was examined by Börgers and Larsen.[64,65] For this cross section γ is given by

$$\gamma = \delta^2 \left(1 - e^{-2/\delta}\right)^{-1} \left[2 - e^{-2/\delta}\left(4\delta^{-2} + 4\delta^{-1} + 2\right)\right]. \tag{124}$$

As $\delta \rightarrow 0$, $\gamma \rightarrow 2\delta^2$, so the $O(\gamma/\delta)$ term in Eq. (16) vanishes in the FP limit. Thus the problem above is asymptotically described by the FP equation as $\delta \rightarrow 0$.

In Figure 14 we plot the scattering ratios derived from the asymptotic form of the scattering cross section moments in Eq. (8) for $A(\mathbf{r}) = 1$, $\gamma = 0$, and various values of δ. We also plot the corresponding scattering ratios of the cross section given in Eq. (123c). As $\delta \rightarrow 0$ we see that the actual scattering ratios approach the asymptotic values. This demonstrates the validity of Eq. (8). Figure 14 also shows us when we might expect our transport solution to be close to the asymptotic Fokker-Planck limit. For example, a P_{15} cross section expansion for $\delta = 0.001$ is very close to the asymptotic expansion, so the corresponding discrete ordinates solution should be close to a pseudospectral Fokker-Planck solution of the same order.

Next we examine S_N solutions to Eq. (123) near the Fokker-Planck limit. For these studies we use $L = 20$ and $\delta = 0.001$. As boundary conditions we use a quasi-Mark approximation to Eqs. (123a) and (123b) in which all incoming fluxes are set to zero except at the quadrature direction $\mu_{\max}$ closest to $\mu = 1$; we set $\psi(0, \mu_{\max}) = w_{\max}^{-1}$, where $w_{\max}$ is the corresponding (non-Galerkin) quadrature weight. This boundary condition has the effect of preserving the contribution to the boundary scalar flux from the beam in Eq. (123a). (We do not report the results of other calculations that use different boundary conditions, such as conditions which preserve the incident current.) Figure 15 shows the scalar flux

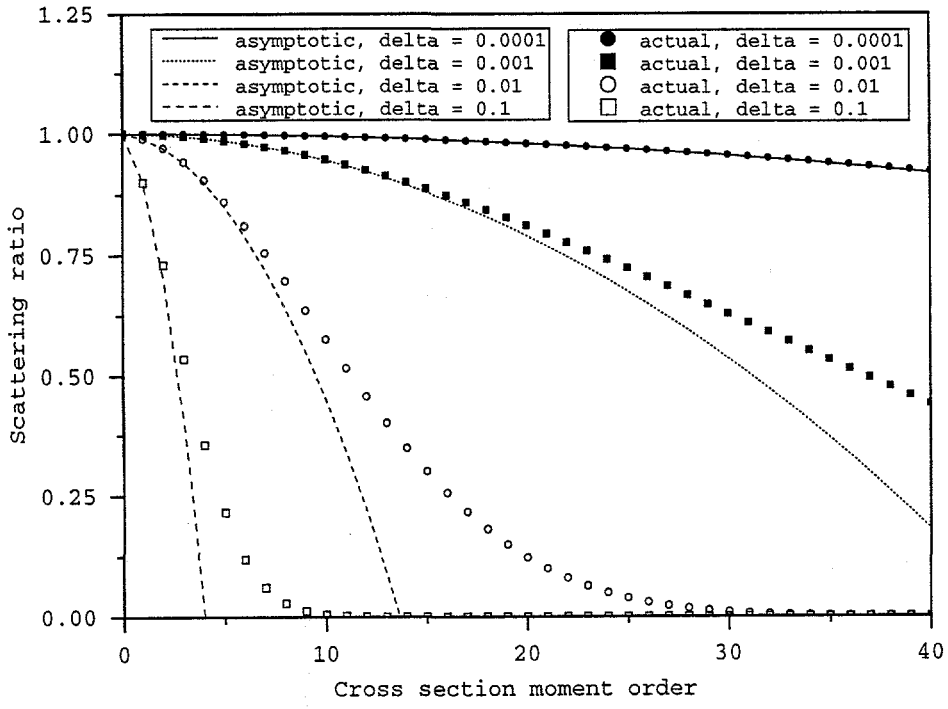

Fig. 14. Scattering ratios vs. cross section moment order, exponential cross section.

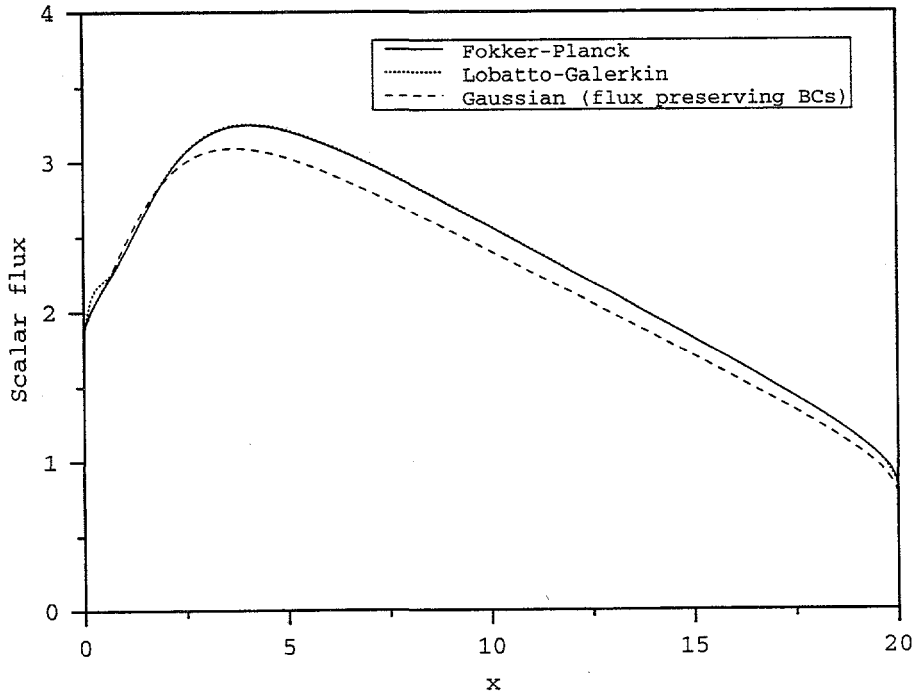

Fig. 15. S_8 scalar fluxes, $\delta = 0.001$.

throughout the slab as calculated by the LM-S_8 method using both the Lobatto-Galerkin and Gaussian quadratures. For these calculations we have used a very fine spatial mesh (200 cells, $\sigma_{tr}\Delta x = 0.01$) to minimize the effects of spatial discretization so that we may concentrate on the effects of the angular differencing. These S_N results compare favorably with a pseudospectral Fokker-Planck solution of order 32. The Lobatto-Galerkin results are especially good; the Lobatto set includes the point $\mu = 1$, so its boundary condition is expected to be better than that used with the Gaussian set. We remark that a stable solution could not be obtained with the Lobatto set without the Galerkin quadrature treatment. These results demonstrate the need to use discrete-to-moments and moments-to-discrete operators that are inverses of each other, as well as the fact that S_N solutions limit to Fokker-Planck solutions under proper conditions.

We now examine the effects of spatial discretization on the S_N solutions. In Figures 16-18 we show DD-, LD-, and LM-S_8 solutions, respectively, as $\delta \rightarrow 0$. We also plot the corresponding DD- and LD-pseudospectral Fokker-Planck solutions as well as the highly refined FP solution that we showed in Figure 15. These figures show that as $\delta \rightarrow 0$, the spatially discrete S_8 solutions approach the spatially discrete FP solutions that we predicted in Chapter III. We note that these discrete FP solutions are fairly accurate, especially the LD results. In Figures 19-21 we show similar results for S_{16} calculations; these solutions also have the expected behavior in the FP limit.

We have not performed any similar computational tests in multidimensional settings, other than to demonstrate that a stable S_N solution can be obtained when the Galerkin treatment is used. However, the excellent agreement with analysis in slab geometry gives us confidence that our FP analyses are accurate.

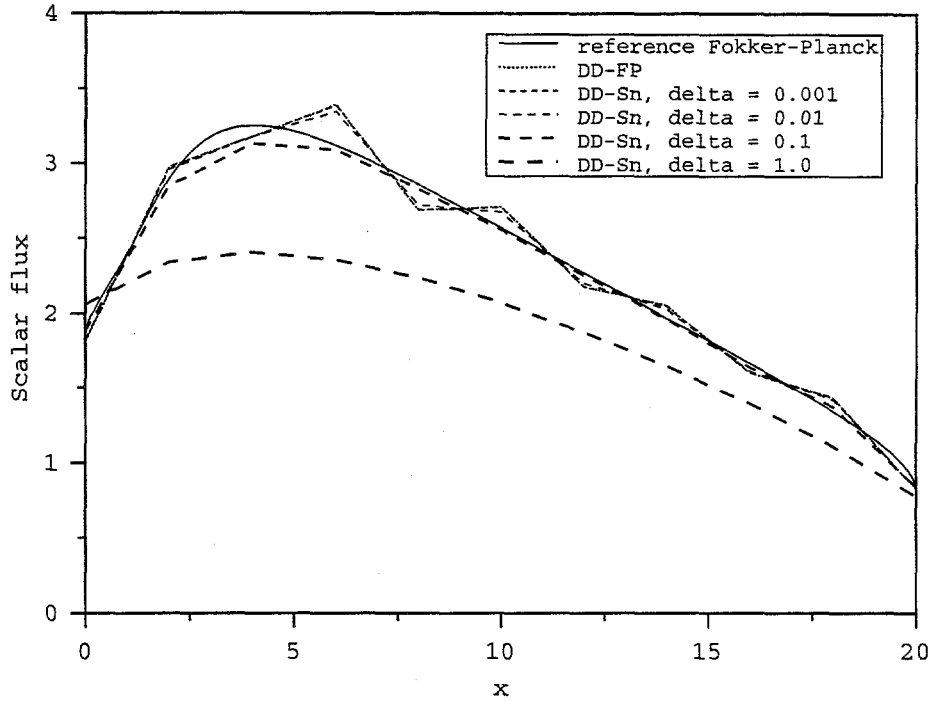

Fig. 16. DD-S_8 scalar fluxes. (The DD-FP and DD-S_8-0.001 curves are nearly coincident.)

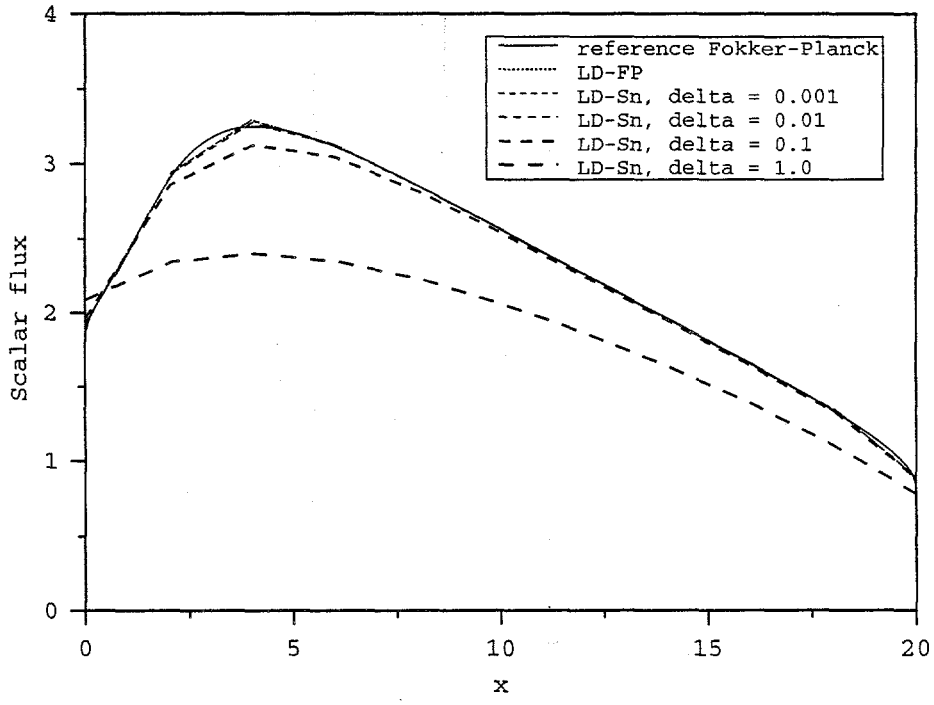

Fig. 17. LD-S_8 scalar fluxes. (The LD-FP and LD-S_8-0.001 curves are nearly coincident.)

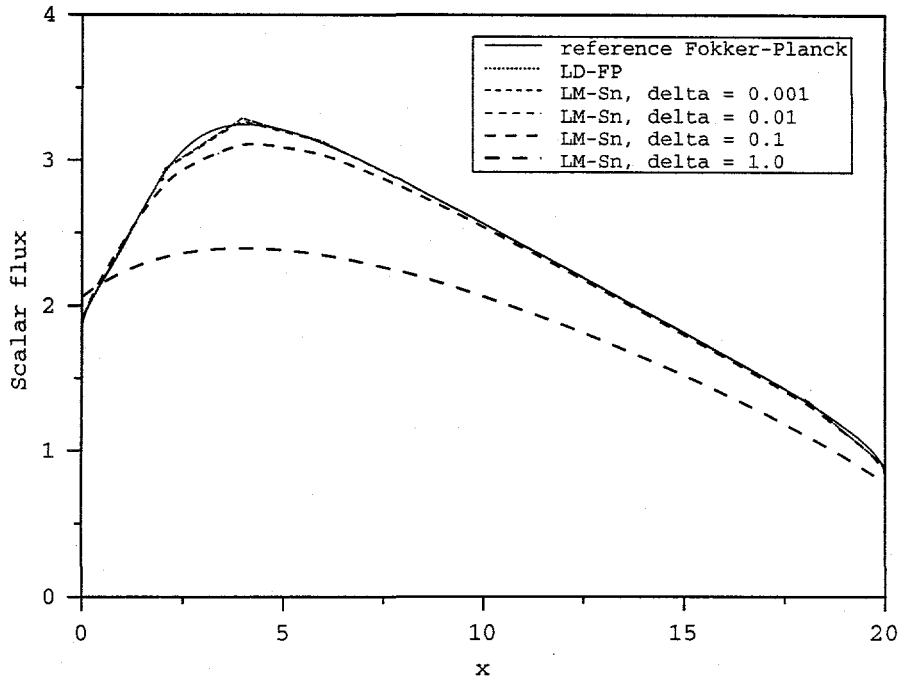

Fig. 18. LM-S_8 scalar fluxes. (The LD-FP and LM-S_8-0.001 curves are nearly coincident.)

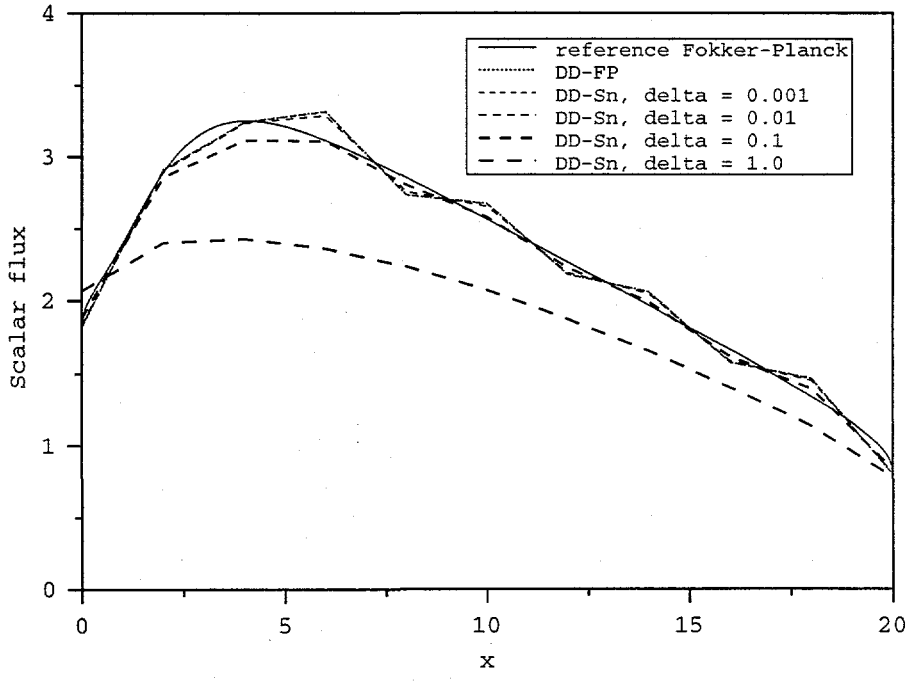

Fig. 19. DD-S_{16} scalar fluxes. (The DD-FP and DD-S_{16}-0.001 curves are nearly coincident.)

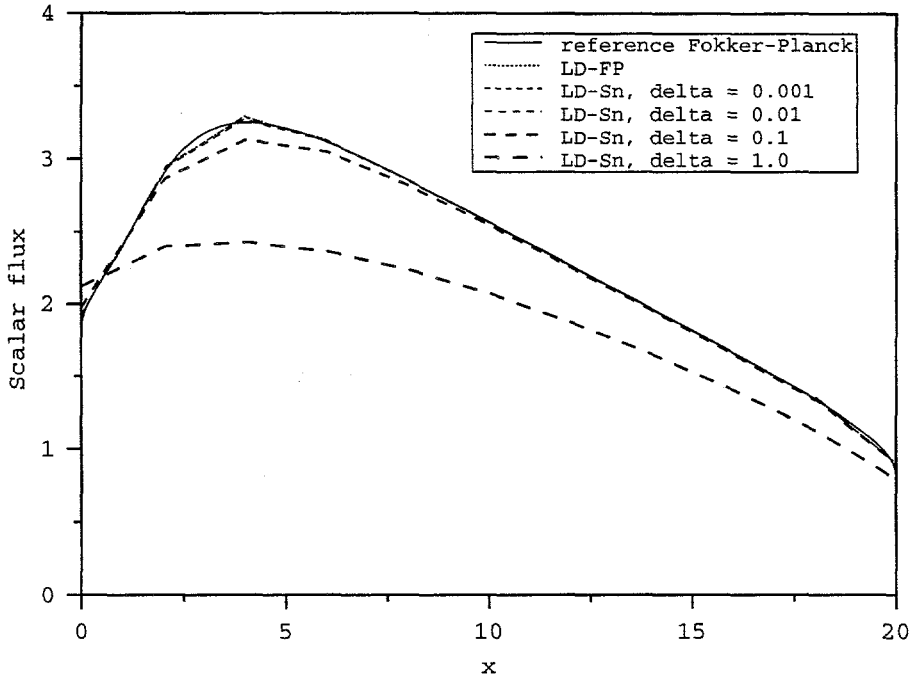

Fig. 20. LD-S_{16} scalar fluxes. (The LD-FP and LD-S_{16}-0.001 curves are nearly coincident.)

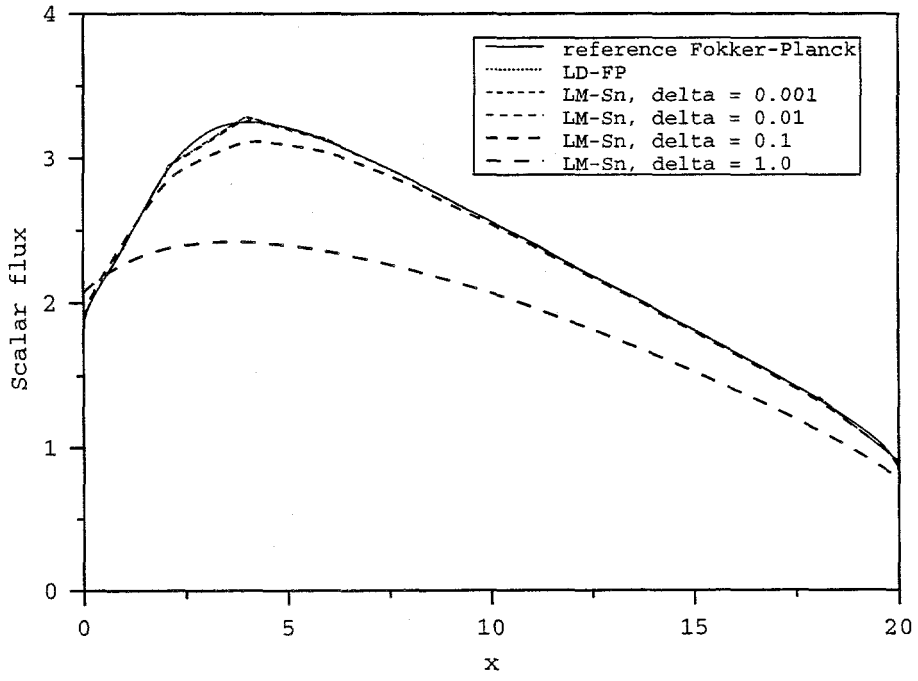

Fig. 21. LM-S_{16} scalar fluxes. (The LD-FP and LM-S_{16}-0.001 curves are nearly coincident.)

VI.B. ANMG Results

In this section we present numerical results that support our ANMG analyses. At first we report results from problems using meshes and quadratures that directly correspond to those used in the Fourier analyses of Chapter V. We also implement the ANMG scheme in more complicated problems that are not amenable to Fourier analysis in order to demonstrate the performance of the ANMG method in realistic situations.

Our numerical results are obtained by means of the PERICLES transport code. PERICLES is an unstructured mesh discrete ordinates code under development at Los Alamos National Laboratory.[137] It can perform calculations on arbitrary generalized hexahedral meshes in one, two, or three dimensions. It uses the family of linear discontinuous methods (LD, BLD, etc.) with or without mass matrix lumping. The modified WLA operator is used for DSA. The Galerkin treatment may be used with the quadrature sets.

VI.B.1. Acceleration of Model Problems

For comparisons with our Fourier analyses we nominally use a 25x25 rectangular mesh with reflective boundary conditions on two adjacent sides and vacuum boundary conditions on the other two sides; since we also use level symmetric quadrature sets this effectively gives us a 50x50 mesh with only vacuum boundaries. We initially perform a source iteration calculation without acceleration for each problem and mesh spacing in order to determine the effect of leakage, since we are trying to confirm infinite-media analysis results. If the resulting spectral radius is less than 0.99 (the spectral radius in infinite media without absorption is unity), the number of elements is doubled in the thinner direction until either the source iteration spectral radius is greater than 0.99 or the mesh size makes it computationally

TABLE XVIII

Mesh Sizes for Numerical Spectral Radii Tests

	$\sigma_{tr}\Delta y$						
$\sigma_{tr}\Delta x$	.001	.01	.1	1	10	100	1000
.001	-						
.01	-	200x200					
.1	-	50x400	50x50				
1	-	25x400	25x50	25x25			
10	-	25x400	25x50	25x25	25x25		
100	-	25x400	25x50	25x25	25x25	25x25	
1000	-	-	25x50	25x25	25x25	25x25	25x25

infeasible to further increase the number of elements. The meshes used for each cell size are reported in Table XVIII. Only a few of the meshes with the thinnest cells yield source iteration spectral radii that are somewhat less than 0.99, so results from spectral radius tests with these meshes are expected to be close to the infinite media results. Meshes have not been created for cells widths $\sigma_{tr}\Delta x < 0.01$ or $\sigma_{tr}\Delta y < 0.01$ because leakage would be so great that the spectral radius results would not be expected to compare well with infinite-medium analyses.

In our tests we use a uniform, isotropic fixed source and an initially random flux distribution. We nominally perform 300 iterations in order to eliminate all but the slowest converging error mode so that a good spectral radius estimate may be obtained, although in some cases it is necessary to use more iterations. The computational spectral radius is estimated by means of the techniques described in Appendix B.

Our first set of tests are the S_4-DSA, S_6-DSA, and S_8-DSA iterations with BLD differencing and optimized FP scattering on a variety of rectangular meshes. We report the results in Tables XIX-XXI. These numerical results correspond to the Fourier analysis results reported in Tables V-VII. Except for some slight differences with the most optically thin

TABLE XIX

Numerical Spectral Radii, BLD S_4-DSA (WLA) Iteration, Optimized FP Scattering

	$\sigma_{tr}\Delta y$						
$\sigma_{tr}\Delta x$	.001	.01	.1	1	10	100	1000
.001	-						
.01	-	0.87					
.1	-	0.90	0.90				
1	-	0.90	0.90	0.90			
10	-	0.96	0.95	0.90	0.90		
100	-	0.99	0.99	0.99	0.90	0.90	
1000	-	-	0.99	0.997	0.99	0.95	0.90

meshes, which we attribute to leakage effects, the spectral radii are generally within 0.01 of the Fourier results for all meshes. Thus we have computationally confirmed these Fourier analyses as well as the need for better acceleration.

Our next set of tests are the S_4-S_2-DSA, S_6-S_4-S_2-DSA, and S_8-S_4-S_2-DSA iterations, also with BLD differencing and optimized FP scattering. The resulting computational spectral radii are reported in Tables XXII-XXIV. These tables correspond to Tables IX-XI. The numerical results are generally within 0.01 of the Fourier analyses. This confirms that the ANMG method is unstable without filtering for optically thin cells but stable when thicker cells are used.

Next we examine the S_4-S_2-DSA-filter, S_6-S_4-S_2-DSA-filter, and S_8-S_4-S_2-DSA-filter iterations with BLD differencing and optimized FP scattering. The results are reported in

TABLE XX

Numerical Spectral Radii, BLD S_6-DSA (WLA) Iteration, Optimized FP Scattering

	$\sigma_{tr}\Delta y$		
$\sigma_{tr}\Delta x$	.01	1	100
.01	0.94		
1	0.95	0.95	
100	0.99	0.99	0.95

TABLE XXI

Numerical Spectral Radii, BLD S_8-DSA (WLA) Iteration, Optimized FP Scattering

	$\sigma_{tr}\Delta y$		
$\sigma_{tr}\Delta x$	.01	1	100
.01	0.97		
1	0.97	0.97	
100	0.997	0.99	0.97

TABLE XXII

Numerical Spectral Radii, BLD S_4-S_2-DSA (WLA) Iteration, Optimized FP Scattering

	$\sigma_{tr}\Delta y$						
$\sigma_{tr}\Delta x$	.001	.01	.1	1	10	100	1000
.001	-						
.01	-	1.86					
.1	-	0.98	0.77				
1	-	0.64	0.64	0.65			
10	-	0.88	0.88	0.78	0.65		
100	-	0.96	0.97	0.98	0.89	0.70	
1000	-	-	0.98	0.995	0.99	0.95	0.73

TABLE XXIII

Numerical Spectral Radii, BLD S_6-S_4-S_2-DSA (WLA) Iteration, Optimized FP Scattering

	$\sigma_{tr}\Delta y$		
$\sigma_{tr}\Delta x$	.01	1	100
.01	1.15		
1	0.61	0.63	
100	0.96	0.98	0.71

TABLE XXIV

Numerical Spectral Radii, BLD S_8-S_4-S_2-DSA (WLA) Iteration, Optimized FP Scattering

	$\sigma_{tr}\Delta y$		
$\sigma_{tr}\Delta x$	.01	1	100
.01	1.48		
1	0.62	0.64	
100	0.97	0.98	0.71

TABLE XXV

Numerical Spectral Radii, BLD S_4-S_2-DSA-filter (WLA) Iteration, Optimized FP Scattering

	$\sigma_{tr}\Delta y$						
$\sigma_{tr}\Delta x$	.001	.01	.1	1	10	100	1000
.001	-						
.01	-	0.58					
.1	-	0.63	0.63				
1	-	0.71	0.64	0.65			
10	-	0.96	0.93	0.79	0.65		
100	-	0.99	0.98	0.98	0.89	0.70	
1000	-	-	0.99	0.996	0.99	0.95	0.73

TABLE XXVI

Numerical Spectral Radii, BLD S_6-S_4-S_2-DSA-filter (WLA) Iteration, Optimized FP Scattering

	$\sigma_{tr}\Delta y$		
$\sigma_{tr}\Delta x$	.01	1	100
.01	0.55		
1	0.82	0.63	
100	0.99	0.98	0.71

TABLE XXVII

Numerical Spectral Radii, BLD S_8-S_4-S_2-DSA-filter (WLA) Iteration, Optimized FP Scattering

	$\sigma_{tr}\Delta y$		
$\sigma_{tr}\Delta x$	.01	1	100
.01	0.74		
1	0.83	0.64	
100	0.99	0.98	0.71

TABLE XXVIII

Numerical Spectral Radii, LBLD S_4-S_2-DSA-filter (WLA) Iteration, Optimized FP Scattering

	$\sigma_{tr}\Delta y$						
$\sigma_{tr}\Delta x$	.001	.01	.1	1	10	100	1000
.001	-						
.01	-	0.58					
.1	-	0.63	0.63				
1	-	0.81	0.64	0.65			
10	-	0.97	0.94	0.83	0.65		
100	-	0.99	0.99	0.98	0.90	0.72	
1000	-	-	0.996	0.997	0.99	0.95	0.74

Tables XXV-XXVII, which correspond to Tables XIII-XV. We again see that the numerical spectral radii are close to the Fourier results. These results confirm that the filtered ANMG method is unconditionally stable and generally effective. The ineffectiveness for large aspect-ratio cells we attribute to the ineffectiveness of the DSA operator and not the ANMG scheme itself.

The final Fourier analysis that we will confirm is the S_4-S_2-DSA-filter iteration with LBLD differencing and optimized FP scattering. The numerical results are reported in Table XXVIII, which corresponds to the Fourier results of Table XVI. The numerical results again are close to the Fourier results, which demonstrates the effectiveness of the filtered ANMG method with LBLD differencing.

The spectral radius tests that we have reported in this section thus far have directly corresponded to problems that we Fourier analyzed in Chapter V. The only difference has been that the numerical tests were performed on finite grids, whereas our Fourier analyses were derived for grids that are infinite in extent. We now will perform spectral radius tests of the ANMG method for some problems that are still "simple", but which are less amenable

TABLE XXIX

Numerical Spectral Radii, Accelerated TLD S_4 Iteration, Optimized FP Scattering

$\sigma_{tr}\Delta x$	DSA spectral radius	ANMG spectral radius
1	0.93	0.80
10	0.94	0.80
100	0.94	0.80
1000	0.94	0.80

to Fourier analysis, in order to demonstrate the applicability of our Fourier results to other situations.

In Chapter IV we stated that we would perform Fourier analyses only for two-dimensional problems; the effectiveness of the ANMG method in three dimensions would be confirmed by numerical testing. We report one such test here. We examine a problem with optimized Fokker-Planck scattering and no absorption on a 25x25x25 grid of cubic elements ($\Delta x = \Delta y = \Delta z$) with reflective boundary conditions on three adjacent faces. We use trilinear discontinuous (TLD) spatial differencing and S_4 level-symmetric angular differencing. Table XXIX records the numerical spectral radii for this problem with DSA and ANMG acceleration for several cell optical thicknesses. The ANMG method is clearly more effective than DSA for these cases. Although we suspect that there will be high-frequency instabilities for much thinner cells and that these instabilities can be eliminated by means of a diffusive filter, numerical tests in three dimensions would require a prohibitive number of elements so that leakage would not dominate the problem.

Next we examine a multimaterial problem in 2D. Figure 22 depicts the physical problem. A central square region of one material is surrounded by a region of a second material. Both materials have FP scattering kernels without absorption. However, σ_{tr} in the first material may be different from that in the second material.

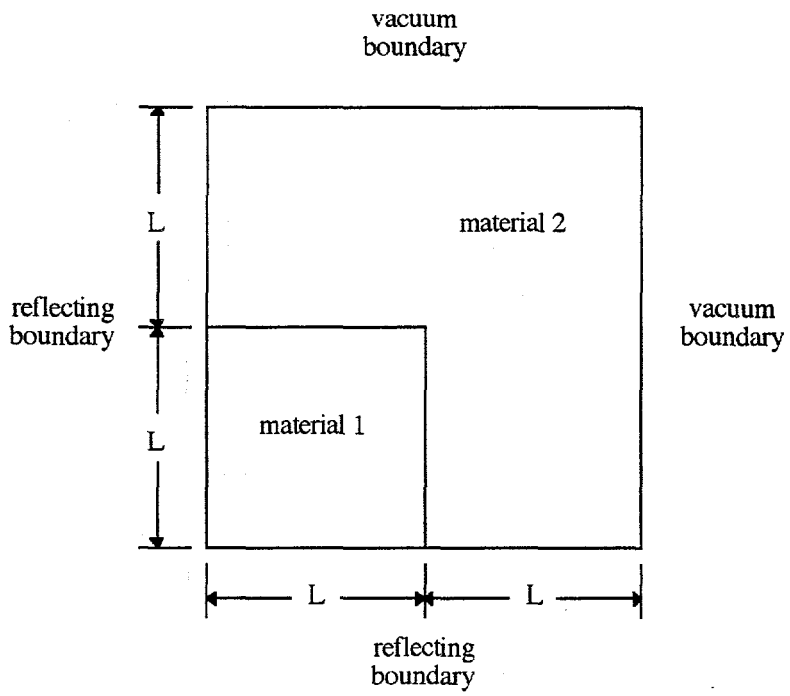

Fig. 22. Multimaterial test problem.

We model this problem with a uniform 50x50 mesh, BLD spatial differencing, and an S_4 quadrature. In Table XXX we report numerical spectral radius results from PERICLES for the case in which the central region is optically thick and the outer region is made increasingly optically thin. In Table XXXI we report similar results for an optically thick outer region and an increasingly thin central region. In all cases ANMG acceleration is at least as effective as DSA acceleration. However, as the differences in the material properties become extreme the effectiveness of both acceleration methods can degrade. The effectiveness of DSA does not degrade unless and until the ANMG spectral radius has become equal to that of DSA. Further increases in material differences may continue to degrade both methods, but their spectral radii are equal to each other then.

TABLE XXX

Numerical Spectral Radii, Multimaterial Test Problem, Optically Thick Inner Region

$\sigma_{tr,1}\Delta x$	$\sigma_{tr,2}\Delta x$	DSA spectral radius	ANMG spectral radius	ANMG (filtered) spectral radius
1000	1000	0.90	0.73	0.73
1000	100	0.90	0.73	0.73
1000	10	0.90	0.73	0.73
1000	1	0.90	0.73	0.73
1000	0.1	0.90	0.81	0.81
1000	0.01	0.90	0.82	0.82
1000	0.001	0.90	0.82	0.82
1000	0.0001	0.90	0.82	0.82

TABLE XXXI

Numerical Spectral Radii, Multimaterial Test Problem, Optically Thick Outer Region

$\sigma_{tr,1}\Delta x$	$\sigma_{tr,2}\Delta x$	DSA spectral radius	ANMG spectral radius	ANMG (filtered) spectral radius
1000	1000	0.90	0.73	0.73
100	1000	0.90	0.73	0.73
10	1000	0.90	0.73	0.73
1	1000	0.90	0.74	0.73
10^{-1}	1000	0.90	0.86	0.86
10^{-2}	1000	0.90	0.90	0.90
10^{-3}	1000	0.90	0.91	0.91
10^{-4}	1000	0.92	0.92	0.92
10^{-5}	1000	0.93	0.93	0.93
10^{-6}	1000	0.93	0.93	0.93

These results lead to several observations. Although there are optically thin regions in some of these cases, the unfiltered ANMG scheme remains stable. In fact, diffusive filtering of the ANMG corrections does not improve the spectral radius at all. If there are localized amplifications of error in the thin regions, then the thick regions may be stabilizing the problem. If a multimaterial problem were constructed that led to ANMG instabilities it is not known how effective a diffusive filter would be at stabilizing the iteration.

It has been observed in other situations that DSA effectiveness can degrade when extreme differences in material properties exist in a problem.[138] We observe here that the ANMG scheme also loses some effectiveness. However, the ANMG method relies on DSA as its lowest-order operator, so the multigrid scheme itself may not be the source of the spectral radius degradation. An effective multigrid method coupled with an increasingly ineffective DSA operator is consistent with our results. If the multigrid scheme is effective at accelerating all but the zeroth moment but the DSA operator is increasingly ineffective at accelerating the zeroth moment when material differences become extreme, then the spectral radius would increase. This behavior is consistent with the ANMG results of Table XXXI. On the other hand, if only DSA acceleration is used in a forward-peaked scattering problem, its inability to accelerate higher moments would control the spectral radius until the multimaterial degradation becomes so severe that the lack of effective zeroth moment acceleration dominates. This behavior is also consistent with the DSA results in Table XXXI. Although we have not proven that there are no multimaterial effects on the angular multigrid method's ability to accelerate higher flux moments, it appears that problems with the DSA operator are the main cause of degradation in ANMG effectiveness for multimaterial problems.

VI.B.2. Acceleration of Electron-Photon Transport Problems

We have analyzed and numerically tested the ANMG method in a variety of model problems. Now we will apply the ANMG method to the solution of a real transport problem. We choose to solve a coupled electron-photon problem. The transport of electrons involves highly forward-peaked scattering, as does photon transport when high-energy Compton scattering predominates. This type of problem is well suited to demonstrate the ANMG method.

Before we describe the particular electron-photon problem to be solved, we will discuss certain features of this class of problems. In the transport of charged particles, including electrons, the energy loss due to Coulomb interactions is nearly continuous. One may separate out this energy loss term from the discrete scattering losses by introducing a $\partial\psi/\partial E$ term in the energy-dependent transport equation. This term is called the continuous slowing-down (CSD) operator. Whereas the discrete energy loss terms are usually modeled by the multigroup method, the CSD operator must be discretized separately to obtain an accurate solution.

Another aspect of electron-photon transport problems is the coupling between the two particle types. Physically, electron interactions with a material may produce photons, and photon interactions may produce electrons. However, if the photon energy is not too high the electrons that it produces are relatively low in energy. These electrons have a short range and their energy is deposited in a small region. For such problems one may assume with little error that all of the electron energy is deposited locally, and therefore one does not need to consider the transport of photon-produced electrons. This decouples the problem; electrons

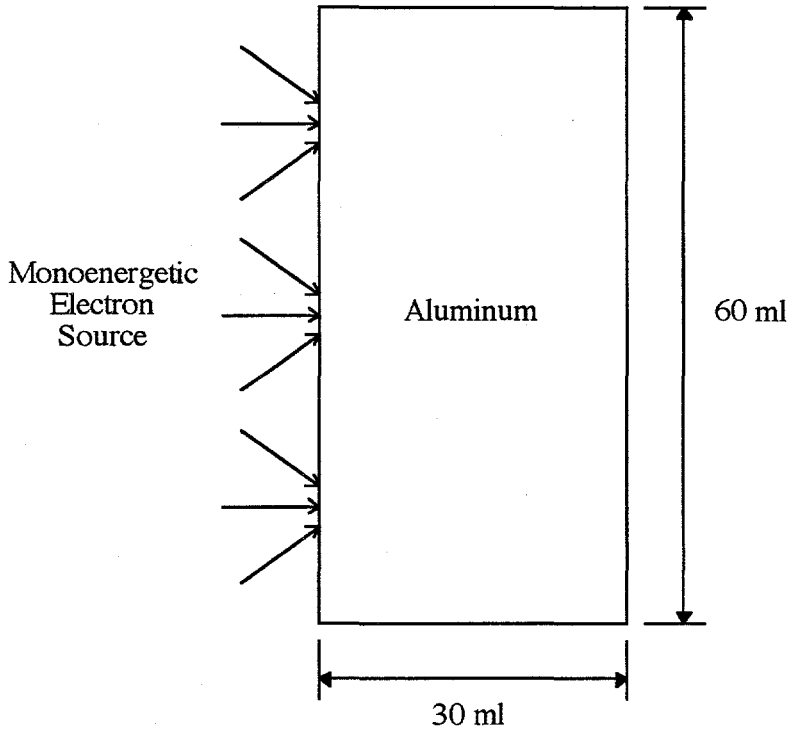

Fig. 23. Electron-photon transport test problem.

produce photons but photons effectively do not produce electrons. Such decoupling aids the solution process.

The physical problem we wish to solve is depicted in Figure 23. An isotropic, monoenergetic source of electrons is incident upon one face of a 2D aluminum shield that is 30 ml thick and 60 ml tall. The energy of the incident electrons is in the range 1-4 MeV. This problem was previously reported by Seltzer[11] and by Datta et al.[28]

In our modeling we mostly duplicate the work of Datta et al. They divided the shield into a 20x40 mesh of square elements, to which they applied step characteristic differencing. They used an S_{12} quadrature with the Galerkin treatment. The electron calculation was decoupled from the photon calculation by assuming that all photon-produced electrons deposit their

TABLE XXXII

Calculated Doses Behind Aluminum Shield in Test Problem

Incident Energy [MeV]	Dose, Datta et al. [MeV/g]	Dose, PERICLES [MeV/g]
1	1.754	2.070
2	2.572	2.168
3	2.931	2.219
4	2.453	2.230

energy locally. The CSD operator was discretized by the diamond difference method and the other energy loss terms were handled by the multigroup method. There were 40 electron groups and 40 photon groups of uniform width with a cutoff energy of 50 keV. Cross sections were obtained from the CEPXS cross section generation code.[139] In our tests we use all of the same discretizations and physical data except that BLD spatial differencing is used instead of step characteristics.

A dose profile in the shield as calculated by PERICLES for 1 MeV incident electrons is depicted in Figure 24. Although we do not have outside results to which we may compare this figure, the dose profile appears to be physically realistic. The cell average dose for one of the two cells in the center of the right side of the shield is reported in Table XXXII for step characteristics calculations[28] and our PERICLES calculations. The two sets of results differ somewhat. However, we are interested primarily in acceleration results rather than accuracy, so we will not attempt to refine the solutions or to determine the main sources of error. Since this calculation is typical our acceleration results for this problem will be practically relevant.

In Table XXXIII we report the number of within-group (inner) iterations and CPU times required by PERICLES to converge the solution to within 10^{-4} relative error with both DSA and ANMG acceleration. The iteration count produced by ANMG acceleration is approximately half that produced by DSA acceleration, as is the CPU time required for the

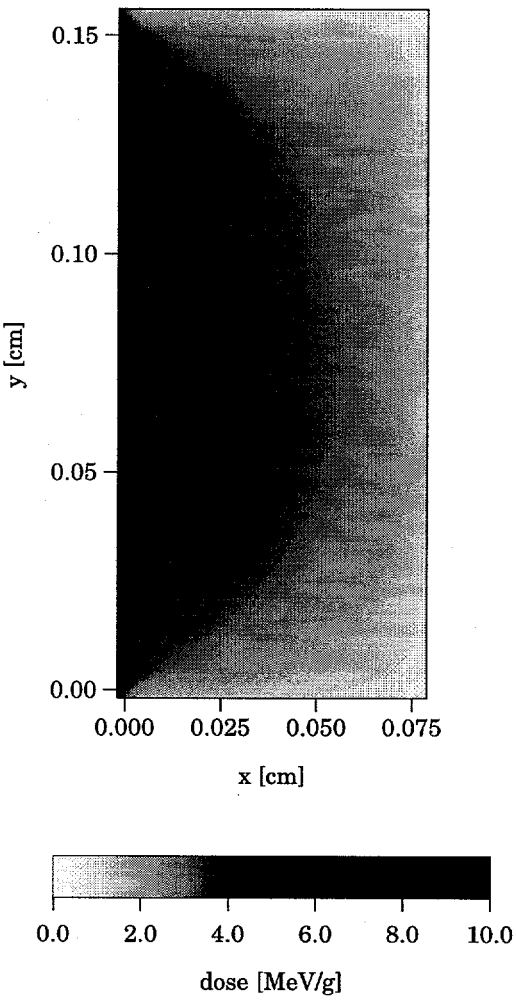

Fig. 24. Dose in aluminum shield, 1 MeV incident electrons.

TABLE XXXIII

ANMG and DSA Performance, Electron-Photon Test Problem, DD-CSD Operator

Incident Energy [MeV]	Iterations, ANMG	Iterations, DSA	Inner CPU [s], ANMG	Inner CPU [s], DSA	Total CPU [s], ANMG	Total CPU [s], DSA
1	337	837	2656	5339	23409	26407
2	448	928	3568	5960	23486	26024
3	459	928	3721	6044	25095	26491
4	465	912	3776	5751	24280	25332

within-group calculations. However, in these problems the total CPU time is dominated by the calculation of downscattering sources; this time increases by the square of the number of energy groups. Since we are using a total of 80 groups, the time necessary for this calculation is significant. Nevertheless, ANMG acceleration does decrease the required total CPU time slightly from that required with DSA acceleration. We note that the performance of the ANMG method relative to DSA may be somewhat understated since we did not guard against false convergence, which would affect the DSA-accelerated calculation more than the ANMG-accelerated one.

There is an option in PERICLES and CEPXS to apply a linear discontinuous discretization to the CSD operator instead of diamond differencing. The linear discontinuous differencing is more accurate, so one may use a coarser group structure to obtain results of similar accuracy. Since a coarser group structure would increase the amount of within-group scattering and reduce the downscattering term, one would expect a greater need for acceleration than with a fine group structure. Therefore we will examine some calculations of the above problem in which we use a linear discontinuous discretization of the CSD operator with a coarser group structure. We use 20 electron groups and 20 photon groups. The results are shown in Table XXXIV. Although the downscattering calculations still require a

TABLE XXXIV

ANMG and DSA Performance, Electron-Photon Test Problem, LD-CSD Operator

Incident Energy [MeV]	Iterations, ANMG	Iterations, DSA	Inner CPU [s], ANMG	Inner CPU [s], DSA	Total CPU [s], ANMG	Total CPU [s], DSA
1	211	710	5403	14138	19517	27703
2	215	665	5501	13278	19569	26900
3	207	614	5226	12284	19094	25910
4	207	579	5238	11636	19124	25235

substantial portion of the CPU time, the time required for the within-group calculations when DSA is applied is significant, whereas when the ANMG method is applied the within-group CPU time is a small fraction of the total CPU time.

The results of this chapter confirm that one may obtain S_N results that are equivalent to discrete Fokker-Planck solutions in the limit of forward-peaked scattering, provided that the scattering source is calculated correctly and that the scattering kernel itself is Fokker-Planck in nature. This chapter also has confirmed that the ANMG method is a stable and effective acceleration method when the ANMG corrections are diffusively filtered and the scattering is highly forward-peaked.

CHAPTER VII

CONCLUSIONS AND RECOMMENDATIONS

VII.A. Conclusions

In this work we analyzed the solutions of certain transport discretizations in the Fokker-Planck (FP) limit. We compared the properties of these solutions to those of the analytic solutions, discovering the conditions under which a reasonable discrete solution will be obtained. We examined the acceleration of the iterative solution of these transport schemes in the FP limit and extended a previously developed angular multigrid scheme to the multidimensional setting. Our analyses show that this acceleration method is effective at reducing the computational cost for the solution of such problems.

The analyses of the spatially analytic discrete ordinates (S_N) equations revealed that if the analytic transport solution does not satisfy a Fokker-Planck equation in the FP limit (a condition determined solely by the scattering kernel) then the discrete solution will not satisfy a discretized Fokker-Planck equation. However, if the analytic solution does satisfy a FP equation and if the moments-to-discrete and discrete-to-moments operators of the S_N method are inverses of each other, then the S_N solution will satisfy a pseudospectral discretization of the Fokker-Planck equation. If the moments-to-discrete and discrete-to-moments operators are not inverses of each other, then the S_N method will fail in the FP limit. Since this is true in most S_N implementations, these methods will fail to produce reasonable results for forward-peaked scattering problems unless their scattering treatments are modified. These results were extended to spatially discretized S_N equations. If the spatially analytic S_N solution satisfies a pseudospectral FP equation, then the solutions to several spatially discrete

S_N schemes will satisfy spatially discretized pseudospectral FP equations. The spatially discrete S_N methods that were examined are, in one-dimensional slab geometry, the diamond difference, linear discontinuous, and linear moments methods, and in two dimensions the bilinear discontinuous, lumped bilinear discontinuous, and simple corner balance methods.

In order to accelerate the iterative solution of S_N methods when the scattering is highly forward-peaked, we extended the angular multigrid (ANMG) acceleration method to multidimensional calculations. Our analyses revealed that a straightforward application of this method is subject to high-frequency instabilities. These instabilities are always present in spatially analytic problems and in spatially discrete problems whose cells are optically thin. We developed a diffusion filter for the multigrid corrections that eliminates these instabilities. The resulting scheme is far more effective than DSA alone for highly forward-peaked scattering problems.

VII.B. Recommendations for Future Work

During the course of this work we identified some areas of research that warrant further attention. In this section we summarize these research topics.

1. *Non-FP limit analysis.* The analysis of transport solutions in the Fokker-Planck limit revealed that for some scattering kernels the analytic solution does not satisfy a Fokker-Planck equation. This forward-peaked limit analysis should be extended to determine if S_N solutions to these problems satisfy a discrete version of the corresponding non-FP limit.

2. *Accuracy of discrete FP equations.* We have found that if the analytic transport solution satisfies a FP equation, then the solution to an S_N scheme that handles the scattering term carefully will satisfy a pseudospectral FP equation. The discretization errors of these FP equations are not entirely known. For example, if the analytic solution contains a delta

function, then the discrete solution cannot strongly converge to the exact solution. However, the weak convergence properties are unknown. Even if the discrete solution is highly inaccurate for pointwise angular flux values, integrated quantities such as scalar fluxes may be more accurate.

3. *Better DSA and filter operators.* The DSA and associated filter operators that were used in most of the analyses and all of the numerical tests become ineffective when the cells have large aspect ratios. This is a general problem; it is not limited to transport problems that have highly forward-peaked scattering. The search for unconditionally effective and easily solved diffusion operators should continue.

4. *Combined angular and spatial multigrid.* The angular multigrid instabilities occur in modes that are attenuated somewhat by source iteration alone; it is not absolutely necessary to accelerate these modes. In order to stabilize the ANMG scheme we actually eliminate the high-frequency corrections anyway. An alternative would be to define a combined angular and spatial multigrid method. Such a method would not produce corrections for those modes that are unstable in the ANMG scheme, assuming that the spatial grid is sufficiently coarsened. It would, however, produce approximately the same corrections for low-frequency modes, since such modes are not greatly affected by spatial discretization. Because of the coarsened spatial mesh this scheme could be more rapidly solved than the ANMG scheme; since no filter would be necessary there would be additional computational savings.

REFERENCES

1. L.V. Spencer, "Theory of Electron Penetration," *Phys. Rev.*, **98**, 1597 (1955).

2. W.T. Scott, "The Theory of Small-Angle Scattering of Fast Charged Particles," *Rev. Mod. Phys.*, **35**, 231 (1963).

3. Z.-M. Luo and A. Brahme, "An Overview of the Transport Theory of Charged Particles," *Radiat. Phys. Chem.*, **41**, 673 (1993).

4. A.B. Chilton, J.K. Shultis, and R.E. Faw, *Principles of Radiation Shielding*, Prentice-Hall, Englewood Cliffs, New Jersey (1984).

5. D.I. Garber, L.G. Strömberg, M.D. Goldberg, D.E. Cullen, and V.M. May, "Angular Distributions in Neutron-Induced Reactions," 3^{rd} ed., BNL-400, Brookhaven National Laboratory (1970).

6. S.C. Klevenhagen, *Physics and Dosimetry of Therapy Electron Beams*, Medical Physics Publishing, Madison, Wisconsin (1993).

7. S. Webb, *The Physics of Radiation Therapy*, Institute of Physics Publishing, Philadelphia (1993).

8. D. Jette, "Electron-Beam Dose Calculations," *Medical Radiology - Radiation Therapy Physics*, Chap. 5, A.R. Smith, Ed., Springer-Verlag, Berlin (1995).

9. L. Reimer, *Scanning Electron Microscopy*, Springer-Verlag, Berlin (1985).

10. L. Reimer, *Transmission Electron Microscopy*, Springer Series in Optical Sciences, Vol. 36, Springer-Verlag, Berlin (1989).

11. S.M. Seltzer, "Electron, Electron-Bremsstrahlung and Proton Depth-Dose Data for Space-Shielding Applications," *IEEE Trans. Nucl. Sci.*, **NS-26**, 4896 (1979).

12. J.F. Ziegler, J.P. Biersack, and J. Littmart, *The Stopping Power and Range of Ions in Solids*, Pergamon, New York (1985).

13. L.G. Henyey and J.L. Greenstein, "Diffuse Radiation in the Galaxy," *Astrophys. J.*, **93**, 70 (1941).

14. J.A. Weinman and S.T. Shipley, "Effects of Multiple Scattering on Laser Pulses Transmitted Through Clouds," *J. Geophys. Res.*, **77**, 7123 (1972).

15. L.B. Stotts, "The Radiance Produced by Laser Radiation Transversing a Particulate Multiple-Scattering Medium," *J. Opt. Soc. Am.*, **67**, 815 (1977).

16. S. Ito and K. Furutsu, "Theory of Light Pulse Propagation Through Thick Clouds," *J. Opt. Soc. Am.*, **70**, 366 (1980).

17. J.J. Ullo, "Use of Multidimensional Transport Methodology on Nuclear Logging Problems," *Nucl. Sci. Eng.*, **92**, 228 (1986).

18. D.E. Bartine, R.G. Alsmiller, F.R. Mynatt, W.W. Engle, Jr., and J. Barish, "Low-Energy Electron Transport by the Method of Discrete Ordinates," *Nucl. Sci. Eng.*, **48**, 159 (1972).

19. T.A. Mehlhorn and J.J. Duderstadt, "A Discrete Ordinates Solution of the Fokker-Planck Equation Characterizing Charged Particle Transport," *J. Comp. Phys.*, **38**, 86 (1980).

20. J.E. Morel, "Fokker-Planck Calculations Using Standard Discrete Ordinates Transport Codes," *Nucl. Sci. Eng.*, **79**, 340 (1981).

21. B.R. Wienke, "ESN: One-Dimensional S_n Transport Module for Electrons," *J. Quant. Spectrosc. Radiat. Transfer*, **28**, 311 (1982).

22. B.R. Wienke, "Electron Transport in One-Dimensional Plasmas," *Nucl. Tech./Fusion*, **4**, 426 (1983).

23. B.R. Wienke, "Suprathermal Electron Energy Deposition in Plasmas with the Fokker-Planck Method," *J. Comp. Phys.*, **51**, 208 (1983).

24. L.J. Lorence, Jr., W.E. Nelson, and J.E. Morel, "Coupled Electron-Photon Transport Calculations Using the Method of Discrete Ordinates," *IEEE Trans. Nucl. Sci.*, **NS-32**, 4416 (1985).

25. L.J. Lorence, Jr., J.E. Morel, and G.D. Valdez, "Results Guide to CEPXS/ONELD: A One-Dimensional Coupled Electron-Photon Discrete Ordinates Code Package," SAND89-2211, Sandia National Laboratory (1990).

26. R.P. Datta, A.K. Ray, and B.R. Wienke, "A Discrete Ordinates Study of Two-Dimensional Electron Transport," *J. Phys. D.* , **26**, 1077 (1993).

27. R.P. Datta and A.K. Ray, "A Spatial Characteristic Scheme for Multigroup Discrete Ordinates Electron Energy Deposition in Two Dimensions," *Phys. Stat. Sol. B*, **180**, 85 (1993).

28. R.P. Datta, S.D. Altekar, A.K. Ray, and J.E. Morel, "Computational Model for Coupled Electron-Photon Transport in Two Dimensions," *Phys. Rev. E*, **53**, 6514 (1996).

29. J.E. Morel and T.A. Manteuffel, "An Angular Multigrid Acceleration Technique for S_n Equations with Highly Forward-Peaked Scattering," *Nucl. Sci. Eng.*, **107**, 330 (1991).

30. G.C. Pomraning, "The Fokker-Planck Operator as an Asymptotic Limit," *Math. Mod. Meth. Appl. Sci.*, **2**, 1, 21 (1992).

31. S. Pautz and M. Adams, "An Asymptotic Study of the Transport Equation in the Fokker-Planck Limit with Angular and Spatial Discretization," *Trans. Am. Nucl. Soc.*, **73**, 193 (1995).

32. N.K. Madsen, "Pointwise Convergence of the Three-Dimensional Discrete Ordinate Method," *SIAM J. Numer. Anal.*, **8**, 2, 266 (1971).

33. P. Nelson, Jr., "Convergence of the Discrete-Ordinates Method for Anisotropically Scattering Multiplying Particles in a Subcritical Slab," *SIAM J. Numer. Anal.*, **10**, 1, 175 (1973).

34. H.D. Victory, Jr., "Convergence Properties of Discrete-Ordinates Solutions for Neutron Transport in Three-Dimensional Media," *SIAM J. Numer. Anal.*, **17**, 1, 71 (1980).

35. P. Nelson, Jr., "Convergence of Two-dimensional Nyström Discrete-Ordinates in Solving the Linear Transport Equation," *Numer. Math.*, **34**, 353 (1980).

36. P. Nelson, Jr., "An Error Estimate for the Multigroup Method with Application to Shielding Calculations," *Ann. Nucl. Energy*, **7**, 297 (1980).

37. E.W. Larsen, "Distributional Solutions of the Transport Equation as a Weak Limit of Regular Solutions of the Discrete Ordinates Equations," *Transp. Theory Stat. Phys.*, **19**, 179 (1990).

38. W.H. Reed and K.D. Lathrop, "Truncation Error Analysis of Finite Difference Approximations to the Transport Equation," *Nucl. Sci. Eng.*, **41**, 237 (1970).

39. R.E. Alcouffe, E.W. Larsen, W.F. Miller, Jr., and B.R. Wienke, "Computational Efficiency of Numerical Methods for the Multigroup, Discrete-Ordinates Neutron Transport Equations: The Slab Geometry Case," *Nucl. Sci. Eng.*, **71**, 111 (1979).

40. E.W. Larsen and W.F. Miller, Jr., "Convergence Rates of Spatial Difference Equations for the Discrete-Ordinates Neutron Transport Equations in Slab Geometry," *Nucl. Sci. Eng.*, **73**, 76 (1980).

41. S.M. Lee and R. Vaidyanathan, "Comparison of the Order of Approximation in Several Spatial Difference Schemes for the Discrete-Ordinates Transport Equation in One-Dimensional Plane Geometry," *Nucl. Sci. Eng.*, **76**, 1 (1980).

42. E.W. Larsen, "Spatial Convergence Properties of the Diamond Difference Method in x,y Geometry," *Nucl. Sci. Eng.*, **80**, 711 (1982).

43. P. Barbucci and F. Di Pasquantonio, "Computational Efficiency of Some Numerical Methods for the Multigroup Discrete Ordinates Solution of Stationary Boltzmann Equations for Neutrons and Gamma Rays in Slab Geometry," *Nucl. Sci. Eng.*, **82**, 448 (1982).

44. E.W. Larsen, "Spectral Analysis of Numerical Methods for Discrete-Ordinates Problems. I.," *Transp. Theory Stat. Phys.*, **15**, 93 (1986).

45. M.L. Adams and W.R. Martin, "Slab Geometry Transport Spatial Discretization Schemes with Infinite-Order Convergence," *Transp. Theory Stat. Phys.*, **15**, 651 (1986).

46. P. Nelson and R. Zelazny, "Some Remarks on Convergence and Stability in Ray-Tracing Calculations," *Nucl. Sci. Eng.*, **93**, 283 (1986).

47. H.B. Keller and P. Nelson, "Closed Linear One-Cell Functional Spatial Approximations: Consistency Implies Convergence and Stability," *Transp. Theory Stat. Phys.*, **17**, 191 (1988).

48. J.E. Morel and E.W. Larsen, "A New Class of S_N Spatial Differencing Schemes," *Proc. Topl. Mtg. Advances in Nuclear Engineering Computation and Radiation Shielding*, Santa Fe, New Mexico, April 9-13, 1989, Vol. 1, p. 1:1 (1989).

49. R.C. De Barros and E.W. Larsen, "A Numerical Method for One-Group Slab-Geometry Discrete Ordinates Problems with No Spatial Truncation Error," *Nucl. Sci. Eng.*, **104**, 199 (1990).

50. J.E. Morel and E.W. Larsen, "A Multiple Balance Approach for Differencing the S_n Equations," *Nucl. Sci. Eng.*, **105**, 1 (1990).

51. R.C. De Barros and E.W. Larsen, "A Numerical Method for Multigroup Slab-Geometry Discrete Ordinates Problems with No Spatial Truncation Error," *Transp. Theory Stat. Phys.*, **20**, 441 (1991).

52. W.F. Miller, Jr., "An Analysis of the Finite Differenced, Even-Parity, Discrete Ordinates Equations in Slab Geometry," *Nucl. Sci. Eng.*, **108**, 247 (1991).

53. P. Nelson and F. Yu, "Worst-Case Errors for Some Spatial Approximations to a Model Problem in Two-Dimensional Transport Theory," *Transp. Theory Stat. Phys.*, **22**, 271 (1993).

54. W.F. Walters and T.A. Wareing, "A Nonlinear Positive Method for Solving the Transport Equation on Coarse Meshes," *Proc. Int. Conf. Radiation Shielding*, Arlington, Texas, April 24-28, 1994, Vol. 1, p. 173 (1994).

55. K. Mathews, G. Sjoden and B. Minor, "Exponential Characteristic Spatial Quadrature for Discrete Ordinates Radiation Transport in Slab Geometry," *Nucl. Sci. Eng.*, **118**, 24 (1994).

56. B. Minor and K. Mathews, "Exponential Characteristic Spatial Quadrature for Discrete Ordinates Radiation Transport with Rectangular Cells," *Nucl. Sci. Eng.*, **120**, 165 (1995).

57. E.W. Larsen, "Diffusion Theory as an Asymptotic Limit of Transport Theory for Nearly Critical Systems with Small Mean Free Paths," *Ann. Nucl. Energy*, **7**, 249 (1980).

58. E.W. Larsen and G.C. Pomraning, "The P_N Theory as an Asymptotic Limit of Transport Theory in Planar Geometry - I: Analysis," *Nucl. Sci. Eng.*, **109**, 49 (1991).

59. E.W. Larsen, J.M. McGhee and J.E. Morel, "The Simplified P_N Equations as an Asymptotic Limit of the Transport Equation," *Trans. Am. Nucl. Soc.*, **66**, 231 (1992).

60. E.W. Larsen, J.E. Morel and J.M. McGhee, "Asymptotic Derivation of the Simplified P_N Equations," *Proc. Joint Int. Conf. Mathematical Methods and Supercomputing in Nuclear Applications*, Karlsruhe, Germany, April 19-23, 1993, Vol. 2, p. 718 (1993).

61. C. Börgers and E.W. Larsen, "Fokker-Planck Approximation of Monoenergetic Transport Processes," *Trans. Am. Nucl. Soc.*, **71**, 235 (1994).

62. E.W. Larsen, J.E. Morel and J.M. McGhee, "Asymptotic Derivation of the Multigroup P_1 and Simplified P_N Equations with Anisotropic Scattering," *Proc. Int. Conf. Mathematics and Computations, Reactor Physics, and Environmental Analyses*, Portland, Oregon, April 30-May 4, 1995, Vol. 1, p. 309 (1995).

63. M.L. Adams, E.W. Larsen and P.F. Nowak, "The Asymptotic Diffusion Limit of Continuous and Discrete Steady-State Multigroup Radiative Transfer Problems," *Proc. Int. Conf. Mathematics and Computations, Reactor Physics, and Environmental Analyses*, Portland, Oregon, April 30-May 4, 1995, Vol. 1, p. 361 (1995).

64. C. Börgers and E.W. Larsen, "The Fermi Pencil Beam Approximation," *Proc. Int. Conf. Mathematics and Computations, Reactor Physics, and Environmental Analyses*, Portland, Oregon, April 30-May 4, 1995, Vol. 2, p. 847 (1995).

65. C. Börgers and E.W. Larsen, "Asymptotic Derivation of the Fermi Pencil-Beam Approximation," *Nucl. Sci. Eng.*, **123**, 343 (1996).

66. G.C. Pomraning, "Higher Order Fokker-Planck Operators," *Nucl. Sci. Eng.*, **124**, 390 (1996).

67. E.W. Larsen, "On Numerical Solutions of Transport Problems in the Diffusion Limit," *Nucl. Sci. Eng.*, **83**, 90 (1983).

68. E.W. Larsen, J.E. Morel and W.F. Miller, Jr., "Asymptotic Solutions of Numerical Transport Problems in Optically Thick, Diffusive Regimes," *J. Comp. Phys.*, **69**, 283 (1987).

69. E.W. Larsen and J.E. Morel, "Asymptotic Solutions of Numerical Transport Problems in Optically Thick, Diffusive Regimes II," *J. Comp. Phys.*, **83**, 212 (1989).

70. M.L. Adams, "Even-Parity Finite-Element Transport Methods in the Diffusion Limit," *Prog. Nucl. Energy*, **25**, 159 (1991).

71. M.L. Adams, "A New Transport Discretization Scheme for Arbitrary Spatial Meshes in XY Geometry," *Proc. Int. Topl. Mtg. Advances in Mathematics, Computations, and Reactor Physics*, Pittsburgh, Pennsylvania, April 28-May 2, 1991, Vol. 3, p. 13.2 2-1 (1991).

72. M.L. Adams, "Discontinuous Finite-Element Transport Solutions in the Thick Diffusion Limit in Cartesian Geometry," *Proc. Int. Topl. Mtg. Advances in Mathematics, Computations, and Reactor Physics*, Pittsburgh, Pennsylvania, April 28-May 2, 1991, Vol. 5, p. 21.1 3-1 (1991).

73. T.A. Wareing, E.W. Larsen and M.L. Adams, "Diffusion Accelerated Discontinuous Finite Element Schemes for the S_N Equations in Slab and X,Y Geometries," *Proc. Int. Topl. Mtg. Advances in Mathematics, Computations, and Reactor Physics*, Pittsburgh, Pennsylvania, April 28-May 2, 1991, Vol. 3, p. 11.1 2-1 (1991).

74. E.W. Larsen, "The Asymptotic Diffusion Limit of Discretized Transport Problems," *Nucl. Sci. Eng.*, **112**, 336 (1992).

75. C. Börgers, E.W. Larsen and M.L. Adams, "The Asymptotic Diffusion Limit of a Linear Discontinuous Discretization of a Two-Dimensional Linear Transport Equation," *J. Comp. Phys.*, **98**, 285 (1992).

76. T.A. Wareing, "Asymptotic Diffusion Accelerated Discontinuous Finite Element Methods for Transport Problems," Ph.D. Dissertation, University of Michigan, Ann Arbor, Michigan (1992).

77. T.S. Palmer and M.L. Adams, "Curvilinear Geometry Transport Discretizations in the 'Thick' Diffusion Limit," *Proc. Joint Int. Conf. Mathematical Methods and Supercomputing in Nuclear Applications*, Karlsruhe, Germany, April 19-23, 1993, Vol. 1, p. 3 (1993).

78. M.L. Adams, W.F. Walters and T.A. Wareing, "Characteristics Methods in Thick Diffusive Problems," *Proc. Int. Conf. Mathematics and Computations, Reactor Physics, and Environmental Analyses*, Portland, Oregon, April 30-May 4, 1995, Vol. 1, p. 349 (1995).

79. C.L. Castrianni and M.L. Adams, "A Nonlinear Corner-Balance Spatial Discretization for Transport on Arbitrary Grids," *Proc. Int. Conf. Mathematics and Computations, Reactor Physics, and Environmental Analyses*, Portland, Oregon, April 30-May 4, 1995, Vol. 2, p. 916 (1995).

80. W.F. Walters and T.A. Wareing, "An Accurate, Strictly-Positive, Nonlinear Characteristic Scheme for the Discrete-Ordinate Equations," *Transp. Theory Stat. Phys.*, **25**, 197 (1996).

81. T. Noh, W.F. Miller, Jr., and J.E. Morel, "The Even-Parity and Simplified Even-Parity Transport Equations in Two-Dimensional *x-y* Geometry," *Nucl. Sci. Eng.*, **123**, 38 (1996).

82. C.L. Castrianni, "Nonlinear Finite Element and Characteristic Based Transport Methods in the Thick Diffusion Limit in Cartesian Coordinates," Ph.D. Dissertation, Texas A&M University, College Station, Texas (1997).

83. C.L. Castrianni and M.L. Adams, "Asymptotic Diffusion Limit of Nonlinear Discontinuous Finite Element Transport Discretizations in One Dimension," *Proc. Joint Int. Conf. Mathematical Methods and Supercomputing for Nuclear Applications*, Saratoga Springs, New York, October 5-9, 1997, Vol. 2, p. 1476 (1997).

84. C.L. Castrianni and M.L. Adams, "A Nonlinear Corner-Balance Spatial Discretization for Transport on Arbitrary Grids," *Nucl. Sci. Eng.*, **128**, 1 (1998).

85. J. Stoer and R. Bulirsch, *Introduction to Numerical Analysis*, 2^{nd} ed., Springer-Verlag, New York (1993).

86. G.D. Smith, *Numerical Solution of Partial Differential Equations: Finite Difference Methods*, 3^{rd} ed., Oxford University Press, New York (1985).

87. C. Johnson, *Numerical Solution of Partial Differential Equations by the Finite Element Method*, Cambridge University Press, New York (1987).

88. S.C. Brenner and L.R. Scott, *The Mathematical Theory of Finite Element Methods*, Springer-Verlag, New York (1994).

89. B.S. Tannenbaum, *Plasma Physics*, McGraw-Hill Book Company, Inc., New York (1967).

90. D. Gottlieb, M.Y. Hussaini and S.A. Orszag, "Theory and Applications of Spectral Methods," *Spectral Methods for Partial Differential Equations*, Chap. 1, R.G. Voigt, D. Gottlieb, and M.Y. Hussaini, Eds., Society for Industrial and Applied Mathematics, Philadelphia (1984).

91. J.E. Morel, "A Hybrid Collocation-Galerkin-S_n Method for Solving the Boltzmann Transport Equation," *Nucl. Sci. Eng.*, **101**, 72 (1989).

92. E.E. Lewis and W.F. Miller, Jr., *Computational Methods of Neutron Transport*, American Nuclear Society, Inc., La Grange Park, Illinois (1993).

93. W.H. Reed, "Spherical Harmonic Solutions of the Neutron Transport Equation from Discrete Ordinate Codes," *Nucl. Sci. Eng.*, **49**, 10 (1972).

94. J.E. Morel, J.E. Dendy, Jr., and T.A. Wareing, "Diffusion-Accelerated Solution of the Two-Dimensional S_n Equations with Bilinear-Discontinuous Differencing," *Nucl. Sci. Eng.*, **115**, 304 (1993).

95. S. Oliveira, "Parallel Multigrid Methods for Transport Equations: The Anisotropic Case," *Parallel Computing*, **22**, 513 (1996).

96. J.E. Morel, "A Synthetic Acceleration Method for Discrete Ordinates Calculations with Highly Anisotropic Scattering," *Nucl. Sci. Eng.*, **82**, 34 (1982).

97. H.J. Kopp, "Synthetic Method Solution of the Transport Equation," *Nucl. Sci. Eng.*, **17**, 65 (1963).

98. E.M. Gelbard and L.A. Hageman, "The Synthetic Method as Applied to the S_n Equations," *Nucl. Sci. Eng.*, **37**, 288 (1969).

99. W.H. Reed, "The Effectiveness of Acceleration Techniques for Iterative Methods in Transport Theory," *Nucl. Sci. Eng.*, **45**, 245 (1971).

100. R.E. Alcouffe, "Diffusion Synthetic Acceleration Methods for the Diamond-Differenced Discrete-Ordinates Equations," *Nucl. Sci. Eng.*, **64**, 344 (1977).

101. W.F. Miller, Jr., "Generalized Rebalance: A Common Framework for Transport Acceleration Methods," *Nucl. Sci. Eng.*, **65**, 226 (1978).

102. E.W. Larsen, "Unconditionally Stable Diffusion-Acceleration of the Transport Equation," *Transp. Theory Stat. Phys.*, **11**, 29 (1982).

103. E.W. Larsen, "Unconditionally Stable Diffusion-Synthetic Acceleration Methods for the Slab Geometry Discrete Ordinates Equations. Part I: Theory," *Nucl. Sci. Eng.*, **82**, 47 (1982).

104. D.R. McCoy and E.W. Larsen, "Unconditionally Stable Diffusion-Synthetic Acceleration Methods for the Slab Geometry Discrete Ordinates Equations. Part II: Numerical Results," *Nucl. Sci. Eng.*, **82**, 64 (1982).

105. E.W. Larsen, "Diffusion-Synthetic Acceleration Methods for Discrete-Ordinates Problems," *Transp. Theory Stat. Phys.*, **13**, 107 (1984).

106. W.F. Miller, Jr. and E.W. Larsen, "Modified Diffusion Synthetic Acceleration Algorithms," *Nucl. Sci. Eng.*, **93**, 403 (1986).

107. Y.Y. Azmy and E.W. Larsen, "Fourier Analysis of the Diffusion Synthetic Acceleration Method for Weighted Diamond-Differencing Schemes in Cartesian Geometries," *Nucl. Sci. Eng.*, **95**, 106 (1987).

108. H. Khalil, "Effectiveness of a Consistently Formulated Diffusion-Synthetic Acceleration Differencing Approach," *Nucl. Sci. Eng.*, **98**, 226 (1988).

109. M.L. Adams and W.R. Martin, "Diffusion Synthetic Acceleration of Discontinuous Finite Element Transport Iterations," *Nucl. Sci. Eng.*, **111**, 145 (1992).

110. J.E. Morel, J.E. Dendy, Jr. and T.A. Wareing, "Diffusion-Accelerated Solution of the 2-D S_n Equations with Bilinear-Discontinuous Differencing," *Proc. Joint Int. Conf. Mathematical Methods and Supercomputing in Nuclear Applications*, Karlsruhe, Germany, April 19-23, 1993, Vol. 2, p. 488 (1993).

111. T.A. Wareing, "New Diffusion-Synthetic Acceleration Methods for the S_N Equations With Corner Balance Spatial Differencing," *Proc. Joint Int. Conf. Mathematical Methods and Supercomputing in Nuclear Applications*, Karlsruhe, Germany, April 19-23, 1993, Vol. 2, p. 500 (1993).

112. M.L. Adams and T.A. Wareing, "Diffusion-Synthetic Acceleration Given Anisotropic Scattering, General Quadratures, and Multidimensions," *Trans. Am. Nuc. Soc.*, **68**, 203 (1993).

113. J.E. Morel and J.M. McGhee, "A Diffusion-Synthetic Acceleration Technique for the Even-Parity S_n Equations with Anisotropic Scattering," *Nucl. Sci. Eng.*, **120**, 147 (1995).

114. T.A. Wareing, W.F. Walters and J.E. Morel, "A Diffusion Accelerated Solution Method for the Nonlinear Characteristic Scheme," *Proc. Int. Conf. Mathematics and Computations, Reactor Physics, and Environmental Analyses*, Portland, Oregon, April 30-May 4, 1995, Vol. 2, p. 1335 (1995).

115. T.A. Wareing, W.F. Walters and J.E. Morel, "A Diffusion-Accelerated Solution Method for the Nonlinear Characteristic Scheme in Slab Geometry," *Nucl. Sci. Eng.*, **124**, 72 (1996).

116. W. Hackbusch, *Iterative Solution of Large Sparse Systems of Equations*, Springer-Verlag, New York (1994).

117. M. Williams, "The Acceleration of Anisotropic Transport Iterations," *Transp. Theory Stat. Phys.*, **13**, 127 (1984).

118. D. Valougeorgis, M. Williams and E.W. Larsen, "Stability Analysis of Synthetic Acceleration Methods with Anisotropic Scattering," *Nucl. Sci. Eng.*, **99**, 91 (1988).

119. K.M. Khattab and E.W. Larsen, "Synthetic Acceleration Methods for Linear Transport Problems with Highly Anisotropic Scattering," *Nucl. Sci. Eng.*, **107**, 217 (1991).

120. E.W. Larsen and W.F. Miller, Jr., "A Two-Step Acceleration Method for Transport Problems," *Trans. Am. Nuc. Soc.*, **52**, 416 (1986).

121. L.J. Lorence, E.W. Larsen and J.E. Morel, "An S_2 Synthetic Acceleration Scheme for the One-Dimensional S_n Equations," *Trans. Am. Nuc. Soc.*, **52**, 417 (1986).

122. L.J. Lorence, Jr., J.E. Morel and E.W. Larsen, "An S_2 Synthetic Acceleration Scheme for the One-Dimensional S_n Equations with Linear Discontinuous Spatial Differencing," *Nucl. Sci. Eng.*, **101**, 341 (1989).

123. T.A. Wareing, W.F. Walters and J.E. Morel, "An S_2-Like Acceleration Method for the Nonlinear Characteristic Transport Scheme," *Trans. Am. Nuc. Soc.*, **71**, 267 (1994).

124. D.Y. Anistratov, M.L. Adams, and E.W. Larsen, "Acceleration of the Nonlinear Corner-Balance Scheme by the Averaged Flux Method," *J. Comp. Phys.*, **135**, 66 (1997).

125. G.L. Ramone, M.L. Adams and P.F. Nowak, "A Transport Synthetic Acceleration Method for Transport Iterations," *Nucl. Sci. Eng.*, **125**, 257 (1997).

126. M.R. Zika, "Iterative Acceleration for Two-Dimensional Long-Characteristics Transport Problems," Ph.D. Dissertation, Texas A&M University, College Station, Texas (1997).

127. M.R. Zika and M.L. Adams, "Transport Synthetic Acceleration for the Long-Characteristics Discretization," *Proc. Joint Int. Conf. Mathematical Methods and Supercomputing for Nuclear Applications*, Saratoga Springs, New York, October 5-9, 1997, Vol. 1, p. 353 (1997).

128. K.D. Lathrop, "Anisotropic Scattering Approximations in the Monoenergetic Boltzmann Equation," *Nucl. Sci. Eng.*, **21**, 498 (1965).

129. G.I. Bell, G.E. Hansen and H.A. Sandmeier, "Multitable Treatments of Anisotropic Scattering in S_N Multigroup Transport Calculations," *Nucl. Sci. Eng.*, **28**, 376 (1967).

130. J.E. Morel, "On the Validity of the Extended Transport Cross-Section Correction for Low-Energy Electron Transport," *Nucl. Sci. Eng.*, **71**, 64 (1979).

131. R.P. Fedorenko, "A Relaxation Method for Solving Elliptic Difference Equations," *U.S.S.R. Comp. Math. and Math. Phys.*, **1**, 4, 1092 (1962).

132. W.L. Briggs, *A Multigrid Tutorial*, Society for Industrial and Applied Mathematics, Philadelphia (1987).

133. R.E. Alcouffe, A. Brandt, J.E. Dendy, Jr. and J.W. Painter, "The Multi-Grid Method for the Diffusion Equation with Strongly Discontinuous Coefficients," *SIAM J. Sci. Stat. Comput.*, **2**, 4, 430 (1981).

134. A. Barnett, J.E. Morel and D.R. Harris, "A Multigrid Acceleration Method for the One-Dimensional S_N Equations with Anisotropic Scattering," *Nucl. Sci. Eng.*, **102**, 1 (1989).

135. J.W. Ruge and K. Stüben, "Algebraic Multigrid," *Multigrid Methods*, Chap. 4, S.F. McCormick, Ed., Society for Industrial and Applied Mathematics, Philadelphia (1987).

136. M.L. Adams, Texas A&M University, Private Communication (1997).

137. T.A. Wareing, J.M. McGhee, and J.E. Morel, "Discontinuous Finite Element S_N Methods for 3D Unstructured Meshes," (in preparation), Los Alamos National Laboratory.

138. Y.Y. Azmy, "Impossibility of Unconditional Stability and Robustness of Diffusive Acceleration Schemes," *1998 American Nuclear Society Radiation Protection and Shielding Division Topical Conference*, Nashville, Tennessee (to appear).

139. L.J. Lorence, Jr., J.E. Morel, and G.D. Valdez, "Physics Guide to CEPXS: A Multigroup Coupled Electron-Photon Cross-Section Generating Code," SAND89-1685, Sandia National Laboratory (1989).

APPENDIX A

DIFFUSION AND FILTER OPERATORS FOR DFEM DISCRETIZATIONS IN *X-Y* GEOMETRY

In Chapter V we performed Fourier analyses of the ANMG method as applied to DFEM discretizations in *x-y* Cartesian geometry. These transport iterations use diffusion operators for DSA and for the filtering of ANMG corrections. We examined two specific diffusion operators in our analyses: the modified 4-step method[109] and the modified WLA method.[137] We present these operators here.

The first method, the modified 4-step method, is a simplification of the well-known 4-step method[103] for deriving DSA operators. A detailed derivation of this method for the general class of DFEM discretizations is presented in reference 109. We will not present the derivation here; we will simply present the resulting equations. Furthermore we will restrict our attention to a uniform, infinite rectangular mesh with constant material properties. The modified 4-step method for the DFEM discretizations presented in Chapter III is given by

$$\frac{\Delta y}{2}\mathbf{G}\begin{bmatrix} J_x^B(x_i) - J_x^B\left(x_{i-\frac{1}{2}}\right) \\ J_x^B\left(x_{i+\frac{1}{2}}\right) - J_x^B(x_i) \\ J_x^T\left(x_{i+\frac{1}{2}}\right) - J_x^T(x_i) \\ J_x^T(x_i) - J_x^T\left(x_{i-\frac{1}{2}}\right) \end{bmatrix}$$

$$+\frac{\Delta x}{2}\mathbf{H}\begin{bmatrix} J_y^L(y_j) - J_y^L\left(y_{j-\frac{1}{2}}\right) \\ J_y^R(y_j) - J_y^R\left(y_{j-\frac{1}{2}}\right) \\ J_y^R\left(y_{j+\frac{1}{2}}\right) - J_y^R(y_j) \\ J_y^L\left(y_{j+\frac{1}{2}}\right) - J_y^L(y_j) \end{bmatrix} + \sigma_a \Delta x \Delta y \mathbf{M}\begin{bmatrix} \varphi_{1,ij} \\ \varphi_{2,ij} \\ \varphi_{3,ij} \\ \varphi_{4,ij} \end{bmatrix}$$

$$= \Delta x \Delta y \mathbf{M} \begin{bmatrix} q_{1,ij} \\ q_{2,ij} \\ q_{3,ij} \\ q_{4,ij} \end{bmatrix}, \tag{A.1a}$$

$$J_x^B(x_i) = -\frac{D}{\Delta x}\left(\varphi_{2,ij} - \varphi_{1,ij}\right), \tag{A.1b}$$

$$J_x^T(x_i) = -\frac{D}{\Delta x}\left(\varphi_{3,ij} - \varphi_{4,ij}\right), \tag{A.1c}$$

$$J_y^L(y_j) = -\frac{D}{\Delta y}\left(\varphi_{4,ij} - \varphi_{1,ij}\right), \tag{A.1d}$$

$$J_y^R(y_j) = -\frac{D}{\Delta y}\left(\varphi_{3,ij} - \varphi_{2,ij}\right) \tag{A.1e}$$

$$J_x^B\left(x_{i-\frac{1}{2}}\right) = \left[\alpha\varphi_{2,i-1,j} + \frac{1}{2}J_x^B(x_{i-1})\right] - \left[\alpha\varphi_{1,ij} - \frac{1}{2}J_x^B(x_i)\right], \tag{A.1f}$$

$$J_x^T\left(x_{i-\frac{1}{2}}\right) = \left[\alpha\varphi_{3,i-1,j} + \frac{1}{2}J_x^T(x_{i-1})\right] - \left[\alpha\varphi_{4,ij} - \frac{1}{2}J_x^T(x_i)\right], \tag{A.1g}$$

$$J_y^L\left(y_{j-\frac{1}{2}}\right) = \left[\alpha\varphi_{4,i,j-1} + \frac{1}{2}J_y^L(y_{j-1})\right] - \left[\alpha\varphi_{1,ij} - \frac{1}{2}J_y^L(y_j)\right], \tag{A.1h}$$

$$J_y^R\left(y_{j-\frac{1}{2}}\right) = \left[\alpha\varphi_{3,i,j-1} + \frac{1}{2}J_y^R(y_{j-1})\right] - \left[\alpha\varphi_{2,ij} - \frac{1}{2}J_y^R(y_j)\right], \tag{A.1i}$$

where $\alpha \approx 0.25$ (the exact value depends on the quadrature set), $D \equiv 1/3\sigma_t$ is the diffusion coefficient, $\mathbf{M}$ is defined in Eq. (46o), and $\mathbf{G}$ and $\mathbf{H}$ are defined as

$$\mathbf{G} = \begin{cases} \frac{1}{3}\begin{bmatrix} 2 & 0 & 0 & 1 \\ 0 & 2 & 1 & 0 \\ 0 & 1 & 2 & 0 \\ 1 & 0 & 0 & 2 \end{bmatrix}, & BLD, LBLD \\ \begin{bmatrix} 1 & 0 & 0 & 0 \\ 0 & 1 & 0 & 0 \\ 0 & 0 & 1 & 0 \\ 0 & 0 & 0 & 1 \end{bmatrix}, & SCB \end{cases}, \tag{A.1j}$$

$$\mathbf{H} = \begin{cases} \frac{1}{3}\begin{bmatrix} 2 & 1 & 0 & 0 \\ 1 & 2 & 0 & 0 \\ 0 & 0 & 2 & 1 \\ 0 & 0 & 1 & 2 \end{bmatrix}, & BLD, LBLD \\ \begin{bmatrix} 1 & 0 & 0 & 0 \\ 0 & 1 & 0 & 0 \\ 0 & 0 & 1 & 0 \\ 0 & 0 & 0 & 1 \end{bmatrix}, & SCB \end{cases} . \tag{A.1k}$$

Here $J_x^B(x_i)$ is the modified 4-step approximation to the net current in the x-direction in the bottom half of the cell, and $J_x^B\left(x_{i-1/2}\right)$ is the net current in the x-direction along the bottom half of the left boundary of the cell. The other J variables have analogous physical interpretations. The exact definition of q depends on how the diffusion operator is applied. In DSA it is the residual scattering source. The above method may also be used as an ANMG filter by replacing σ_a with σ_t and by defining q to be the product of σ_t and one of the moments of the ANMG correction term.

The modified 4-step method has been shown to be an unconditionally stable and effective DSA operator for many different DFEM discretizations. In Chapter V we demonstrated its effectiveness as an ANMG filter for a few DFEM discretizations. However, in multidimensional calculations the modified 4-step equations are generally difficult to solve. Wareing[137] has developed an approximation to these equations that is less effective but easier to solve. It consists of a continuous FEM diffusion equation (which is easier to solve); the continuous solution is used to construct an approximate discontinuous solution. To derive this method we begin with Eq. (A.1), but we ignore the definitions of the boundary currents in Eqs. (A.1f)-(A.1i), yielding the following intermediate set of equations:

$$\frac{\Delta y}{2}\mathbf{G}\begin{bmatrix} -\frac{D}{\Delta x}\left(\varphi_{2,ij}-\varphi_{1,ij}\right)-J_x^B\left(x_{i-\frac{1}{2}}\right) \\ J_x^B\left(x_{i+\frac{1}{2}}\right)+\frac{D}{\Delta x}\left(\varphi_{2,ij}-\varphi_{1,ij}\right) \\ J_x^T\left(x_{i+\frac{1}{2}}\right)+\frac{D}{\Delta x}\left(\varphi_{3,ij}-\varphi_{4,ij}\right) \\ -\frac{D}{\Delta x}\left(\varphi_{3,ij}-\varphi_{4,ij}\right)-J_x^T\left(x_{i-\frac{1}{2}}\right) \end{bmatrix}$$

$$+\frac{\Delta x}{2}\mathbf{H}\begin{bmatrix} -\frac{D}{\Delta y}\left(\varphi_{4,ij}-\varphi_{1,ij}\right)-J_y^L\left(y_{j-\frac{1}{2}}\right) \\ -\frac{D}{\Delta y}\left(\varphi_{3,ij}-\varphi_{2,ij}\right)-J_y^R\left(y_{j-\frac{1}{2}}\right) \\ J_y^R\left(y_{j+\frac{1}{2}}\right)+\frac{D}{\Delta y}\left(\varphi_{3,ij}-\varphi_{2,ij}\right) \\ J_y^L\left(y_{j+\frac{1}{2}}\right)+\frac{D}{\Delta y}\left(\varphi_{4,ij}-\varphi_{1,ij}\right) \end{bmatrix}+\sigma_a\Delta x\Delta y\mathbf{M}\begin{bmatrix}\varphi_{1,ij}\\ \varphi_{2,ij}\\ \varphi_{3,ij}\\ \varphi_{4,ij}\end{bmatrix}$$

$$= \Delta x\Delta y\mathbf{M}\begin{bmatrix}q_{1,ij}\\ q_{2,ij}\\ q_{3,ij}\\ q_{4,ij}\end{bmatrix}, \tag{A.2}$$

We now derive a continuous FEM diffusion equation from Eq. (A.2). We first assume that all four flux values located at the same vertex are equal:

$$\varphi_{1,ij}=\varphi_{2,i-1,j}=\varphi_{3,i-1,j-1}=\varphi_{4,i,j-1}\equiv\varphi_{i-\frac{1}{2},j-\frac{1}{2}}. \tag{A.3}$$

Next we add the individual equations from Eq. (A.2) that are associated with the same node, i.e. the first row of Eq. (A.2) as defined in cell i,j, the second row as defined in cell $i-1,j$, etc. Given the definition of $\mathbf{G}$ and $\mathbf{H}$ in Eq. (A.1), the edge current terms all cancel, yielding a single equation in terms of the nodal fluxes:

$$\beta_{ij}\varphi_{i-\frac{1}{2},j-\frac{1}{2}}+\beta_{i-1,j}\varphi_{i-\frac{3}{2},j-\frac{1}{2}}+\beta_{i+1,j}\varphi_{i+\frac{1}{2},j-\frac{1}{2}}$$

$$+\beta_{i,j-1}\varphi_{i-\frac{1}{2},j-\frac{3}{2}}+\beta_{i,j+1}\varphi_{i-\frac{1}{2},j+\frac{1}{2}}+\beta_{i-1,j-1}\varphi_{i-\frac{3}{2},j-\frac{3}{2}}$$

$$+\beta_{i-1,j+1}\varphi_{i-\frac{3}{2},j+\frac{1}{2}} + \beta_{i+1,j-1}\varphi_{i+\frac{1}{2},j-\frac{3}{2}} + \beta_{i+1,j+1}\varphi_{i+\frac{1}{2},j+\frac{1}{2}}$$

$$= \Delta x \Delta y \left(M_{1,1} Q_1 + M_{1,2} Q_2 + M_{1,3} Q_3 \right), \tag{A.4a}$$

$$\beta_{ij} = 2G_{1,1}\frac{D\Delta y}{\Delta x} + 2H_{1,1}\frac{D\Delta x}{\Delta y} + 4M_{1,1}\Delta x \Delta y \sigma_a, \tag{A.4b}$$

$$\beta_{i-1,j} = \beta_{i+1,j} = -G_{1,1}\frac{D\Delta y}{\Delta x} + H_{1,2}\frac{D\Delta x}{\Delta y} + 2M_{1,2}\Delta x \Delta y \sigma_a, \tag{A.4c}$$

$$\beta_{i,j-1} = \beta_{i,j+1} = G_{1,4}\frac{D\Delta y}{\Delta x} - H_{1,1}\frac{D\Delta x}{\Delta y} + 2M_{1,2}\Delta x \Delta y \sigma_a, \tag{A.4d}$$

$$\beta_{i-1,j-1} = \beta_{i-1,j+1} = \beta_{i+1,j-1} = \beta_{i+1,j+1}$$

$$= -G_{1,4}\frac{D\Delta y}{2\Delta x} - H_{1,1}\frac{D\Delta x}{2\Delta y} + M_{1,3}\Delta x \Delta y \sigma_a, \tag{A.4e}$$

$$Q_1 = q_{1,ij} + q_{2,i-1,j} + q_{3,i-1,j-1} + q_{4,i,j-1}, \tag{A.4f}$$

$$Q_2 = (q_2 + q_4)_{ij} + (q_1 + q_3)_{i-1,j} + (q_2 + q_4)_{i-1,j-1} + (q_1 + q_3)_{i,j-1}, \tag{A.4g}$$

$$Q_3 = q_{3,ij} + q_{4,i-1,j} + q_{1,i-1,j-1} + q_{2,i,j-1}. \tag{A.4h}$$

In defining Eq. (A.4) we have made use of the symmetries of $\mathbf{M}$, $\mathbf{G}$, and $\mathbf{H}$. Equation (A.4) is a symmetric nine-point operator (five-point for SCB), which may be solved easily by a variety of methods. Although we derived it differently here, this equation is actually an asymptotic diffusion limit of the DFEM schemes we are studying.[73] Therefore we can expect it to give reasonable acceleration of diffusive error modes.

Since the discretizations we are examining are discontinuous, we need to somehow map the continuous solution onto the discontinuous variables. One simple way is to use the assumption of Eq. (A.3), i.e. to let the "discontinuous" solution be in fact continuous. An

alternative approach is to consider all the variables in a given cell as unknowns but to use the continuous solution in adjacent cells to construct an incoming partial current; this decouples all of the cells, each of which can be easily inverted directly. To construct the discontinuous update equations with this approach we first express the net currents at the boundaries as the difference between the incoming and outgoing partial currents:

$$J_x^B\left(x_{i-\frac{1}{2}}\right) = J_x^{B+}\left(x_{i-\frac{1}{2}}\right) - J_x^{B-}\left(x_{i-\frac{1}{2}}\right), \tag{A.5a}$$

$$J_x^T\left(x_{i-\frac{1}{2}}\right) = J_x^{T+}\left(x_{i-\frac{1}{2}}\right) - J_x^{T-}\left(x_{i-\frac{1}{2}}\right), \tag{A.5b}$$

$$J_y^L\left(y_{j-\frac{1}{2}}\right) = J_y^{L+}\left(y_{j-\frac{1}{2}}\right) - J_y^{L-}\left(y_{j-\frac{1}{2}}\right), \tag{A.5c}$$

$$J_y^R\left(y_{j-\frac{1}{2}}\right) = J_y^{R+}\left(y_{j-\frac{1}{2}}\right) - J_y^{R-}\left(y_{j-\frac{1}{2}}\right). \tag{A.5d}$$

where the outgoing currents may be expressed in terms of the upstream values:

$$J_x^{B-}\left(x_{i-\frac{1}{2}}\right) = \frac{\varphi_{1,ij}}{4} - \frac{J_x^B\left(x_i\right)}{2}, \tag{A.6a}$$

$$J_y^{L-}\left(y_{j-\frac{1}{2}}\right) = \frac{\varphi_{1,ij}}{4} - \frac{J_y^L\left(y_j\right)}{2}, \tag{A.6b}$$

$$J_x^{B+}\left(x_{i+\frac{1}{2}}\right) = \frac{\varphi_{2,ij}}{4} + \frac{J_x^B\left(x_i\right)}{2}, \tag{A.6c}$$

$$J_y^{R-}\left(y_{j-\frac{1}{2}}\right) = \frac{\varphi_{2,ij}}{4} - \frac{J_y^R\left(y_j\right)}{2}, \tag{A.6d}$$

$$J_x^{T+}\left(x_{i+\frac{1}{2}}\right) = \frac{\varphi_{3,ij}}{4} + \frac{J_x^T\left(x_i\right)}{2}, \tag{A.6e}$$

$$J_y^{R+}\left(y_{j+\frac{1}{2}}\right) = \frac{\varphi_{3,ij}}{4} + \frac{J_y^R\left(y_j\right)}{2}, \tag{A.6f}$$

$$J_x^{T-}\left(x_{i-\frac{1}{2}}\right) = \frac{\varphi_{4,ij}}{4} - \frac{J_x^T(x_i)}{2}, \tag{A.6g}$$

$$J_y^{L+}\left(y_{j+\frac{1}{2}}\right) = \frac{\varphi_{4,ij}}{4} + \frac{J_y^L(y_j)}{2}. \tag{A.6h}$$

Next we recognize that in the continuous diffusion solution the sum of these partial currents is related to the corresponding nodal fluxes:

$$2\alpha\varphi_{i-\frac{1}{2},j-\frac{1}{2}} = J_x^{B+}\left(x_{i-\frac{1}{2}}\right) + J_x^{B-}\left(x_{i-\frac{1}{2}}\right) = J_y^{L+}\left(y_{j-\frac{1}{2}}\right) + J_y^{L-}\left(y_{j-\frac{1}{2}}\right), \tag{A.7a}$$

$$2\alpha\varphi_{i+\frac{1}{2},j-\frac{1}{2}} = J_x^{B+}\left(x_{i+\frac{1}{2}}\right) + J_x^{B-}\left(x_{i+\frac{1}{2}}\right) = J_y^{R+}\left(y_{j-\frac{1}{2}}\right) + J_y^{R-}\left(y_{j-\frac{1}{2}}\right), \tag{A.7b}$$

$$2\alpha\varphi_{i+\frac{1}{2},j+\frac{1}{2}} = J_x^{T+}\left(x_{i+\frac{1}{2}}\right) + J_x^{T-}\left(x_{i+\frac{1}{2}}\right) = J_y^{R+}\left(y_{j+\frac{1}{2}}\right) + J_y^{R-}\left(y_{j+\frac{1}{2}}\right), \tag{A.7c}$$

$$2\alpha\varphi_{i-\frac{1}{2},j+\frac{1}{2}} = J_x^{T+}\left(x_{i-\frac{1}{2}}\right) + J_x^{T-}\left(x_{i-\frac{1}{2}}\right) = J_y^{L+}\left(y_{j+\frac{1}{2}}\right) + J_y^{L-}\left(y_{j+\frac{1}{2}}\right). \tag{A.7d}$$

By combining Eqs. (A.5)-(A.7) we obtain alternative expressions for the net edge currents that contain unknown values from only a single cell:

$$J_x^B\left(x_{i-\frac{1}{2}}\right) = 2\alpha\left(\varphi_{i-\frac{1}{2},j-\frac{1}{2}} - \varphi_{1,ij}\right) + J_x^B(x_i), \tag{A.8a}$$

$$J_x^B\left(x_{i+\frac{1}{2}}\right) = 2\alpha\frac{\varphi_{2,ij} - \varphi_{i+\frac{1}{2},j-\frac{1}{2}}}{2} + J_x^B(x_i), \tag{A.8b}$$

$$J_x^T\left(x_{i+\frac{1}{2}}\right) = 2\alpha\left(\varphi_{3,ij} - \varphi_{i+\frac{1}{2},j+\frac{1}{2}}\right) + J_x^T(x_i), \tag{A.8c}$$

$$J_x^T\left(x_{i-\frac{1}{2}}\right) = 2\alpha\left(\varphi_{i-\frac{1}{2},j+\frac{1}{2}} - \varphi_{4,ij}\right) + J_x^T(x_i), \tag{A.8d}$$

$$J_y^L\left(y_{j-\frac{1}{2}}\right) = 2\alpha\left(\varphi_{i-\frac{1}{2},j-\frac{1}{2}} - \varphi_{1,ij}\right) + J_y^L(y_j), \tag{A.8e}$$

$$J_y^R\left(y_{j-\frac{1}{2}}\right) = 2\alpha\left(\varphi_{i+\frac{1}{2},j-\frac{1}{2}} - \varphi_{2,ij}\right) + J_y^R(y_j), \tag{A.8f}$$

$$J_y^R\left(y_{j+\frac{1}{2}}\right) = 2\alpha\left(\varphi_{3,ij} - \varphi_{i+\frac{1}{2},j+\frac{1}{2}}\right) + J_y^R\left(y_j\right), \tag{A.8g}$$

$$J_y^L\left(y_{j+\frac{1}{2}}\right) = 2\alpha\left(\varphi_{4,ij} - \varphi_{i-\frac{1}{2},j+\frac{1}{2}}\right) + J_y^L\left(y_j\right). \tag{A.8h}$$

We substitute Eqs. (A.8) into Eq. (A.1a), which eliminates the currents. The resulting discontinuous update equation is:

$$\begin{aligned}
&\left(\alpha\Delta y\mathbf{G} + \alpha\Delta x\mathbf{H} + \sigma_a\Delta x\Delta y\mathbf{M}\right)\begin{bmatrix}\varphi_{1,ij}\\ \varphi_{2,ij}\\ \varphi_{3,ij}\\ \varphi_{4,ij}\end{bmatrix} \\
&= \left(\alpha\Delta y\mathbf{G} + \alpha\Delta x\mathbf{H}\right)\begin{bmatrix}\varphi_{i-\frac{1}{2},j-\frac{1}{2}}\\ \varphi_{i+\frac{1}{2},j-\frac{1}{2}}\\ \varphi_{i+\frac{1}{2},j+\frac{1}{2}}\\ \varphi_{i-\frac{1}{2},j+\frac{1}{2}}\end{bmatrix} + \Delta x\Delta y\mathbf{M}\begin{bmatrix}q_{1,ij}\\ q_{2,ij}\\ q_{3,ij}\\ q_{4,ij}\end{bmatrix}.
\end{aligned} \tag{A.9}$$

The DSA method of Wareing is unconditionally stable and easily solved, but it loses effectiveness as the cells become highly elongated. The analyses of Chapter V show that this method is stable when used as an ANMG filter and effective when cell aspect ratios are not too large.

APPENDIX B

NUMERICAL ESTIMATION OF COMPLEX EIGENVALUES

In Chapter VI we performed numerical tests of the ANMG method by means of the transport code PERICLES. Our main objective was to determine the iterative spectral radii in order to confirm our Fourier analyses. Although the numerical estimation of a spectral radius is relatively simple when the dominant eigenvalue is real, a good estimate is more difficult to obtain when a complex conjugate pair of eigenvalues is dominant. Since our Fourier analyses reveal that most of our iterations with forward-peaked scattering have dominant eigenvalues that are complex, this is an important subject to consider. We describe here a method for obtaining a numerical estimate of the spectral radius in such a situation.

We begin by examining the case when the dominant eigenvalue is real. Let A be a real linear iteration matrix for a system of equations with solution $\mathbf{\Phi}$, and let $\mathbf{\Phi}^{(0)}$ be an initial guess at the solution. We may rewrite $\mathbf{\Phi}^{(0)}$ in terms of $\mathbf{\Phi}$ and the error $\mathbf{e}^{(0)}$:

$$\mathbf{\Phi}^{(0)} = \mathbf{\Phi} + \mathbf{e}^{(0)}. \tag{B.1}$$

Let $\{\mathbf{v}_1, \cdots, \mathbf{v}_l\}$ be the eigenvectors of A. We may rewrite the error in terms of these eigenvectors:

$$\mathbf{e}^{(0)} = \sum_{i=1}^{l} c_i \mathbf{v}_i. \tag{B.2}$$

The following expression for the error at an arbitrary iteration is well known:

$$\mathbf{e}^{(n)} = A^n \mathbf{e}^{(0)} = \sum_{i=1}^{l} c_i A^n \mathbf{v}_i = \sum_{i=1}^{l} c_i \omega_i^n \mathbf{v}_i, \tag{B.3}$$

where ω_i is the eigenvalue associated with eigenvector $\mathbf{v}_i$. Therefore the approximate solution at any iteration is given by

$$\mathbf{\Phi}^{(n)} = \mathbf{\Phi} + \mathbf{e}^{(n)} = \mathbf{\Phi} + \sum_{i=1}^{l} c_i \omega_i^n \mathbf{v}_i. \tag{B.4}$$

Now we assume that the dominant eigenvalue, $\omega_{\max}$, is real and distinct, i.e. that $|\omega_{\max}| = \omega_{\max} \equiv \sigma$. For n sufficiently large all other components of the error become negligible compared to the dominant component, yielding the following asymptotic form for the approximate solution:

$$\mathbf{\Phi}^{(n)} = \mathbf{\Phi} + c_{\max} \sigma^n \, \mathbf{v}_{\max}. \tag{B.5}$$

The usual method for estimating σ during an iterative calculation is to take the ratio of the norms of successive residuals:

$$\frac{\left\|\mathbf{r}^{(n+1)}\right\|}{\left\|\mathbf{r}^{(n)}\right\|} = \frac{\left\|\mathbf{\Phi}^{(n+1)} - \mathbf{\Phi}^{(n)}\right\|}{\left\|\mathbf{\Phi}^{(n)} - \mathbf{\Phi}^{(n-1)}\right\|} = \frac{|c_{\max}| \left(\sigma^{n+1} - \sigma^n\right) \left\|\mathbf{v}_{\max}\right\|}{|c_{\max}| \left(\sigma^n - \sigma^{n-1}\right) \left\|\mathbf{v}_{\max}\right\|} = \sigma \tag{B.6}$$

Equation (B.6) is exact when the error is composed of only the dominant eigenvector. It will be inexact when there are other error modes present, but its accuracy will increase as the iterations continue and the non-dominant modes are effectively eliminated.

Now let us assume instead that A has a pair of complex conjugate eigenvalues that are dominant. We will further assume that there are no other eigenvalues of equal magnitude. The dominant component of the initial error then is given by

$$\mathbf{e}^{(0)} = (a_0, ib_0) \, \mathbf{v}_{\max} + (a_0, -ib_0) \, \mathbf{v}^*_{\max}, \tag{B.7}$$

where $\mathbf{v}^*_{\max}$ is the complex conjugate of $\mathbf{v}_{\max}$. Therefore after n iterations the dominant component of the error is

$$\mathbf{e}^{(n)} = \omega^n_{\max}\left(a_0, ib_0\right)\mathbf{v}_{\max} + \omega^{*n}_{\max}\left(a_0, -ib_0\right)\mathbf{v}^*_{\max}. \tag{B.8}$$

Let $\omega_{\max}$ be given in complex polar coordinates by (σ, ϕ) and let $\mathbf{v}_{\max}$ be given in complex Cartesian coordinates by $(\mathbf{f}, i\mathbf{g})$. Substitution of these values into Eq. (B.8) yields, in Cartesian coordinates,

$$\mathbf{e}^{(n)} = \left(\sigma^n\left\{\mathbf{F}\cos\left(n\phi\right) + \mathbf{G}\sin\left(n\phi\right)\right\}, 0\right), \tag{B.9}$$

where

$$\mathbf{F} = 2\left(a_0\mathbf{f} - b_0\mathbf{g}\right), \tag{B.10a}$$

$$\mathbf{G} = -2\left(b_0\mathbf{f} + a_0\mathbf{g}\right). \tag{B.10b}$$

Since both the error and the solution are real, we will suppress the complex notation in the rest of the analysis. If we combine Eqs. (B.4) and (B.9) and assume that a sufficient number of iterations has been completed to effectively eliminate the non-dominant error modes, we obtain the following expressions for the iterative solution and residual:

$$\mathbf{\Phi}^{(n)} = \mathbf{\Phi} + \sigma^n\left[\mathbf{F}\cos\left(n\phi\right) + \mathbf{G}\sin\left(n\phi\right)\right], \tag{B.11a}$$

$$\begin{aligned}\mathbf{r}^{(n)} = {} & \mathbf{F}\left[\sigma^n\cos\left(n\phi\right) - \sigma^{n-1}\cos\left(\left(n-1\right)\phi\right)\right] \\ & +\mathbf{G}\left[\sigma^n\sin\left(n\phi\right) - \sigma^{n-1}\sin\left(\left(n-1\right)\phi\right)\right].\end{aligned} \tag{B.11b}$$

Note how the residual differs from that of Eq. (B.6), where the dominant eigenvalue is real. If we attempt to use Eq. (B.6) to estimate the spectral radius when the dominant eigenvalues are complex conjugates, our estimate could be very inaccurate. For example, if $\mathbf{G} = \mathbf{0}$ then the real spectral radius estimate is given by

$$\sigma_{est} = \sigma \left| \frac{\sigma \cos\left((n+1)\,\phi\right) - \cos\left(n\phi\right)}{\sigma \cos\left(n\phi\right) - \cos\left((n-1)\,\phi\right)} \right|. \tag{B.12}$$

Depending on the value of n and ϕ, the estimate can cycle through a wide (even infinite) range of values. Clearly we need an estimate that takes into account the potentially complex nature of the eigenvalues.

If we examine Eq. (B.11b) we see that the unknown quantities are $\mathbf{F}$, $\mathbf{G}$, σ, and ϕ; we obtain $\mathbf{r}^{(n)}$ from our computations at each iteration. We are most interested in σ and perhaps ϕ. We can obtain expressions for $\mathbf{F}$ and $\mathbf{G}$ in terms of the other parameters by using two successive residuals:

$$\mathbf{F} = \frac{1}{\det} \left\{ \begin{array}{c} \mathbf{r}^{(n)} \left[\sigma^{n+1} \sin\left((n+1)\,\phi\right) - \sigma^{n} \sin\left(n\phi\right)\right] \\ -\mathbf{r}^{(n+1)} \left[\sigma^{n} \sin\left(n\phi\right) - \sigma^{n-1} \sin\left((n-1)\,\phi\right)\right] \end{array} \right\}, \tag{B.13a}$$

$$\mathbf{G} = \frac{1}{\det} \left\{ \begin{array}{c} \mathbf{r}^{(n+1)} \left[\sigma^{n} \cos\left(n\phi\right) - \sigma^{n-1} \cos\left((n-1)\,\phi\right)\right] \\ -\mathbf{r}^{(n)} \left[\sigma^{n+1} \cos\left((n+1)\,\phi\right) - \sigma^{n} \cos\left(n\phi\right)\right] \end{array} \right\}, \tag{B.13b}$$

where

$$\begin{aligned} \det = {} & \sigma^{2n} \left[\cos\left(n\phi\right) - \sigma^{-1} \cos\left((n-1)\,\phi\right)\right] \left[\sigma \sin\left((n+1)\,\phi\right) - \sin\left(n\phi\right)\right] \\ & -\sigma^{2n} \left[\sigma \cos\left((n+1)\,\phi\right) - \cos\left(n\phi\right)\right] \left[\sin\left(n\phi\right) - \sigma^{-1} \sin\left((n-1)\,\phi\right)\right]. \end{aligned} \tag{B.14}$$

We need the next two residuals to obtain independent equations for σ and ϕ:

$$\begin{aligned}\mathbf{r}^{(n+2)} &= \mathbf{F}\left[\sigma^{n+2}\cos\left((n+2)\,\phi\right) - \sigma^{n+1}\cos\left((n+1)\,\phi\right)\right] \\ &\quad +\mathbf{G}\left[\sigma^{n+2}\sin\left((n+2)\,\phi\right) - \sigma^{n+1}\sin\left((n+1)\,\phi\right)\right], \qquad \text{(B.15a)}\end{aligned}$$

$$\begin{aligned}\mathbf{r}^{(n+3)} &= \mathbf{F}\left[\sigma^{n+3}\cos\left((n+3)\,\phi\right) - \sigma^{n+2}\cos\left((n+2)\,\phi\right)\right] \\ &\quad +\mathbf{G}\left[\sigma^{n+3}\sin\left((n+3)\,\phi\right) - \sigma^{n+2}\sin\left((n+2)\,\phi\right)\right]. \qquad \text{(B.15b)}\end{aligned}$$

If we substitute Eqs. (B.13) into Eqs. (B.15) we obtain two nonlinear vector equations with the two unknowns σ and ϕ. There are actually only two independent scalar equations; the equations from any non-zero element of the residuals are equivalent to those obtained from any other component. Therefore in practice we may simply choose an arbitrary algebraically non-zero component of the residuals in order to determine σ and ϕ.

The two nonlinear equations derived above require a nonlinear solution method. For our computational experiments we use a method similar to the one we used to determine the theoretical spectral radii in the Fourier analyses of Chapters IV and V. We define a grid of points in (σ, ϕ) space and substitute each set of values into the right sides of Eqs. (B.15) to obtain two estimated residuals. We add the absolute values of the differences between these estimates and the actual residuals to define an error. The (σ, ϕ) pair that has the lowest error is used as the center for a finer set of grid points and the process is repeated. Successively finer sets of test points are used until the error is smaller than some tolerance. We note that because of the sinusoidal terms in Eqs. (B.15) there may be multiple roots; we have not developed a solution strategy to avoid false roots. In practice this has not been a serious problem.

Note some qualitative differences between this spectral radius estimate and the simpler one, which is valid only for real eigenvalues. In the real case we only calculate a ratio, whereas in the nonlinear case we must find the roots of two nonlinear equations. This requires the implementation of a good nonlinear root solver. In practice this has not been difficult, nor has it appreciably increased the computational time. In the real case we take a norm of the residual, whereas in the complex case we only examine the values of a single component of the residual; applying a norm to these residuals would greatly complicate the equations and probably make their solution impractical. Finally, in the real case the iteration count n is effectively eliminated from Eq. (B.6); in the complex case it cannot easily be eliminated. However, since $\mathbf{e}^{(0)}$ is arbitrary, we may define any iteration as the initial iteration in order to reduce n and simplify our equations.

The complex eigenvalue estimate is, like the real estimate, subject to the constraint that all but the dominant error modes have been eliminated; during the transient phase the complex estimate will not be exact. The estimate also may be in error if there are other eigenvalues of the same magnitude as the "dominant" eigenvalue pair but with different phases; our analysis has not included this case.

As a demonstration of the behavior of these two methods we perform an S_4-DSA calculation in PERICLES with BLD differencing and optimized FP scattering. Our first test is on a mesh with $\sigma_{tr}\Delta x = \sigma_{tr}\Delta y = 1$. From Table XIX we see that the theoretical spectral radius is 0.90; the dominant eigenvalue is complex. We report the spectral radius estimates for certain iterations in Table XXXV. The estimate obtained by assuming that the dominant eigenvalue is real varies greatly and never approaches a single value. The complex estimate, however, fluctuates between good and poor estimates during the early

TABLE XXXV

Numerical Spectral Radius Estimates, Complex Dominant Eigenvalue

n	σ: Eq. (B.6)	σ: Eqs. (B.15)	ϕ: Eqs. (B.15)
10	0.3603	0.9299	0.4159
20	1.4071	1.3849	0.0628
30	0.7053	0.6899	-0.0628
40	8.1874	0.9031	0.4407
50	0.9405	0.9038	0.4422
60	0.2722	0.9035	0.4412
70	1.3046	1.2899	-0.0628
80	0.6684	0.6549	-0.0628
90	4.7604	0.9035	0.4412
100	0.9058	0.8949	-0.0628
110	0.1886	0.9037	0.4412
120	1.2304	1.2199	0.0628
130	0.6329	0.6199	-0.0628
140	3.0688	0.9038	0.4413
150	0.8751	0.8649	-0.0628
160	0.1509	0.9038	0.4412
170	1.1720	1.1649	-0.0628
180	0.5966	0.5849	-0.0628
190	2.3844	0.9039	0.4412
200	0.8462	0.9038	0.4412
225	4.1773	0.9039	0.4412
250	0.8183	0.9038	0.4411
275	4.8405	0.9040	0.4412
300	0.7906	0.9038	0.4411
325	3.5989	0.9040	0.4412
350	0.7626	0.9038	0.4411
375	2.7451	0.9040	0.4412
400	0.7342	0.9038	0.4411
425	2.2545	0.9041	0.4411
450	0.7050	0.7049	-0.0628
475	1.9480	0.9041	0.4411
500	0.6747	0.9042	0.4411

iterations and eventually settles on a single good estimate. It is not surprising that there are fluctuations during the initial iterates, since even if the dominant error mode is larger than the other modes, its complex nature occasionally causes it to assume a low real value, and the corresponding residual is more greatly affected by the other modes. Eventually, however, these other modes become so small compared to the dominant eigenmode that poor estimates are rarely obtained.

TABLE XXXVI

Numerical Spectral Radius Estimates, Real Dominant Eigenvalue

n	σ: Eq. (B.6)	σ: Eq. (B.15)	ϕ: Eq. (B.15)
10	0.3606	0.8955	0.4436
20	1.4046	1.3949	-0.0628
30	0.7024	0.6899	-0.0628
40	8.9839	0.9031	0.4430
50	0.9344	0.9199	-0.0628
60	0.2520	0.9023	0.4411
70	1.2849	1.2649	-0.0628
80	0.6587	0.6399	-0.0628
90	3.2789	0.8946	0.4425
100	0.8987	0.8949	-0.0628
110	0.7182	0.9480	0.4662
120	1.0483	0.7689	0.5520
130	0.9587	0.8786	0.2815
140	0.9895	1.2950	0.1634
150	0.9871	0.9999	0.0000
160	0.9883	0.9200	0.0116
170	0.9890	0.9648	0.0428
180	0.9898	0.9946	0.0000
190	0.9906	0.9932	0.0000
200	0.9914	0.9861	0.0112
225	0.9931	0.9953	0.0000
250	0.9944	0.9956	0.0000
275	0.9952	0.9957	0.0000
300	0.9957	0.9959	0.0000
325	0.9961	0.9960	0.0000
350	0.9962	0.9960	0.0000
375	0.9964	0.9961	0.0000
400	0.9964	0.9961	0.0000
425	0.9965	0.9962	0.0000
450	0.9965	0.9962	0.0000
475	0.9966	0.9962	0.0000
500	0.9966	0.9962	0.0000

To demonstrate the behavior of the spectral radius estimates when the actual dominant eigenvalue is real, we perform the same computation on a mesh in which $\sigma_{tr}\Delta x$ is increased to 1000. The results are reported in Table XXXVI. During the early transient period the real estimate fluctuates greatly, whereas the complex estimate gives more reasonable values. Sometimes the complex estimate has a value close to the spectral radius of the previous case (0.90); this particular eigenvalue must still be present, even if it is not the dominant one now. After sufficient iterations have occurred both the real and the complex estimates approach a value close to unity, and the estimated phase is zero. This is close to the spectral radius predicted by the Fourier analysis in Table XIX. Since a real eigenvalue is a special case of a complex eigenvalue, the complex estimate works well in this situation. Therefore we observe that the spectral radius estimation method that takes into account the potentially complex nature of the dominant eigenvalue is more robust than the one that assumes that the eigenvalue is real.

Finally, we note that a somewhat better real estimate may be obtained by calculating a geometric mean over several iterations. In the special case when a complex conjugate pair of eigenvalues are dominant and $\mathbf{G} = \mathbf{0}$, we have the estimate

$$\begin{aligned} \sigma_{est} &= \left| \frac{\sigma^{n+k} \cos\left((n+k)\,\phi\right) - \sigma^{n+k-1} \cos\left((n+k-1)\,\phi\right)}{\sigma^{n} \cos\left(n\phi\right) - \sigma^{n-1} \cos\left((n-1)\,\phi\right)} \right|^{\frac{1}{k}} \\ &= \sigma \left| \frac{\sigma \cos\left((n+k)\,\phi\right) - \cos\left((n+k-1)\,\phi\right)}{\sigma \cos\left(n\phi\right) - \cos\left((n-1)\,\phi\right)} \right|^{\frac{1}{k}}, \end{aligned} \tag{B.16}$$

where k is the number of iterations over which the geometric mean is taken. A similar but more complicated relation is obtained if $\mathbf{G} \neq \mathbf{0}$. Although the absolute value term in Eq. (B.16) will fluctuate as much as the absolute value term in Eq. (B.12), taking its kth root

makes it closer to unity. For k sufficiently large the estimate becomes $\sigma_{est} \approx \sigma$. In practice, however, k needs to be quite large for the estimate to be decent, and in the cases studied the complex estimate has always had greater precision.